Republic of Iraq

Ministry of Higher Education and Scientific Research

University of Babylon

College of Engineering

Civil Engineering Department


# Optimal Design of Barrage Considering the Challenges of The Presence of Collapsible Soil

A Thesis

Submitted to the College of Engineering / University of Babylon in Partial Fulfilment of the Requirements for the Master Degree in Engineering /Civil Engineering /Water Resources

*By:*

***Shahlaa Ali Kadhim Aliwi***

*Supervised by:*

***Asst.Prof. Dr. Imad Habeeb Obead***

***Asst.Prof. Dr. Zaid Hameed Majeed***

**2023 A.D** **1444 A.H**

بِسْمِ اللَّهِ الرَّحْمَنِ الرَّحِيمِ

{وَقُلْ رَبِّ زِدْنِي عِلْمًا}

صدق الله العلي العظيم

**سورة طة{الأية:114}**

# *Dedications*

*"To Al-Mahdí Al-Montadar (may Allah hasten his reappearance)"*

"To the loved ones of my heart, my husband and my children, Mohammad and Rayhana"

"To my beloved parents"

"To martyrs of Iraq"

***With love and respect***

***Shahlaa Ali***

# *Acknowledgements*

***In The Name of Allah, The Most Gracious, the Most Merciful***

First, great thanks are to ***ALLAH HIS MAJESTY*** for enabling me to complete this work.

I would like to express my sincere appreciation and deepest gratitude to ***Asst. Prof. Dr. Imad Habeeb Obead & Asst. Prof. Dr. Zaid Hameed Majeed***, for their generous advice, constructive suggestions, valuable guidance and continuous encouragement throughout this thesis.

Appreciation is also extended to my thesis examining committee members for their time and efforts.

Great thanks to the Dean of the College of Engineering Head and Staff of the Civil Engineering Department in the (University of Babylon) for their appreciable support.

Thanks, are also extended to the College of Engineering Civil Engineering Department, (Staff of the Soil Mechanics Laboratory) & (Staff of the sanitary engineering laboratory) at the University of Babylon for their help in using the various facilities during the experimental work.

Also, I would like to thank the Head and Staff of Al-Ma'awal company for the soil investigations for their assistance in completing the examinations.

Many thanks to my uncle (**Abu- Amir)**, who helped me obtain gypsum stone from Al-Najaf cement factory, and thanks also to the staff and management of Al-Najaf cement factory for their assistance in providing me with gypsum.

As I stand here, I can't express enough thanks to my support in life, my husband (***Dr. Mustafa Kareem Mousa***) who worked tirelessly for me, encouraged and supported me at every step of the way.

Many thanks to everyone who supported and prayed for me throughout my study, especially my uncle Kareem, my mother Umm-Haider, all my sisters and brothers, and all my close friends.

***Shahlaa Ali***

# Abstract

Hydraulic structures, such as dams, weirs, and barrages, are often exposed to water seepage underneath their foundations due to high water retention levels. This water seepage can cause significant problems when the structures are built on collapsible soils. In this study, a barrage constructed on gypseous soil (known to be collapsible due to the dissolution of gypsum minerals when exposed to water seepage) is being examined to determine the optimal design of the barrage profile. To achieve this goal, gypsiferous soil samples were prepared using the weight replacement method, with varying levels of gypsum content of 20%, 25%, and 35% of the weight of the fine portion in the natural soil samples. Six soil samples are collected from the Euphrates River bank in Al-Kifl, Babil governorate, Iraq. Various laboratory tests are conducted on the natural and gypsiferous soil samples, including physical tests, chemical tests, saturated permeability tests, leaching tests, and direct shear tests to measure the strength parameters of the gypsiferous soil samples before and after leaching. As the leaching process progresses, the soil's permeability increases due to increase and development of void spaces within the soil mass, allowing for more water infiltration resulting from the dissolution of gypsum salts.

GeoStudio software's SEEP/W 2D module are used to conduct a numerical analysis of steady state seepage beneath the barrage. A total of 200 section runs are performed to evaluate various dimension configurations, all sections are analyzed in non-dimensionlized form under the assumption of fully closed gates. The parametric analysis of seepage beneath the barrage floor shows that the seepage rate decreases by 39.24% when upstream cutoff depth ($z_2$) increases from (1.35 to 2.25), and total floor length of the barrage increase

from (4.07 to 5.11). The exit gradient decreases with increased downstream cutoff wall depth; the results show that the minimum value of the exit gradient when the total floor length and cutoff wall depth are equal to (5.24 and 2.38) respectively.

In order to optimize the hydraulic design of a barrage a Genetic Algorithm (GA) are used. The objective is to minimize construction volume material of barrage and seepage flux beneath the barrage. The GA algorithm was carried out with different population sizes (200, 600, 1000, and 1400). The results indicated that a population size of 600 is sufficient to obtain a solution of the optimization problem for the optimal hydraulic design of the barrage. Design charts are introduced to apply the optimization problem, using Abu-Sukhair barrage as a design example to re-design the optimal dimensions of the barrage from the present design charts. The results revealed that all dimensions of the barrage decreased, except for the depth of the upstream cutoff wall and the thickness of the inverted filter. The design criteria in terms of safety against piping of the barrage were calculated in which the actual exit gradient computed from barrage dimensions is 0.0445, and from the optimal dimensions is 0.0433, which is less than the critical exit gradient (0.976).

# List of Contents

## List of Content (Continue)

**List of Content (Continue)**



# List of Figures

# List of Figures (Continue)

# List of Figures (Continue)

## List of Figures (Continue)

## List of Figures (Continue)

## List of Figures (Continue)

## List of Figures (Continue)

## List of Figures (Continue)



## List of Tables

# List of Tables (Continue)

## List of Tables (Continue)

## List of Tables (Continue)



## List of Abbreviations

| Abbreviation | Description |
|---|---|
| ASTM | American Society for Testing Materials |
| AL | After Leaching Test |
| BL | Before Leaching Test |
| BS | British Standards |
| $Cl^-$ | Chloride Content |
| EC | Electric Conductivity |
| GA | Genetic Algorithms |
| L.L | Liquid Limit |
| ML | Silt Soil of Low Plasticity |
| MOPs | Multi-Objective Optimization Problems |

## List of Abbreviations (Continue)

| | |
|---|---|
| P. L | Plastic Limit |
| P. I | Plasticity Index |
| ppm | parts per million |
| $SO_3$ | Sulphate Content |
| TDS | Total Dissolved Salts |
| USCS | Unified Soil Classification System |

## List of symbols

| Symbol | Description | Dimension |
|---|---|---|
| A | The cross-section of the soil sample | $L^2$ |
| a | The cross-section of the standpipe | $L^2$ |
| C | Cohesion | $M/L^2$ |
| $d_{50}$ | Mean particle size | L |
| $d_{SU}$ | Depth of sheet piles in upstream | L |
| $d_{SD}$ | Depth of sheet pile in downstream | L |
| $e_{Max}$ | Max. void ratio | Dimensionless |
| $e_{Min.}$ | Min. void ratio | Dimensionless |
| $F_{sliding}$ | Factor of safety against sliding | Dimensionless |
| $G_s$ | Specific Gravity | Dimensionless |
| $H_{F.h}$ | The high flood head in upstream | L |
| $H_{N.h}$ | The normal operation head in upstream | L |
| $H_D$ | The downstream water flood head | L |
| $H_s$ | The seepage head | L |

## List of symbols (Continue)

| | | |
|---|---|---|
| $h_1$ | Normal operation head in normalized form | Dimensionless |
| $h_2$ | high flood head in downstream in normalized form | Dimensionless |
| $h$ | The flow head in porous media | L |
| $i_{exit}$ | The exit gradient | Dimensionless |
| $i_{critical}$ | The critical exit gradient | Dimensionless |
| k | Coefficient of permeability | L/T |
| $k_{xx}$ | The coefficient of permeability in $x$ direction | L/T |
| $k_{yy}$ | The coefficient of permeability in $y$ direction | L/T |
| L | Height of the soil sample column | L |
| $L$ | The creep line length | L |
| $L_{PU}$ | The length of upstream protection | L |
| $L_U$ | Length of upstream floor | L |
| $L_{Cr}$ | Crest length of the barrage | L |
| $L_{SF}$ | The projection length of inclined floor | L |
| $L_s$ | The stilling basin length | L |
| $L_{Inv}$ | Length of inverted filter | L |
| $q$ | The outflow / inflow rate | $L^3/T$ |
| $R^2$ | The Coefficient of Determination | Dimensionless |
| SG | the specific weight of concrete | Dimensionless |
| T | Thickness of soil layer beneath of the barrage foundation | L |

## List of symbols (Continue)

| | | |
|---|---|---|
| $t_s$ | Thickness of soil layer beneath of the barrage foundation in normalized form | Dimensionless |
| t | Time | T |
| $t_{PU}$ | Thickness of upstream protection | L |
| $t_U$ | Thickness of upstream floor | L |
| $t_U$ | Thickness of upstream floor | L |
| $t_{SF}$ | Thickness of the crest | L |
| $t_D$ | Thickness of the downstream floor | L |
| $t_{inv.}$ | Thickness of inverted filter | L |
| $w_c$ | Water content | Dimensionless |
| $\boldsymbol{x_1}$ | Length of the launching apron and protection in upstream in normalized form | Dimensionless |
| $\boldsymbol{x_2}$ | Length of upstream floor in normalized form | Dimensionless |
| $\boldsymbol{x_3}$ | The projection length of inclined floor in normalized form | Dimensionless |
| $\boldsymbol{x_4}$ | Length of stilling basin in normalized form | Dimensionless |
| $\boldsymbol{x_5}$ | Length of inverted filter drain in normalized form | Dimensionless |
| $\boldsymbol{x}_6$ | length of crest in normalized form | Dimensionless |
| $y_1$ | Per-jump depth of water | L |
| $y_2$ | Post-jump depth of water. | L |
| $\boldsymbol{z_1}$ | thickness of the launching apron and protection layers in normalized form | Dimensionless |

## List of symbols (Continue)

| | | |
|---|---|---|
| $z_2$ | Depth of the upstream cutoff wall in normalized form | Dimensionless |
| $z_3$ | Thickness of upstream floor in normalized form | Dimensionless |
| $z_7$ | Depth of the downstream cutoff wall in normalized form | Dimensionless |
| $z_8$ | Thickness of the inverted filter drains in normalized form | Dimensionless |
| $z_9$ | pre-jump depth of water in normalized form | Dimensionless |
| $z_{10}$ | post-jump depth of water in normalized form | Dimensionless |
| $\chi$ | Gypsum content | Dimensionless |
| $\gamma_w$ | Wet field density | $M/L^3$ |
| $\gamma_d$ | Dry field density | $M/L^3$ |
| $\gamma_{Max}$ | Max. dry density | $M/L^3$ |
| $\gamma_{sat}$ | Saturation weight density of soil | $M/L^3$ |
| $\phi$ | Angle of internal friction | Dimensionless |
| $\alpha$ | angle of inclined floor of barrage | Dimensionless |
| $\varphi$ | The specific storage coefficient of the porous media | $L^{-1}$ |
| $\beta$ | Angle of inclined floor of barrage in normalized form | Dimensionless |
| $\varphi_1$ | The objective function for total volume of construction materials | $L^3$ |
| $\varphi_2$ | the objective function of seepage discharge | $L^3/T$ |

# CHAPTER ONE

# INTRODUCTION

## 1.1 General

Many hydraulic structures are constructed on collapsible soils, such as gypseous soils. The term of gypseous soils is known as the soil that has a kind of salt is gypsum which can be dissolve in water, leading to many problems underneath these structures. Collapsible soils or metastable soils are unsaturated soils that undergo a considerable volume change upon saturation with or without additional load (Clemence and Finbarr, 1981). Gypseous soils are consider collapsible soils which defined as any unsaturated soil that goes through a radical rearrangement of particles and susceptible to large abrupt volume changes and sudden collapses when such soils are wetted, or leached with water (Schanz and Karim, 2018).

The dissolution of gypsum salts by water flow through soil mass and the leaching of gypseous soil particles causes several problems that were observed in the soil layers beneath the foundation of many buildings and engineering structures due to the continuous changes in the engineering properties of soil with time. The soil problem appears to become more complex particularly when seepage water flows through soil mass and causes loss of mass due to leachate of soil and removal of soluble salt. Leaching in gypseous soil can be defined as a process of dissolution and washing away of soluble salts; this will lead to a collapse of soil structure and affects structures established on such soil (Al-Damluji, et. al., 2018).

Gypseous and gypsiferrous soils, the two terms are used interchangeably, for soils plus gypsum ($CaSO_4.2H_2O$) in an amount enough to change or affect their engineering properties (Al-Damluji, et. al., 2018). The structure of these soils considers strong and has good properties when

they are in dry conditions, but a significant loss of such soil strength occurs when subjected to the water due to their solubility characteristics. When such soils are found in the foundation of hydraulic structure such as barrages it causes many problems because these types of structure are exposed to seepage of water beneath its foundation leading to dissolution and leaching of gypsum in soil which is soluble salt causes collapse of soil structure due to the breakdown of the bonds between soil particles provided by the gypsum.

Barrages are relatively low-level dams constructed across a river to raise the water level sufficiently or to divert the flow in whole or part into a supply canal or conduit for irrigation, power generation, navigation, flood control, and domestic and industrial uses (Novak et al., 2008).

Barrage is subjected to two hydraulic conditions: subsurface and surface flow. Subsurface flow occurs when water seepage occurs beneath the barrage's foundation because of the difference between the upstream and downstream water levels. Seepage of water beneath the hydraulic structure endangers its stability and may cause failure by piping or direct uplift pressure. The seepage problem become more complex when the foundation of such structure contains gypseous soil due to increase of dissolution of soluble salts leading to increases piping within soil mass. Barrage is considered a costly structure, and its design and construction have been a focus of attention for hydraulic researchers and field engineers (Singh, 2011). The characteristics of surface and subsurface flows are considered while designing a barrage. Surface flow considerations mainly govern the crest level, downstream floor length, and minimum depths of U/S and D/S cutoffs. The cost of a barrage largely depends upon the depth of the cutoffs wall, the length of the floor, and its thickness, which is governed by subsurface flow conditions; in this study, reducing the cost of the barrage by reducing the quantity of construction materials in addition to reducing

seepage flow beneath the foundation as objective functions of the optimization problem.

## 1.2 Problem of the Present Research

The serious problem with hydraulic structures such as barrages laid on gypseous soils is seepage beneath the structure site through such soil. Gypseous soil contain of gypsum salt which is a sulphatic acid soluble salt. At natural moisture content, gypseous soils can withstand a heavy load but with only a little amount of compression or deformation. When wetting presents, such as in the seepage of water beneath a hydraulic structure, a reduction in soil volume occurs due to dissolved salt causing soil collapse.

## 1.3 Aim and Objectives

The aim of the research is to determine the optimum hydraulic design for a barrage profile with the presence of collapsible soil, specifically gypsiferous soil on the foundation of a hydraulic structure, and on the overall barrage performance.

## 1.4 Methodology of The Present Study

1. Preliminary investigation and identification of the soil sampling location.
2. Conduct laboratory tests for soil samples under consideration by preparing samples of manufactured gypsiferous soil, then conducting laboratory tests for hydro-mechanical properties including permeability leaching tests, and shear strength properties.
3. In order to face the pose of the gypsiferous soil in the foundation of a barrage, an optimal hydraulic design approach is considered. This approach targets to minimize the construction material required and reduce the seepage flow underneath the foundation of the structure.
4. Addressing the challenge of achieving optimal design for a barrage by using the genetic algorithm method to solve the multi-objective optimization problem. The solutions generated will be presented in the

form of design charts and tables, in order to facilitate visualization and understanding of the optimal design options. As well as, predicting the optimal hydraulic design of the barrage profiles and seepage control measures. This will develop a comprehensive and effective solution that can be applied to the design of similar structures.

## 1.5 Assumption and Limitation of the Present Study

1. Design of hypothetical barrage laid on gypsiferous soil based on subsurface flow considerations.
2. The soil foundation beneath barrage floor contains gypsiferous soil of higher gypsum content in this study (i.e., $\chi$=35%).
3. The soil foundation beneath barrage floor is saturated and isotropic ($K_y/K_x$ =1).
4. Analyses of steady state seepage using SEEP/W 2D for fully closed gates conditions were the boundary condition in U/S equal to high flood head ($H_{F.h}$).
5. The high flood head in this study is equal to 8.10 m, which the maximum flood head for the barrages that constructed on the Euphrates River from Al-Hindiya downstream.
6. The dimensions of the barrage were investigated by surveying the barrages profiles constructed on the Euphrates River in Iraq from Al-Hindiya Barrage to Abu-Sukhair Barrage, including four barrages (Al-hindiya, Al-kufa, AL-Shamiya, and Abu-Sukhair).
7. The analyses of the seepage problem were done in non-dimensionlized form. In which all the design variables are put in normalization form by dividing all dimensions of the design variable on high flood head ($H_{F.h}$).

# CHAPTER TWO

# REVIEW OF LITERATURES

## 2.1 Challenges of Problematic Soils

Problematic or collapsible soils were extensively investigated due to their riskness consequences. According to Ayadat and Hanna, (2005), it was defined as any unsaturated soil that goes through a radical rearrangement of particles associated with significant volume loss upon wetting with or without additional loading. Collapsible soil layers are widely distributed around the world. Gypseous soil is considered a widely spread type of collapsible soil particularly in Iraq. In which exhibits high volume change during wetting and drying cycles. The gypsum content in such soils are sulphatic acid-soluble salts and a member of the evaporates family; it is typically a sedimentary common mineral and is associated with sandstone, shales, and carbonate rocks (Nashat, 1990). Gypsum is a mineral and rock is a soluble salt widely distributed in sedimentary rocks of various geologic formations with different ages. Its composition is calcium sulfate, and its chemical symbol is $CaSO_4.2H_2O$. Gypseous soils can support a heavy load in their natural moisture content with only a tiny amount of compression or deformation. Still, when wetting occurs, such as in the seepage of water beneath a hydraulic structure, the soil problem appears to become more complex; they significantly reduce volume because soluble salt leads to increased cavity and sinkhole and collapse of the soil.

James and Kirkpatrick, (1980) stated that ″dissolution of soluble materials can constitute a risk in terms of potential settlements and leakage paths within the foundations of dams″. Soil containing sufficient quantities of gypsum that influence on their engineering properties is considered gypseous

soil (Majeed, 2000). A classification of gypseous soil according to its gypsum content was introduced by Barzanji, (1973) as given in table (2.1).

Table (2.1): Classification of gypseous soil (after Barazanji, 1973).

| **Gypsum content (%)** | **Classification** |
|---|---|
| ≤ 0.3 | Non-gypseous soil |
| 0.3 - 3 | Very slightly gypseous soils |
| 3 - 10 | Slightly gypseous soils |
| 10 - 25 | Moderately gypseous soils |
| 25 - 50 | Highly gypseous soils |
| ≥ 50 | Gypseous soils with other soil, such as sandy gypseous soil |

Al-Dabbas et al., (2010) gives an engineering classification of gypsiferous soil. This classification depends on soil texture, mineralogy, geochemistry and engineering properties. The study areas are located within the Mesopotamian plain and include four locations, namely, Najaf, Karbala, Falluja and Samarra. Moreover, they classified gypsiferous soils into two groups: gypsiferous soils of low gypsum content of less than 25% and the second one is gypsiferous soils of higher gypsum content of more than 25%, according to their gypsum content and initial void ratio, coefficient of curvature, coefficient of uniformity, the collapse potential, the compressive strength, cohesion, plasticity index, content of fines, and the total dissolve solids (TDS) of the soil water extracts. The proposed classification for gypseous soils can be applied to other locations and be helpful to other soil scientists and engineers. This classification is given in table (2.2).

Table (2.2): Classification of gypseous soil (after Al-Dabbas et al., 2010).

| **Gypsum content (%)** | **0.5-25** | **25-50** |
|---|---|---|
| Class | Gypsiferous soil | Highly gypsiferous soil |
| Initial void ratio | < 0.45 | ≥ 0.45 |
| Coefficient of curvature | < 2.5 | ≥ 2.5 |
| Uniformity coefficient | < 25 | ≥ 25 |
| Collapse potential (%) | < 1.5 | ≥ 1.5 |
| Comp. strength (mN/m2) | < 1 | ≥ 1 |
| Cohesion (kN/m2) | < 15 | ≥ 15 |
| Plasticity Index (%) | < 10 | ≥ 10 |
| Fine-grained soils (%) | < 50 | ≥ 50 |
| Total dissolved salt of soil water (ppm) | < 350 | ≥ 350 |

Gypsum's action as a cementing agent between soil particles as links greatly affects the strength parameters. When the moisture content in the gypsum soil increases, it works to reach the water to the gypsum grains that begin to melt, causing weak cohesion between the soil grains and reducing the value of friction. The process removes materials in solution (e.g., salts) and cementation agent from a section in the soil profile, which is defined as the leaching process. Accordingly, gypseous soils undergo several changes in their characteristics due to the continuous loss in their mass and due to the alteration in properties of the material constituents during leaching (AL-Mufty, 1997).

Fattah et al., (2014) studied the effect of grouting material on gypseous soil characteristics. Four types of gypseous soil were taken from Karbala and AL-Najaf in Iraq. The soils have various features and different gypsum

contents. In this study, undisturbed soil specimens were tested to calculate the compressibility subjected to many conditions; the experimental work included classification tests, physical and chemical tests, and mechanical and direct shear tests. An acrylate liquid was used as grouting material to treat soil specimens. The results showed that the acrylate liquid could decrease the compressibility of the gypseous soil by more than 60–70%; this is attributed to the acrylate liquid film coating the gypsum particles isolating them from wetting. Also, grouting material affected collapse potential in which acrylate liquid leads to decreased collapse potential in treated soil by more than 50–60% compared with untreated soil. For shear strength parameters of the gypseous soil, the treated material is affected by increasing cohesion and decreasing the angle of internal friction.

Yaqoob et al., (2019) studied the properties of gypseous soils and investigated the behavior of such soils under several conditions by making a particular large-scale model leaching system. Three types of soils are natural gypseous soil from Tikrit city, gypsified soil prepared in the lab and artificial gypseous soil. it was found that artificial gypseous soil has low permeability due to decreased void ratio and reduced water flow through the soil. In contrast, natural and gypsified soil has a high increase in permeability during the leaching test. They also observed salt dissolution by measuring (total dissolved salt (TDS), pH, and temperature).

Fattah et al., (2019) performed a leaching study on collapsible gypseous soil from Bahr Al-Najaf in AL-Najaf city in Iraq. The sample was taken from three sites with different gypsum content. The x-ray diffraction techniques (XRD), and scanning electron microscopy (SEM) were studied to analyze the changes in the surface matrix and chemical composition due to the reaction between minerals of gypseous soil and micro-fabrics of soil with gypsum. An

SEM analysis has shown an increase in the total change of voids and cavities for higher gypsum content, and collapse potential increased after the leaching test. The increase ranged between (46-66) % from its value in the natural state. Also, they found that the total dissolved salt (TDS) increased with increasing gypsum content and leaching period.

Obead et al., (2021) made a database that describes the leaching-permeability behavior of collapsible gypseous soil. The data were implemented to develop artificial neural network (ANN) prediction models for predicting permeability coefficients in a saturated state and the percentage of total dissolved salt by weight. The ANNs model has a reliable capability to find predictions with high accuracy where the coefficient of correlation ($R^2$) ranged between 99.99% and 99.93%.

Al-Gharbawi et al. (2021) studied the leaching of treated and untreated gypseous soils from Tikrit city, Iraq, with a gypsum content of 49%. Two types of leaching tests were carried out odometer permeability test and a modified permeability-leaching test on gypseous soil treated with two types of treated materials (magnesium oxide and carbonated magnesium oxide). It was found that these treatments improved the characteristics of gypseous soil and reduce the coefficient of permeability.

Obead et al., (2022) studied the effects of soluble materials on the hydro-mechanical properties of collapsible gypseous soil. A set of laboratory tests were carried out on disturbed gypseous soil samples taken from three sites from Bahr Al-Najaf in AL-Najaf in, Iraq. a laboratory leaching-permeability test was carried out on soil samples, and the results were analyzed to understand the effect of this test on properties of the gypseous soil. The results showed that the leaching test affected the geotechnical properties, which appeared to increase the sand percentage, void ratio, and coefficient of permeability; the

coefficient of permeability increases and tends to be higher because of increases in the dissolution of soluble minerals. At the same time, the gravel percentage, specific gravity, acceptable percentage, and shear strength parameters were shown to be less affected by the leaching test. For shear strength parameters, the leaching process caused a significant reduction in cohesion and a slight decrease in internal friction; this behavior may be attributed to dissolve of cementation bonds between soil particles.

## 2.2 Piping Risk in the Foundation of Hydraulic Structures

Hydraulic structures like dams, weirs, barrages, head regulators, and cross-drainage works are probably having a problem with construction on an impervious solid or permeable rock foundation comprised of collapsible formations. These hydraulic structures are subjected to seepage of water beneath the floor, in addition to all other forces to which exerted the higher seepage forces threaten the stability of the structure and may cause its failure by:

1. Exit gradient and piping: The exit gradient is the hydraulic gradient of the seepage flow under the base of the barrage floor. The rate of seepage increases with the increase in exit gradient, and such an increase would cause ‘boiling’ of surface soil, the soil being washed away by the percolating water. The flow concentrates into the resulting depression thus removing more soil and creating progressive scour backwards (i.e., upstream). This phenomenon is called (piping). The exit gradient as shown in figure (2.1), and according to the creep flow theory proposed by Bligh is:

$$i_{exit} = \frac{H_S}{L} \qquad (2.1)$$

Where $H_s$, the seepage head, is the difference in the water levels upstream and downstream of the barrage. and $L$ is the total creep length equal to ($2d_1+b+2d_2$), in which $d_1$ and $d_2$ being the depths of the upstream and downstream cut-off piles respectively and $b$ the horizontal floor length between the two piles.

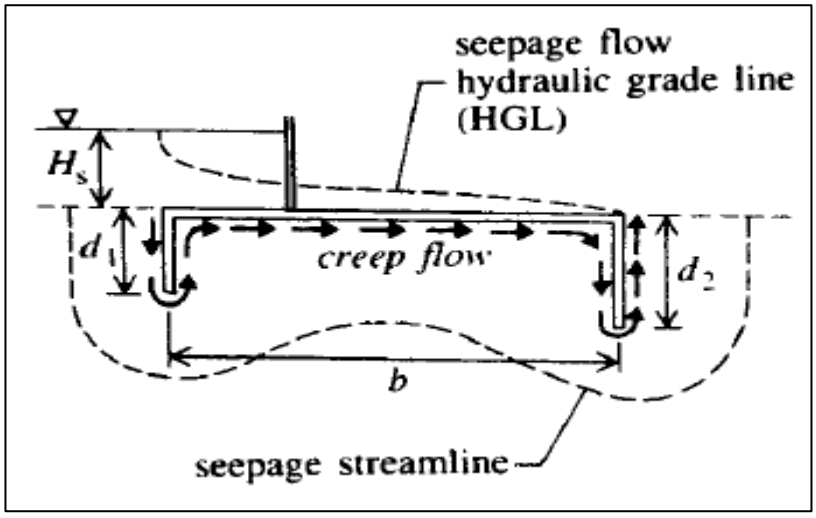


Figure (2.1): Seepage flow hydraulic gradient line (Novak et al., 2008).

The piping phenomenon can be minimized by reducing the exit gradient, i.e., by increasing the creep length. The creep length can be increased by increasing the impervious floor length and by providing upstream and downstream cut-off piles.

2. Direct uplift pressure: The base of the impervious floor is subjected to uplift pressures as the water seeps through below it. The uplift upstream of the weir is balanced by the weight of water standing above the floor in the pond, whereas on the downstream side there may not be any such balancing water weight. The design consideration must assume the worst possible loading conditions, (i.e., when the gates are closed and the downstream side is practically dry).

Numerous researchers investigated the piping phenomena beneath dams, weirs, barrages, and other hydraulic structures. But, the cases of distressed hydraulic structures caused by the solution of gypsum from their foundations were less studied.

Khassaf et al., (2009) studied seepage analysis underneath the weir foundation, Diyala weir was considered a case study. In this research, the effect when one of the sheet piles under the weir was cancelled, the quantity of seepage, pressure head, and exit gradient were calculated using GeoStudio software SEEP/W finite element model. It was found that the Diyala weir is safe against piping and uplift pressure if all parts of the weir were working successfully and the weir foundation and downstream floor problems cracks, and displacement were due to corrosion of the sheet piles especially in upstream.

Mohammed-Ali, (2011) used the finite difference method with a relaxation technique to analyze seepage below the hydraulic structures and show the effect of the middle sheet pile on the uplift pressure under the hydraulic structure. A hydraulic structure was used with horizontal floor and upstream and downstream cutoffs of depths D1, D2 and inserted the middle sheet pile by a depth equal to the depth of the sheet pile in downstream D2 with different distances over the length of the floor and compared all cases with the standard condition. It was concluded that the use of middle sheet pile decreased uplift pressure under the hydraulic structure. This decrease in uplift pressure increased when the distance between the middle sheet pile and the downstream sheet pile decreased.

Obead, (2013) conducted a comprehensive parametric study for the effect of position and inclination angle of the cutoff wall on seepage control in the

foundation of dam structure by using a finite element model for the state seepage condition for the angle of inclination $\beta^{o}$ values ranged between $30^{o}$ to $150^{o}$. The seepage rate behind the inclined cutoff wall, the exit gradient, and the pressure head at key points were determined. It was concluded that when the angle of inclination increased towered the downstream ($\beta > 90^{o}$) the pressure head ratio decreased with $\beta$. Until $\beta$ equal to $120^{o}$, an inclined cutoff wall caused a reduction in exit gradient along the end base of the structure. The seepage discharges behind the dam decreased as the angle of inclination increased, and the minimum value of seepage occurred when $\beta$ value was around $60^{o}$, then the seepage increases rapidly for ($\beta \geq 90^{o}$).

Obead et al., (2014) investigated the influence of drainage holes on the reduction of the impact of uplift pressure on the floor of a concrete dam structure by using the finite element method. In this study, the diameter of the drainage hole d= (15, 20, 25, 30, and 35 cm), the constant head water level upstream (H1= 5 m), and downstream (H2= 0 m). three types of drainage holes (S1, S2, S3), as shown in figure (2.2) were presented to study the effect of longitudinal distance (X) and transverses spacing (S) of drainage holes, S1 at transverses spacing (S=0) and longitudinal distance (X=8 m) from upstream, S2 at transverses distance (S=4 m) and longitudinal distance (X= 8m) from upstream, and S3 at a transverse distance (S= 0) and longitudinal distance (X=10 m) from upstream. The results show that the reduction in the uplift pressure increased as the diameter of the drainage hole increased because of increasing the drainage area, which yields maximum reduction when using two drainage holes of the same longitudinal distance. The effect of transverse spacing (S) is small and effects on the shape of the uplift pressure diagram.

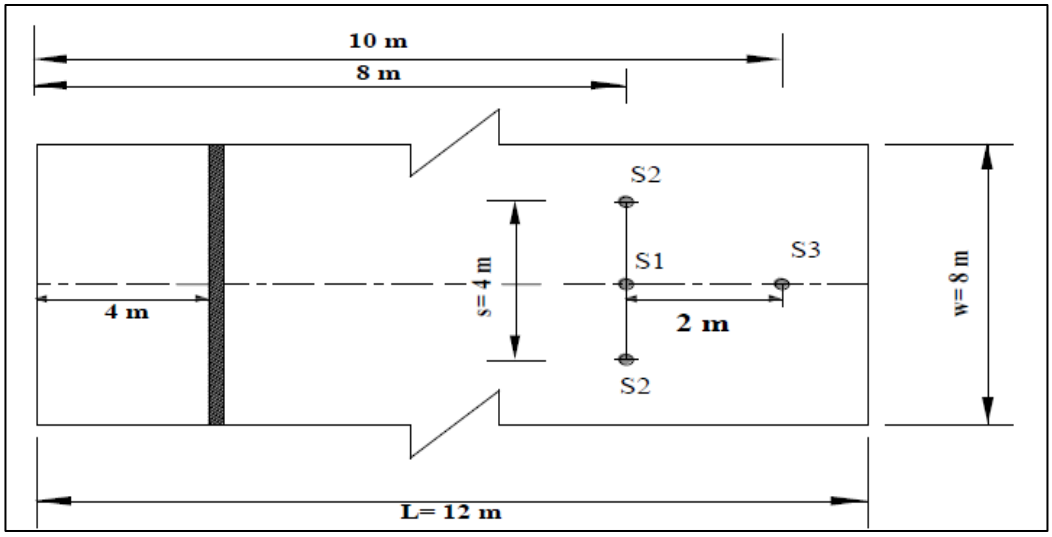


Figure (2.2): plane view of dam structure (Obead et al., 2014).

Nassralla and Rabea, (2015) studied the seepage characteristics in the foundation of hydraulic structures supported by sheet piles in multi-layers soil. In this study, different cases were used (different water heads acting on hydraulic structure, the depth and location of sheet pile, and arrangement of the sub-layer under the floor of the hydraulic structure) to investigate the influence of these cases on seepage flow, uplift pressure, and hydraulic gradient. Experimental tests were conducted by using the sand model, and a numerical solution for the seepage problem was performed by using the finite element method under GeoStudio software via the Seep/W model. It was found that the obtained results show good agreement between experimental and numerical results.

Saleh, (2018) studied the seepage phenomena under a concrete dam with two sheet piles resting on isotropic homogenous soil. A SEEP/W and artificial neural network model has been developed to study seepage flow and exit gradient under a concrete dam. Seven input variables have involved this study, these variables were the depths of upstream and downstream sheet piles L1 and L2 that taken as (8, 6, 4m), head differences (H) were taken as (6, 7, and 8m),

the distance between piles (S) that taken as (5, 10, 15m), the coefficient of permeability (K) that was taken as ($1\times10^{-5}$, $1\times10^{-6}$, and $1\times10^{-7}$m/sec.), and the inclination angle for the upstream and downstream piles with respect to the horizontal direction ($\theta$, $\alpha$) that was taken as ($30^{o}$, $60^{o}$, and $90^{o}$). The overall runs in this research were 2187 for all cases, the seepage rate and exit gradient for each case were estimated. It was found a good agreement between predicted and observed values for seepage rates and exit gradients obtained from ANN and SEEP/W models, that the distance between sheet piles was a more effective variable where the seepage rate and exit gradient decreased when the space between sheet piles was increased. This decreasing ratio was seen more in the exit gradient than the seepage rate for the same cases.

Rasool, (2018) studied the effect of mutual interference pile on seepage properties under hydraulic structures using the finite element program ANSYS. In this research a hydraulic structure of a horizontal floor of length 50 m, the water level upstream and downstream were (4 and 0.5) m, and sheet piles under hydraulic structure at upstream, downstream, and intermediate. The study included many cases for sheet pile depth, and the distance between the upstream and intermediate sheet pile is variable with X= (2, 5, 10, 15, 20, 25, 30, 35, 38). It was found that increasing the distance between sheet piles and the depth of U/S sheet piles reduced the uplift pressure, seepage rate, and exit gradient. The effect of increased depth of the intermediate sheet pile led to increasing uplift pressure at the U/S sheet pile and intermediate sheet pile from the U/S side, reducing the pressure at the intermediate sheet pile from the D/S side and sheet pile in D/S. Increased depth of sheet piles downstream led to increased uplift pressure at sheet piles and reduced the seepage rate and exit gradient.

Salim & Othman, (2021) studied the effect of inclined intermediate sheet piles on seepage, uplift pressure, and exit gradient under hydraulic structure

using the SEEP/W program. This study, at the beginning, was carried out to find the best depth of three sheet pile and the best distance between the three-sheet pile, after using seven angles of incline intermediate sheet pile θ these angles (30°, 45°, 60°, 90°, 120°, 135°, 150°), and three angles (30°, 60°, 90°) for upstream and downstream sheet pile. For each case of run, the quantity of flow rate, uplift pressure, and exit gradient at the toe of the hydraulic structure was determined to develop an empirical equation. It was found that when the depth of three sheet pile increases and the distance between the intermediate sheet pile and downstream sheet pile decreases, the uplift pressure, exit gradient, and flow rate will decrease, and the minimum value of the exit gradient and flow rate when the angle of intermediate sheet pile is 135° and 120° respectively.

From the previous review, major remarks can be drawn,

1. A hydraulic structure such as weir, and concrete dam of horizontal floor, and with control devices such as cut-off walls of different depths, position, and angle of inclination, and drainage holes were studied using finite element program.
2. Different cases for sheet pile depth, distance, angle of inclination, drainage hole diameters, and position of these holes were studied to find its effects on the seepage properties beneath the hydraulic structure, were many cases had a good effect in decreasing seepage flow, uplift pressure, and exit gradient.
3. All the studies were done for hydraulic structure laid on permeable foundation free from gypseous soil.

## 2.3 Optimization based Hydraulic Design of Hydraulic Structure

Optimization is a problem or solution procedure that aims to find the optimal solutions to the objective function. optimization can be defined as the

process of finding the conditions that give the maximum or minimum value of a function. Modern optimization methods have emerged as powerful and popular methods for solving complex engineering optimization problems in recent years. It is also sometimes called nontraditional optimization methods (Rao, 2009). These methods include genetic algorithms (GA), simulated annealing, ant colony optimization, neural network-based optimization, particle swarm optimization, and fuzzy optimization. GA is the most popular evolutionary algorithm used in the design optimization community. Genetic algorithms are applied to a variety of optimization problems that are not well suited for standard optimization algorithms, including problems in which the objective function is discontinuous, non-differentiable, stochastic, or highly nonlinear (Haestad et al. 2003). Many researchers used GA to find the optimal design of hydraulic structures such as weirs, and barrages. The optimal design of the barrages is one of the important issues along with water storage, diversions, and flood mitigation (Singh, 2011).

Garg et al., (2002) Studied the optimization problem to determine an optimal profile of a barrage consisting typically of minimizing the cost of construction volume, earthwork, cut-off walls, and impervious floor length.

Singh, (2011) studied the optimization problem for minimizing the total cost of construction of the barrage by using the genetic algorithm method, classical optimization technique, and conventional method. Seepage analysis for subsurface flow was found by using Kaslo method. The overall objective of the optimization problem consists of minimizing the total cost of the construction of the barrage consisting of concrete floor, the depth of sheet piles in U/S and D/S, and the number of earthworks in excavation and filling, and the constraints is that the uplift pressures must be balanced by a suitable thickness of floor at different key points along the floor length of the barrage,

the depth of sheet piles, and the length of the floor be such that the exit gradients is within the safe exit gradient (SEG) limit. From the results of this study, the solution of optimization problems by classical and conventional methods are costlier than solving them by genetic algorithm method where the cost reduction by GA is about 16.73% from conventional method.

Hassan, (2015) studied the optimal hydraulic design of a barrage using a genetic algorithm. The optimization problem involves minimizing the barrage's overall cost in addition to ensuring safety against the flow conditions-induced failure of the structure. The objective function included optimizing maximum permissible afflux (m), Gated spillway span (m), depth of the upstream sheet-pile (m), depth of the downstream sheet-pile(m), and impervious floor length (m). The optimization model was solved by genetic algorithm, and compare the results by solving the model by the conventional method. The result showed that the genetic algorithm minimized the overall cost of the barrage; the cost reduction was 20.103% from the cost obtained by the conventional method. It was found that flood discharge has the most significant effect on the total cost followed by seepage head value as a hydrological parameter.

Hassan, (2019) carried out an optimization-based solution for the problem of finding the optimal angle of inclination, and the cutoff location in the floor of the barrages. The finite element method used SEEP2D GMS software with genetic algorithm technique was studied. This study uses a hydraulic structure with a cutoff wall of inclined angle (θ) and the cutoff depth (d), length of impervious floor (b), and depth of the foundation soil layer (T) with various anisotropic ratios. Regression non-linear models were used to predict exit gradient and uplift pressure for different degrees of inclination (θ), relative location (b1/ b) from U/S, and relative depth (d/b). The result obtained

by this study showed that the optimum cutoff relative locations and angles of inclination were affected by changing the anisotropic ratio and relative cutoff depth.

Hassan et al., (2022) developed a GA-FEM model to determine the optimal design of the hydraulic structure. The genetic algorithm model and finite element program were proposed in this study to find the optimum depth and location of the cutoff. Also, the effect of anisotropic ratio and coefficient of permeability of soil foundation under hydraulic structure were investigated. It was found that the developed model was more economical, efficient, and safe in the design of hydraulic cutoff walls.

## 2.4 Summary

From the introduced review of literatures, analyses of the steady state seepage problem were conducted to find the optimal design of the barrage structures that laid on permeable foundation free from gypseous soil. In this study analyses and design of a barrage laid on permeable foundation contain gypsiferous soil. An optimal hydraulic design of the barrages is regarded in this study for the case of the presence of gypsiferous soil in the foundation by minimizing the volume of construction material for the barrage structure and seepage flow beneath the foundation. The selection of this study was the actual need to find the effects of such soils on hydraulic structures like barrages; where many of these structures are constructed on such types of soils. The existence of collapsible soil in the foundation of the hydraulic structure will affect the hydro-mechanical behaviors of the foundation layers, and the hydraulic functions of seepage flow beneath hydraulic structures.

# CHAPTER THREE

# EXPERIMENTAL WORKS

## 3.1 Description of the Study Area

The study area is located on the banks of the Euphrates River about one kilometer from Al-Kifl Bridge, in Babil province, Iraq as shown in figure (3.1). This district is situated between the Babylon, Al-Najaf, and Karbala cities in middle Iraq along the Euphrates River. The geographic coordinates are extended from longitudes 44°21′29.4″ to 44°36′34″ East, and latitudes from 32°32′13.7″ to 32°22′11 North, the average elevation of the land in the area by using GPS is about 30 m above mean sea level. Table (3.1) shows the summary of locations, depths and coordinates of the extracted soil samples.

Table (3.1): Summary for locations, depths and coordinates for samples of natural soil.

| Soil Samples | Location | Depth of Soil Sample Pit in (m) | coordinates | |
|---|---|---|---|---|
| | | | Latitude (North) | Longitude (East) |
| $S_1$ | Left bank | 1 | 32°13′7″ | 44°21′49.4″ |
| $S_2$ | | 0.75 | 32°12′34″ | 44°21′55″ |
| $S_3$ | | 0.5 | 32°12′58″ | 44°21′55″ |
| $S_4$ | Right bank | 0.5 | 32°21′22″ | 44°36′50″ |
| $S_5$ | | 1 | 32°20′63″ | 44°36′50″ |
| $S_6$ | | 0.75 | 32°20′11″ | 44°36′34″ |

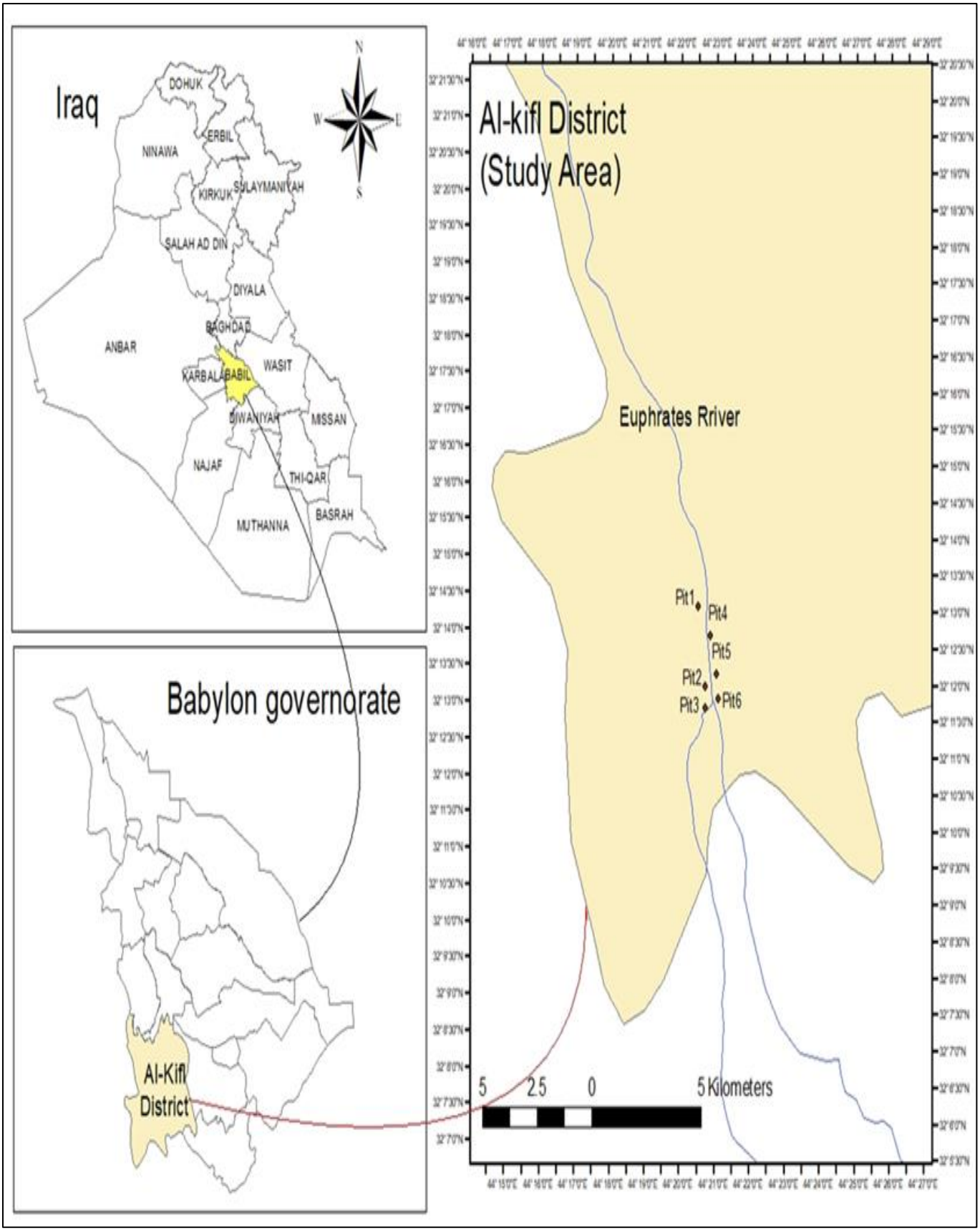


Figure (3.1): Layout of the study area.

## 3.2 Materials and Methods

### 3.2.1 Samples of Natural Soil

Samples of natural soil were taken from the right and left banks of the Euphrates River in the kifl district, six disturbed samples were extracted manually from depths (0.5-1m) below the ground surface to avoid the impurities such as roots, stems of plants, and organic matter. Three samples from each bank were extracted and then packed in double nylon bags to prevent losing their moisture content, after that, the samples were transported to the laboratory of soil mechanics, in Department of Civil Engineering, College of Engineering, University of Babylon.

### 3.2.2 Gypsum Rocks

In order to prepare gypsiferous soil samples, rocks of gypsum were brought from Al-Najaf Al-Ashraf cement factory for cement industries, it weighed about 5 kg as shown in figure (3.2). The sulfate content ($SO_3$) in these rocks was 43.29%, therefore, the gypsum content was up to 93.07%.

Figure (3.2): Crushed gypsum rocks used in this study.

The following section describes the experimental tests, apparatus and procedures that were used in this study. The test procedures of the basic tests are presented in the flowchart shown by figure (3.3).

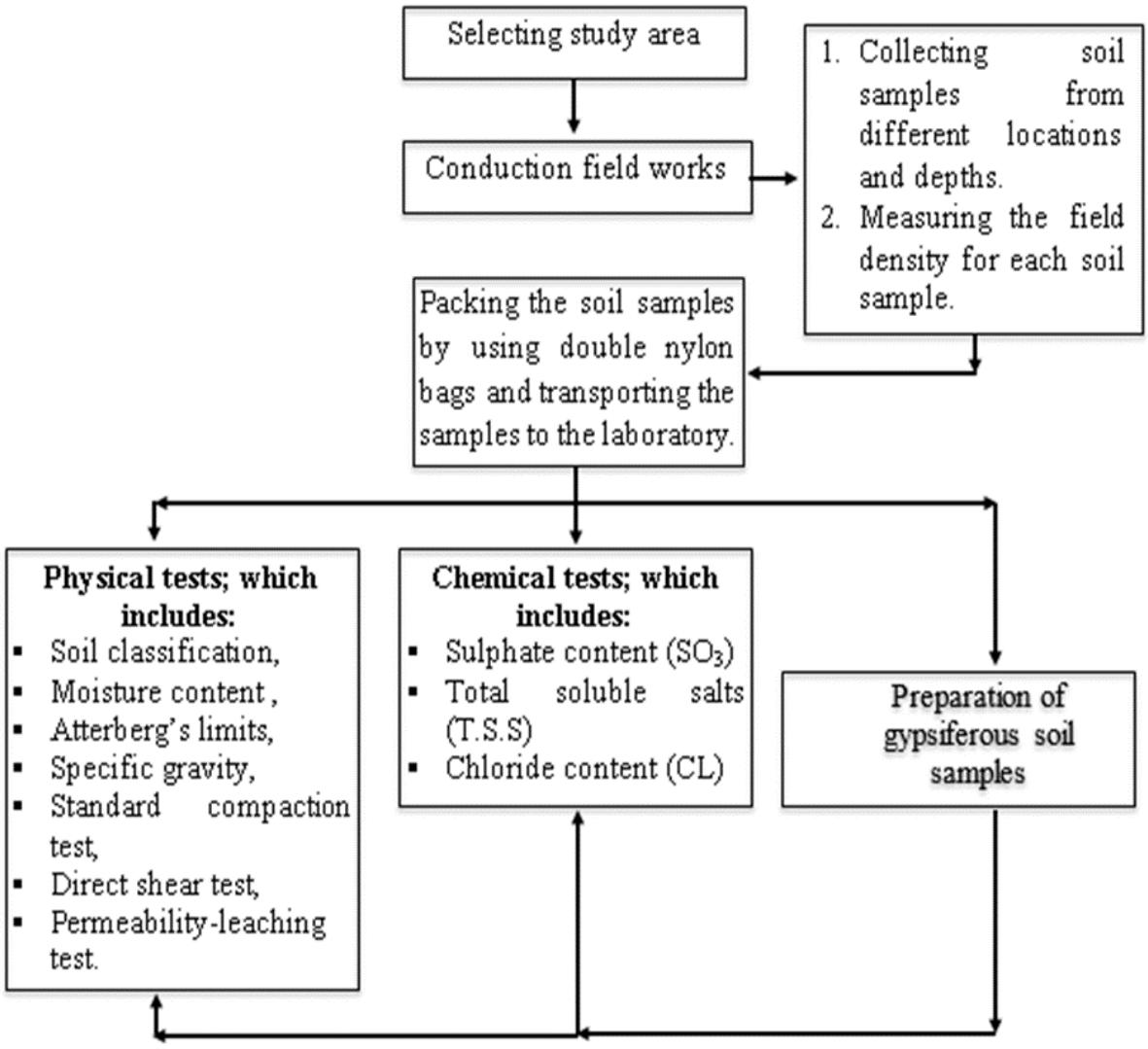


Figure (3.3): Methodology of the basic tests conducted in this study.

## 3.3 Classification Tests for Natural Soil Samples

### 3.3.1 Physical Tests

The Physical properties such as field density, moisture content, specific gravity, particle size distribution, Atterberg's limits (liquid limit and plastic limit), and compaction properties were investigated for the soil samples.

#### 3.3.1.1 Field Density

The field density for samples of soil in their natural (in situ) state was conducted according to BS 1377-9:1990 standard (British standard, 1999)as shown in figure (3.4).

Figure (3.4): In situ field density test by using core device.

### 3.3.1.2 Grain Size Distribution

The grain size distributions were carried out in accordance with ASTM D1140 (2017) specification via the wet sieving method, and the classification of soil was under the unified soil classification system USCS, figure (3.5) shows the experimental laboratory work.


Figure (3.5): Experimental laboratory work for wet sieving method and hydrometer.

Six soil samples were analysed by sieve analyses wet method. The properties, and the classification of the soil samples are the same and their percentage of fine are very closer, so, sample 1 of depth was selected for the

purpose of preparing gypsiferous soil samples. The experimental laboratory works for wet sieving method were done by washing soil samples on sieve No. 200. The percent of passing for the selected sample from sieve No. 200 was 89.3 % and the remaining was 10.7 %. Figure (3.6) shows the particle size distribution curve for soil sample S1.

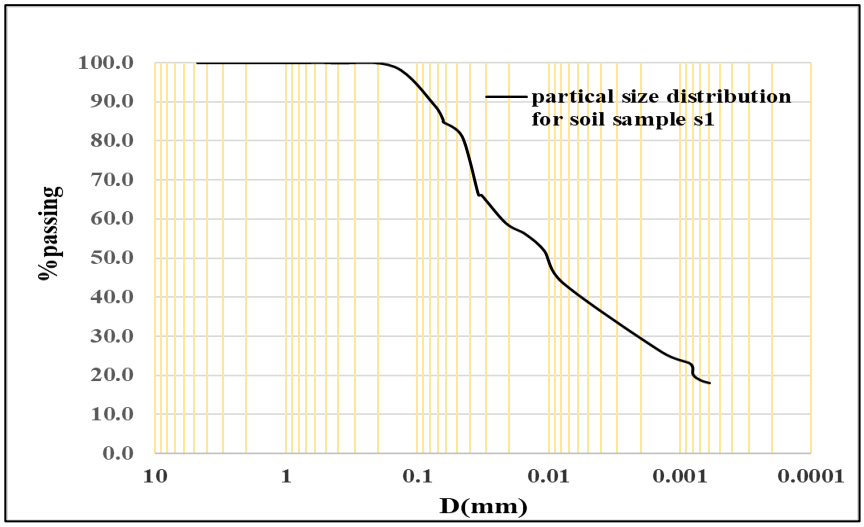


Figure (3.6): particle size distribution for soil sample $S_1$.

### 3.3.1.3 Water Content of Soil Samples

The initial water content for natural soil sample was determined by oven drying test in accordance with ASTM D 2216 (2010) specifications. In this study, a standard drying temperature to dry samples were ranged between 105°C to 110°C for a duration of 24 hours.

### 3.3.1.4 Atterberg's limits

The Atterberg's limits were measured according to the method presented by ASTM D 4318 (2010) specifications. However, the soil samples were detected to have a low plastic behavior.

### 3.3.1.5 Specific Gravity

The specific gravity for the soil under consideration was measured by using ASTM D 854 (2010) standards. A pycnometer test with distilled water was used in this study for specific gravity determination. Figure (3.7) shows the specific gravity test.

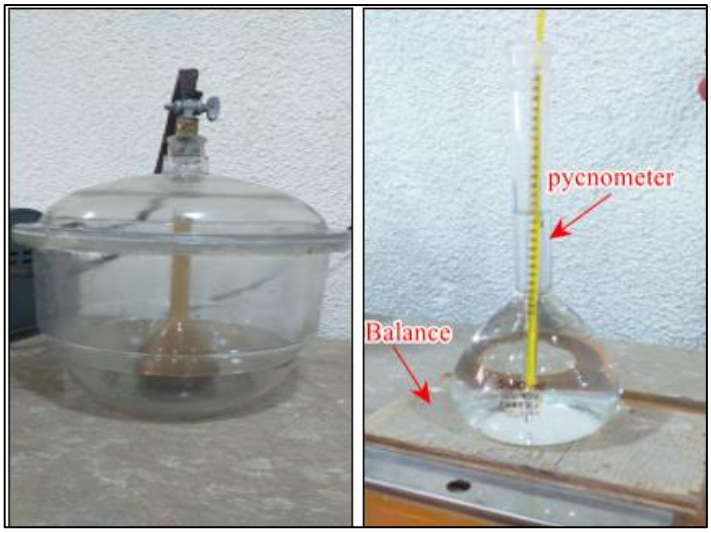


Figure (3.7): specific gravity apparatus.

The summary of physical properties and classification characteristics tests are shown in table (3.1).

Table (3.2): Summery of physical properties and classification characteristics for the natural soil sample $S_1$.

| | **Physical properties** | | | | |
|---|---|---|---|---|---|
| **Parameter** | **Specific gravity ($G_s$)** | **Wet field density*** **$\rho_w$ ($gm/cm^3$)** | **Dry field Density*** **$\rho_d$ ($gm/cm^3$)** | **Max. dry Density**** **$\rho_{Max.}$ ($gm/cm^3$)** | **Water content $w_c$%** |
| **Value** | 2.63 | 2.117 | 1.577 | 1.670 | 34.25 |

| | **Classification characteristics** | | | | | | | | | |
|---|---|---|---|---|---|---|---|---|---|---|
| **Parameter** | **liquid Limit (L.L.)** | **Plastic Limit (P.L.)** | **Plasticity Index (P.I.)** | **Gravel %** | **Sand %** | **Fine %** | **Silt %** | **Clay %** | **$d_{50}$(mm)** | **Classification USCS** |
| **Value** | 34 | 30 | 4 | 0 | 10.7 | 89.3 | 59.3 | 30 | 0.01 | ML*** |

* The natural water content,
** Corresponding to an optimum moisture content of 19%,
*** Silt soil of low plasticity.

### 3.3.1.6 Standard Compaction Test

A standard test method for laboratory compaction characteristics of soil using modified effort were utilized in this study according to the ASTMD1557 (2012). The results of this test are shown in figure (3.8).

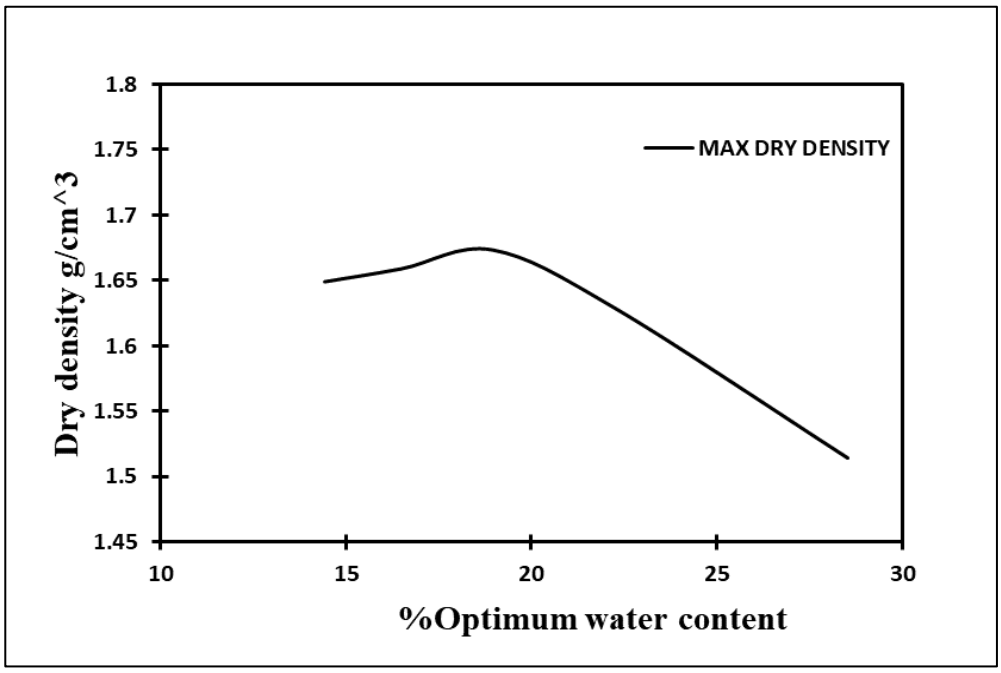


Figure (3.8): Result of standard compaction test for the soil sample $S_1$.

### 3.3.2 Chemical Tests

Chemical properties are measured for the soil in its natural state in the laboratory of sanitary engineering in Civil Engineering Department, College of Engineering, University of Babylon. The tests were done in accordance with British Standards (BS 1377 – 1990). Such tests are including:

1. The total dissolved salts (T.D.S),
2. Sulphate content ($SO_3$) %,
3. Chloride content ($Cl^-$) %,
4. The percentage of gypsum content,

The results of chemical tests are shown in table (3.3), the devices used to measure the gypsum content is shown in figure (3.9).

Table (3.3): Chemical test results for the natural soil samples.

| **$SO_3$ Content (%)** | **Gypsum Content (%)** | **Total dissolved salt (TDS) (ppm)** | **$Cl^-$ Content (%)** |
|---|---|---|---|
| 0.210 | 0.451 | 1.060 | 0.0058 |

Figure (3.9): Apparatus for measuring Sulphate content ($SO_3$) in soil samples.

## 3.4 Preparing Gypsiferous Samples of Soil

In order to prepare the gypsiferous samples of soil, the following steps were followed the method proposed by (Al-Obaidi, 2015), and modified by the author.

1. Free gypsum samples of natural soil were prepared, then dried, weighed, and divided into three soil samples.
2. Each one of the three samples of soil was sieved and separated on sieve No. 200 to split the finer part that passed from that sieve and calculate the percentage of the passed portion.
3. The prescribed percentage of gypsum content that have to add to each soil sample was calculated. The addition percentage are (20%, 25%, and

35% of the total sample weight, but replacement and addition were from the fine part passing through sieve No. 200. These percentages of gypsum content were chosen based on previous studies, which showed that the percentages of gypsum present in the areas along the Euphrates River, starting from AL-Hindia barrage, range within these percentages of gypsum.

4. Preparation of the gypsum powder that has to be mixed with soil sample each according to the prescribed mixing ratio as presented in table (3.4). A rubber hammer was used to crush the big pieces of gypsum rocks manually, then a mechanical crusher was used to complete the crushing process and the resultant mixture was sieved on sieve No.200 to get the fine portion of gypsum crystals before being added to the natural soil. Figure (3.10) shows gypsum powder.
5. The final step is mixing process, which carried out by replacing part of the natural soil (according to the specific weight to produce a soil sample with a specific ratio of gypsum content), the mixing process was continued for a while about 10 minutes to ensure the homogeneity of soil portions.

Table (3.4): The proportion of gypsum in soil samples for manufacturing gypsiferous samples.

| **Soil sample** | **$W_s$[a] (gm)** | **$W_{fine}$[b] (gm)** | **% Fine[c]** | **% Gypsum[c]** | **$W_G$[d] (gm)** | **% Gypsum (from total weight)** |
|---|---|---|---|---|---|---|
| 1 | 3200 | 2180.3 | 68 | 29 | 632.3 | 20 |
| 2 | 3200 | 2202.5 | 69 | 37 | 814.9 | 25 |
| 3 | 3200 | 2250.6 | 70 | 50 | 1125.3 | 35 |

[a] Weight of soil sample,[b] weight of fine in sample,[c] in natural soil sample,[d] weight of gypsum from fine portion of natural soil sample,

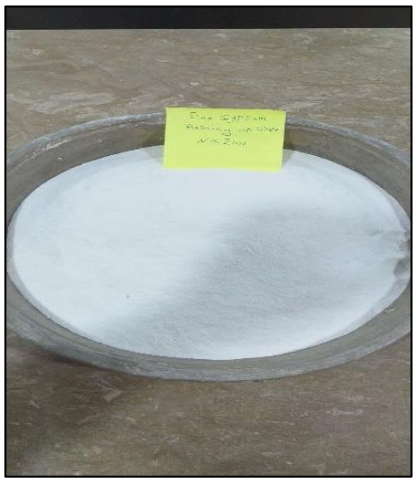

Figure (3.10): Gypsum powder for preparing gypsiferous soil.

## 3.5 Test of Direct Shear

The shear strength parameters (cohesion c, and angle of internal friction ϕ) were obtained by using the direct shear test. In this study, such tests were performed for the soil samples in the natural state, and then the tests were repeated for gypsiferous soil samples for both dry and wet states. The same series of tests were performed after completing the experiments of permeability-leaching. The direct shear test was performed in accordance of ASTM D3080 by using the test device as shown in figure (3.11).


Figure (3.11): Direct shear device.

For the natural soil samples, direct shear tests were performed in the dry and wet states with a soil moisture content of 34.35%. On the other hand, for gypsiferous soils, tests were performed for three samples before the

leaching test in its dry and in the wet state in which the water was added to samples to rise their moisture content to about 34.25 %.

In order to measure the effect of leaching of dissolved minerals, particularly the gypsum material from the soil, a series of direct shear tests were conducted for the gypsiferous samples of soil after carrying out the leaching experiments. The flowchart presented in figure (3.12) shows the steps of this work. The overall results of direct shear tests were shown in table (3.5).

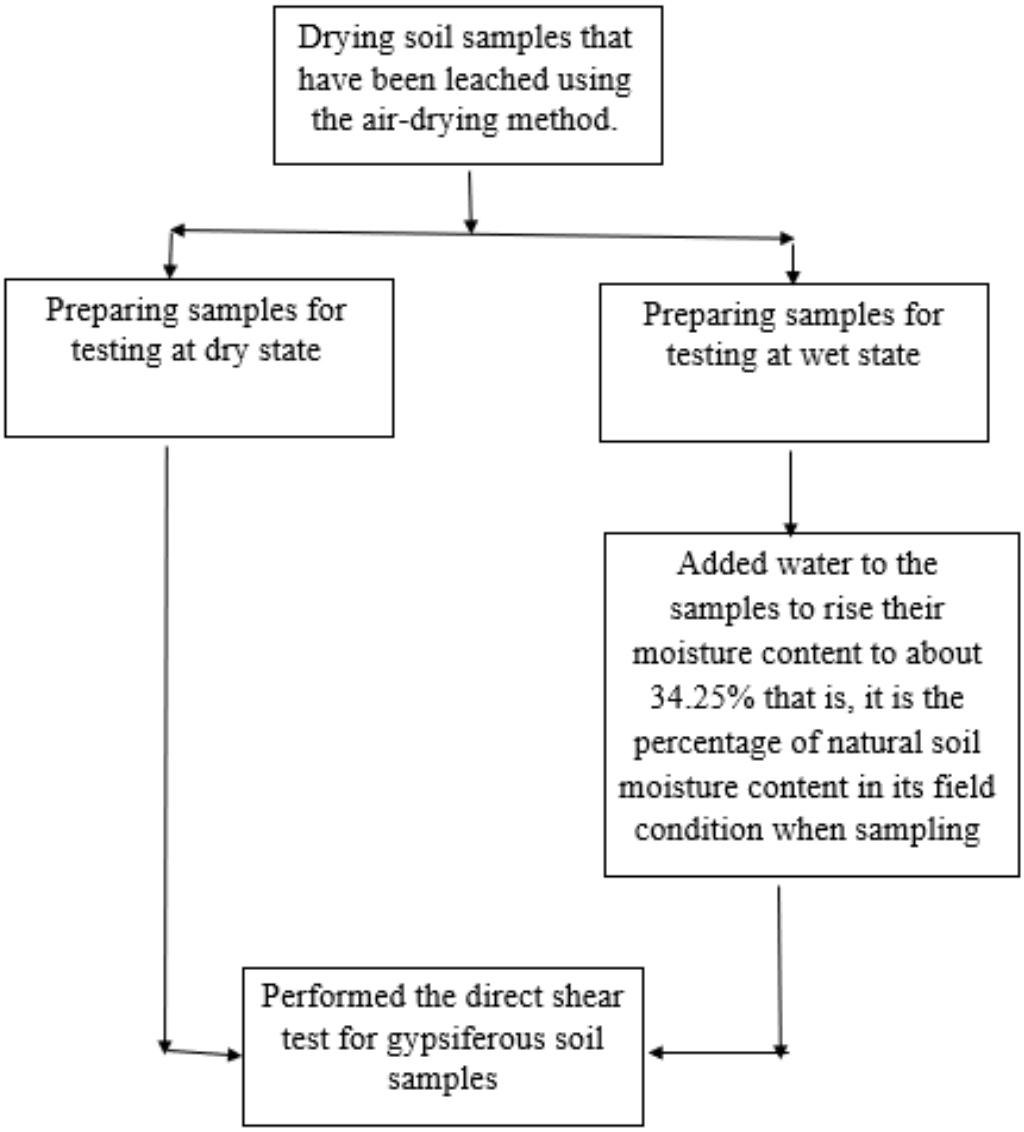


Figure (3.12): Methodology of perform the direct shear test for gypsiferous soil samples after leaching test.

Table (3.5): Summary of direct shear tests for the soil samples in this study.

| | Soil Status | Before Leaching | | After Leaching | |
|---|---|---|---|---|---|
| | Parameter / Soil Type | Cohesion $C$ (kN/m$^2$) | Angle of Internal friction $\phi$ (deg.) | Cohesion $C$ (kN/m$^2$) | Angle of Internal friction $\phi$ (deg.) |
| | Natural | 10.82 | 34.1 | 15.3 | 30.2 |
| Gypsiferous | with $\chi^{**}$=20% (dry) | 28.64 | 31.6 | 12.91 | 44.3 |
| | with $\chi$=20% (wet$^{*}$) | 26.48 | 33.6 | 12.65 | 36.7 |
| | with $\chi$=25% (dry) | 7.91 | 43.3 | 11.96 | 43.8 |
| | with $\chi$=25% (wet) | 10.07 | 40.1 | 14.32 | 39.7 |
| | with $\chi$=35% (dry) | 4.71 | 44.2 | 10.26 | 43.7 |
| | with $\chi$=35% (wet) | 20.82 | 37.6 | 7.42 | 40.7 |

$^{*}$ At the moisture content of the natural soil.
$^{**}$ gypsum content

From the results of table (3.5), it was evident that in the case before the leaching test and for gypsiferous soils at a dry state, the cohesion increases for the soil sample with 20% gypsum content by 62% from cohesion of natural soil (free from gypsum), this is because gypsum works as a binding material between soil particles; then cohesion starts of decreasing for soil samples with gypsum content of 25% and 35%, and this is because when this percentage of gypsum content is exceeded, acts as a material that separates soil grains and ruptures the bonds, which loosens the soil structure.

Also, before the leaching test, in the wet state, the cohesion slightly decreased for the soil sample with a gypsum content of 20% due to the wetting causing the dissolution of some gypsum salt resulting in a decrease in cohesion between soil particles. But; for soil samples with 25% and 35% gypsum content, the wetting led to increased cohesion due to increased binding material between soil particles. The cohesion for soil samples after

the leaching test in dry and wet states decreases with increasing gypsum content. This is because the dissolution of some gypsum particles during the leaching test decreases the binding between soil particles.

The angle of internal friction for gypsiferous soils at dry state before leaching increases for gypsiferous soil samples because of increasing the friction between soil and gypsum particles and between gypsum particles themselves.

While at wet state, the angle of internal friction increases for soil samples with gypsum content of 20%, and this result is due to the different factors that influence shear strength parameters; according to Sa'eed, (2006) the important factors affecting shear strength are the mineral composition of the granules, the shape, size, and distribution of the granules, void ratio and moisture content, stress change during the sample preparation process, and test method. The reason for this result was probably attributed to the non-uniformity in the preparation of soil samples for direct shear tests; this was real as the mixing procedure was carried out manually. For soil samples with 25% and 35% gypsum content, the angle of internal friction decreases as gypsum content increases due to the wetting effects which cause the dissolution of gypsum particles.

The angle of internal friction $\phi$ was increased after the leaching test and these results indicated that not all of the gypsum in the soil sample was leached. This was evidenced by a decrease in total dissolved salt (TDS) in the leachate samples, which did not reach the TDS of the tap water used. It can be inferred that a certain amount of gypsum remained undissolved. If the leaching period is extended beyond 10 days, more free gypsum salt likely dissolved, leading to a reduction in the angle of internal friction. Peterukhin and Arakelyan, (1985)**,** and AL-Obaidi, (2003) showed the same result on gypseous sandy soil and clayey sand soil respectively.

## 3.6 Permeability – Leaching Tests

In this study, the falling head test was used to measure the coefficient of permeability of gypsiferous samples of soil. The falling head permeameter as shown in figure (3.14) was used to conduct the experiments by permitting water to infiltrate into the soil sample from a standpipe that was connected to the device cylinder. The diameter of the standpipe depends on the permeability of the tested soil. Before starting the flow measurements, the soil sample was saturated, and the standpipes were filled with water to a specified level. The test was then started by closing the water valve and allowing water to flow through the soil sample until the water in the standpipe reached the desired lower limit. The time required for the water in the standpipe to drop from the upper to the lower level was recorded. The standpipe was refilled, and the test was repeated several times (Irshayyid, 2015). figure (3.13) shows the permeameter cell for the falling head test.

Figure (3.13): permeameter cell for falling head test.

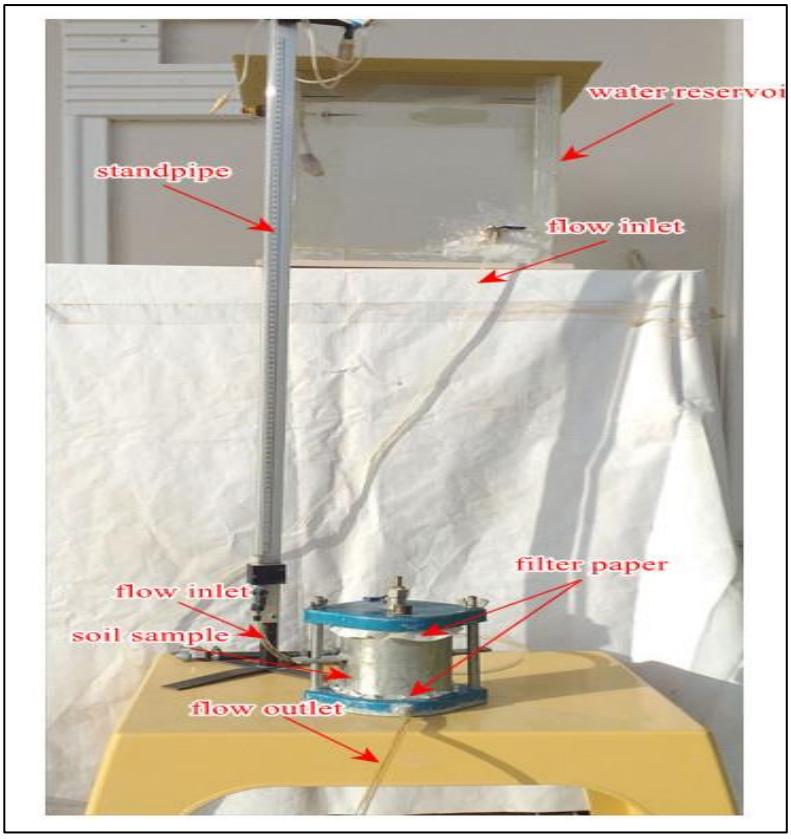


Figure (3.14): The falling head permeameter.

The formula for determining the coefficient of permeability of the soil can be expressed as:

$$K = 2.3\left(\frac{a \times L}{A \times t}\right) \log_{10}\left(\frac{h_1}{h_2}\right) \qquad (3.1)$$

Where;

K= coefficient of permeability in (L/T),

a = the cross-section of the standpipe ($L^2$).

L = height of the soil sample column(L).

A = soil sample cross-section ($L^2$).

t = time for the water to infiltrate through the sample (T).

$h_1$and $h_2$ = upper and lower water levels in the standpipe measured using the same water head reference (L).

A leaching test was conducted for gypsiferous soil samples by using a flowing tap water with total dissolved salt TDS of about 800 ppm (on average) through soils with hydraulic gradient of 9.69. The sample diameter

was (10 cm), and its height was (13cm). The leachate's total dissolved salt (TDS) was monitored twice daily every 12 hours by a portable, digital TDS meter. The leaching test started by closing the water supply valve for the sample and allowing water in the standpipe to flow through the sample until the water in the standpipe reached a given lower limit. At the beginning of the leaching test, the soil sample was soaked for 24 hours then the standpipes were filled with de-aired water to a pre-specified level.

The required period for the leachate water in the standpipe to drop down level was recorded. Then, the standpipe was refilled with water, and the test is repeated twice a period. The soil sample was installed in the permeameter cell in layers with compaction by a rubber hammer to reach the required field dry density. The leaching test procedure measured the permeability, TDS., EC., and temperature of leachate water and the quantity of leachate water collected and measured. The present leaching test procedure was performed by following the method described by Ismael, (1993), and (Fattah et al., 2019).The leaching process was terminated when the reading of T.D.S. values exhibited no further decrease. The leaching period was ten days for each tested soil sample. Figures 3.15, and 3.16 show TDS apparatus, and EC apparatus that used in leaching test process.

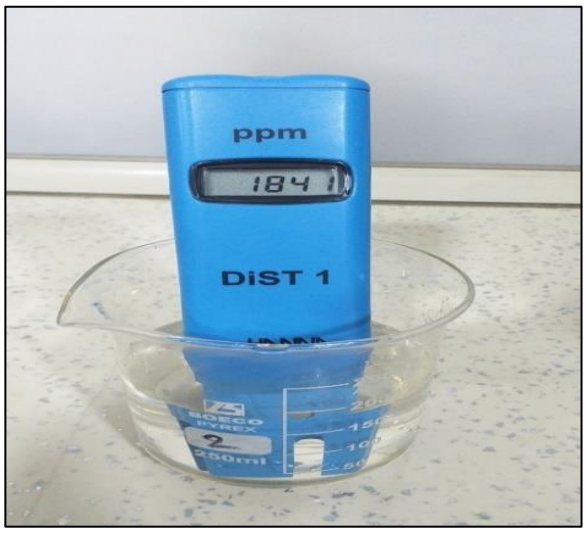


Figure (3.15): TDS apparatus.


Figure (3.16): EC apparatus.

### 3.6.1 Effect of Leaching on the Permeability of Soil

The variation of the coefficient of permeability versus time for different gypsum contents is shown in figure (3.17).

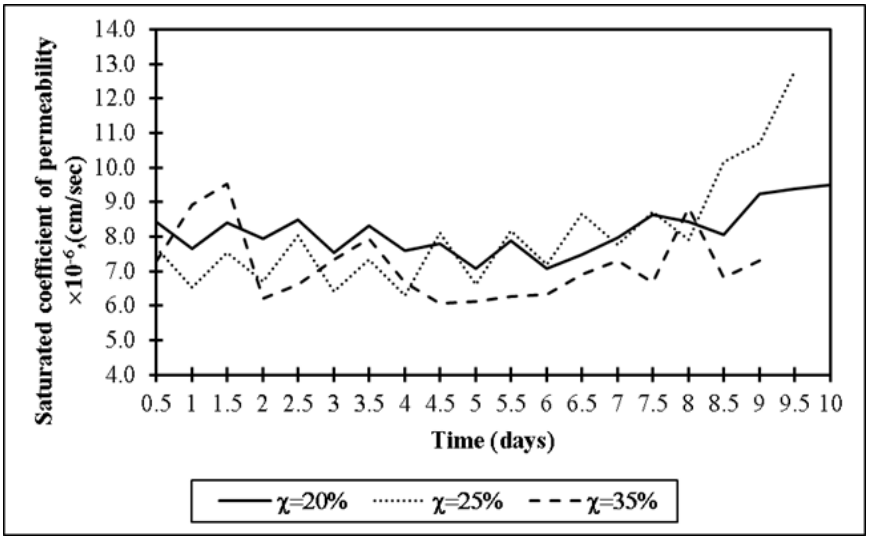


Figure (3.17): Variation of saturated permeability coefficient with leaching time for different gypsum content in soil samples.

As shown in figure (3.17), the range of changes in the coefficient of permeability shows very little change between soils, and it ranges from about $6.0\times 10^{-6}$ to $12\times10^{-6}$ cm/sec for all tested soil samples. In the soil samples with gypsum content of 20% and 25%, the permeability fluctuated in leached period for 8 days. The permeability of the soil sample with gypsum content of 25% increased sharply for the rest of the leaching period (10 days) when (TDS) reading didn't give any change. On the other hand, in the soil sample with gypsum content of 35%, the coefficient of permeability abruptly

increased and decreased for the first four days of the leaching process, followed by reduction until the end of the leached period at the 9th day; this behavior was attributed to the reduction in the void ratio as a result of collapse soil during the leaching process. The variations of TDS with leaching time are displayed in figure (3.18).

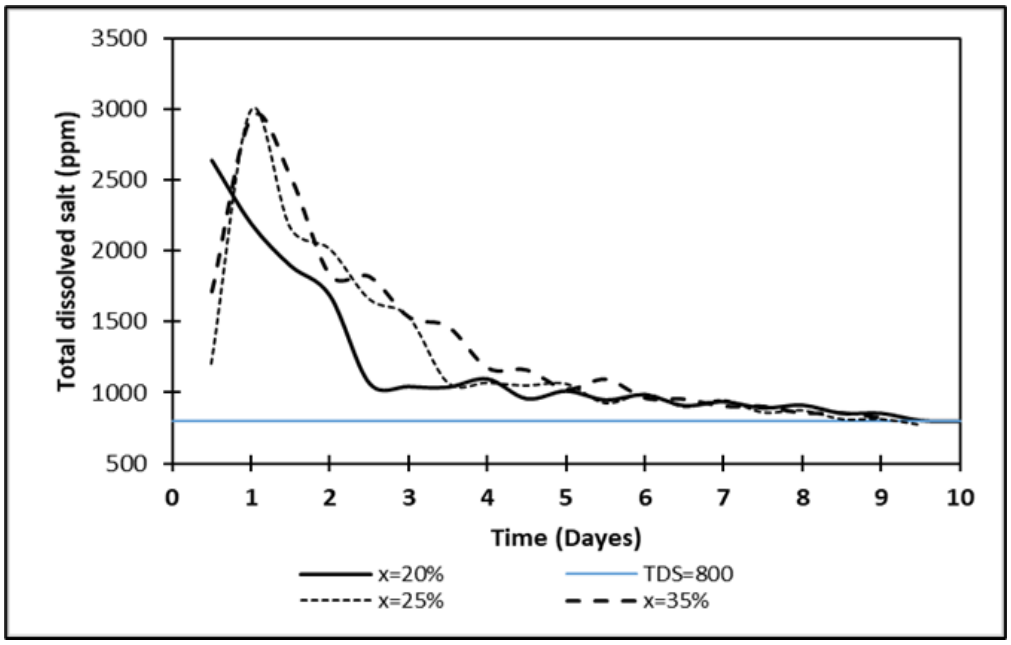


Figure (3.18): Variation of concentration of total dissolved salts of gypsiferous soils with leaching time.

Obviously, for soil samples of higher gypsum content of 25% and 35%, the dissolution of total salts increased rapidly at the beginning; after that, the dissolution of total dissolved salts decreased and then became rather constant throughout the rest of the leaching period. For the soil sample with a gypsum content of 20%, the dissolution of total salts at the beginning of leaching is higher than the soil samples with higher gypsum content. This reason is due to non-homogeneity in preparing this sample for the leaching test being artificial soil; its properties cannot be controlled.

To detect the correlation between the coefficient of saturated permeability and the gypsum content in soil samples implicitly relevant

through the concentration of total dissolved salts, a scatter plot was presented in figure (3.19).

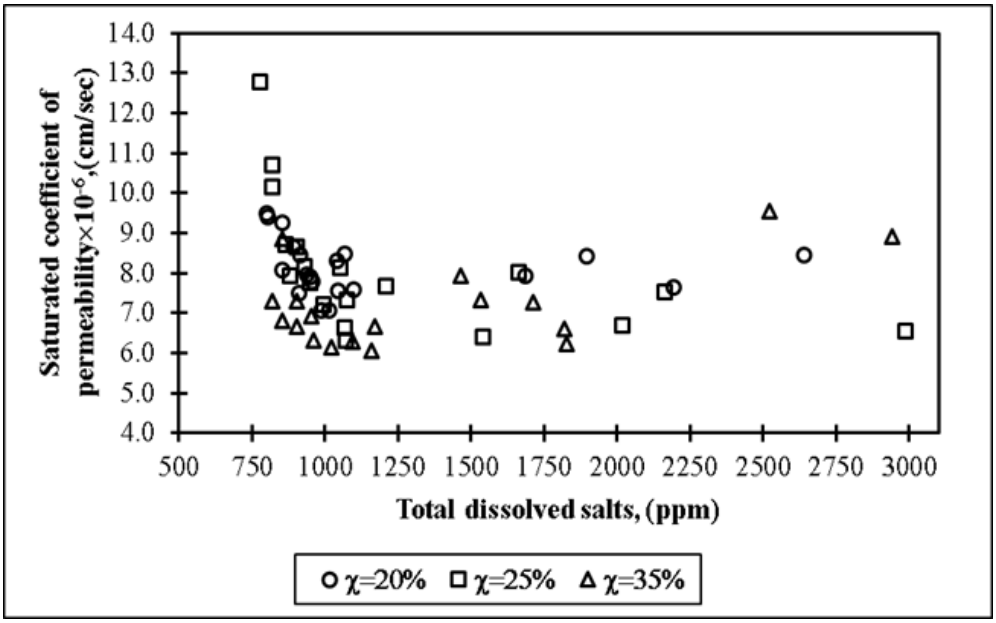


Figure (3.19): Scatter plot for the coefficient of permeability versus the concentration of total dissolved salts for gypsiferous soils.

It was evident that when the initial gypsum content increased in the soil sample, the permeability of the soil increased as the gypsum salt was leached progressively due to the dissolution in the flowing water, leading to increased permeability. This was attributed to the development of voids within soil mass, permitting more volume of infiltrated water under the exerted hydraulic head.

## 3.6.2 Influence of the Leaching Process on the Shear Strength Parameters

The evaluation of the leaching on the strength parameters of the gypsiferous soils was obtained by using relative difference ($R_D$) as:

$$R_D = \frac{X_{ref.} - X_{measured}}{X_{ref.}} \quad (3.2)$$

Where;

$X_{ref.}$ = strength parameter for the natural soil sample (either in dry or in wet status)

$X_{measured}$ =measured strength parameter for the gypsiferous soil sample.

Figures (3.20 and 3.21) show the changes in cohesion C and internal friction ϕ, respectively, at different states of soil samples.

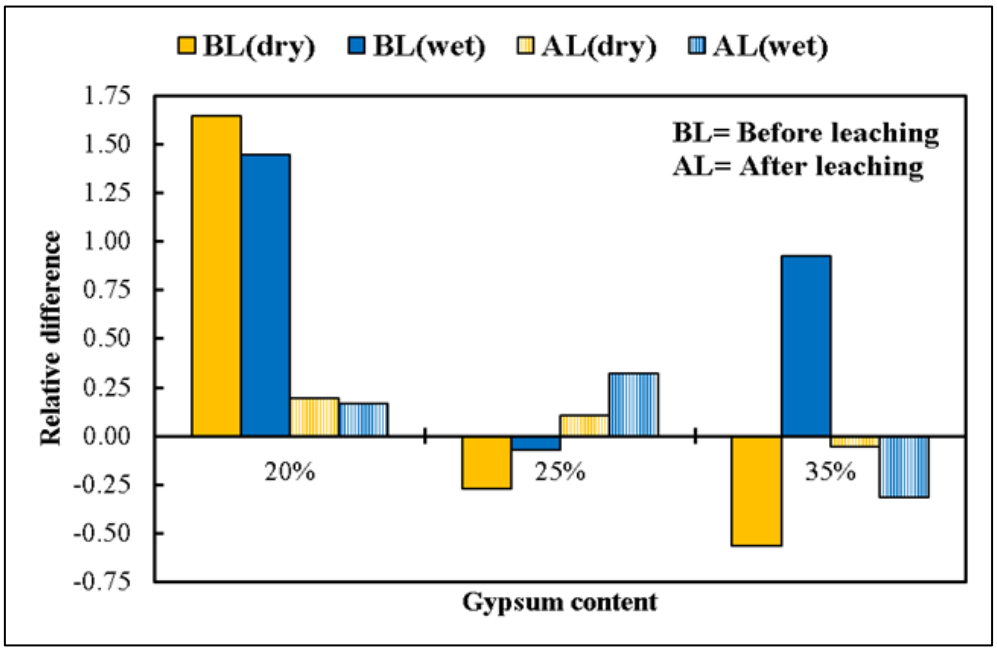


Figure (3.20): Relative difference in soil cohesion versus gypsum content in soil samples for dry and wet states.

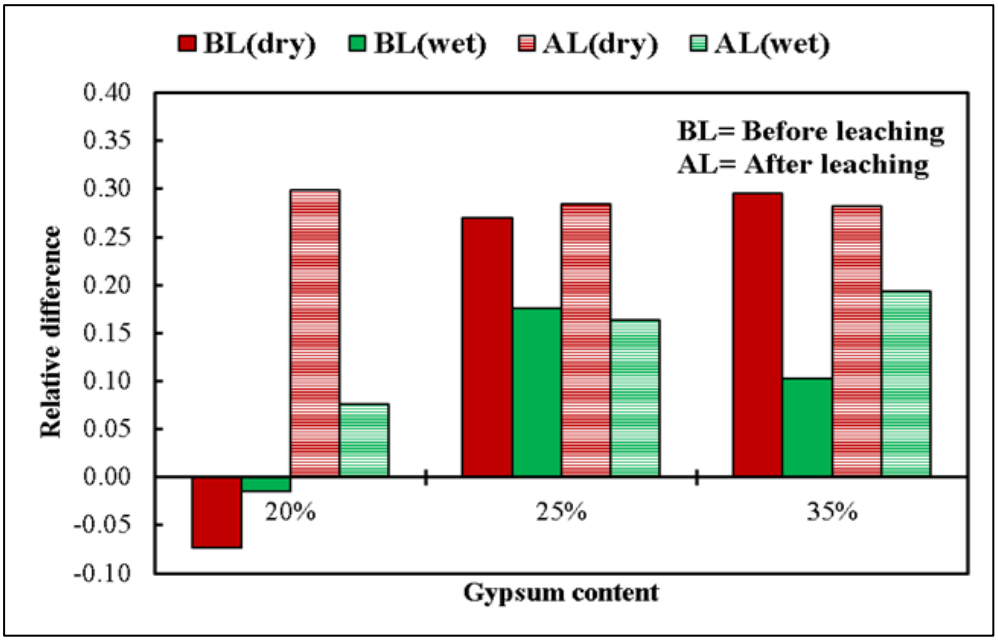


Figure (3.21): Relative difference in internal friction angle versus gypsum content in soil samples for dry and wet states.

As revealed in figure 3.20, a higher increase in soil cohesion occurred before leaching for the gypsiferous soil sample with a gypsum content of 20% in the dry state. At the same time, a significant decrease has occurred for soil samples of 35% gypsum content in the dry state because the increase in gypsum led to separate the bonding material between soil particles.

Furthermore, the results indicated that the gypsiferous soil sample with initial gypsum content of 25% significantly increased cohesion by 32.3 as a percentage of relative deference in the wet state after the leaching that the remaining gypsum in the soil sample after the leaching test was working as a binding material when it dissolved by wetting. In particular, the soil samples with higher initial gypsum content lost significant cohesion after leaching when the gypsiferous soil was at its natural moisture content.

Figure 3.21 shows that for the gypsiferous sample with lower gypsum content (i.e., 20%), the angle of internal friction ($\phi$) reduced slightly than the natural soil for both dry and wet states before leaching. The internal friction for the gypsiferous samples of higher gypsum content of 35% increased for almost all conditions (i.e., dry, wet, before, and after leaching).

# CHAPTER FOUR

# ANALYSIS OF SUBSURFACE FLOW BENEATH BARRAGE

## 4.1 Introduction

The subsurface flow in the foundation of a barrage can be a significant challenge for hydraulic engineers. This flow can cause erosion, instability, and other issues that can compromise the structural integrity of the barrage. Engineers must take into account factors such as soil composition, water flow rate and direction, and other variables when designing and constructing a barrage to ensure that subsurface flow is properly managed. The presence of problematic layers such as gypseous soils that are characterized by their higher solubility when exposed to the flow of water leads to many problems in the foundation of these structures, so anti-seepage measures or control devices must be provided to decrease the seepage flux to a minimum as possible. These control devices are cutoff walls in U/S, D/S, and at intermediate, if needed, protection layers in U/S, and inverted filter layers at D/S of the structure.

## 4.2 Statement of Problem

A typical schematic section of a barrage is shown in figure (4.1). Analysis and design of the hypothetical barrage are carried out based on subsurface flow considerations. However, for a specified profile of the barrage, the subsurface flow in fully closed gates conditions involve protection against piping, uplift, and exit gradient.

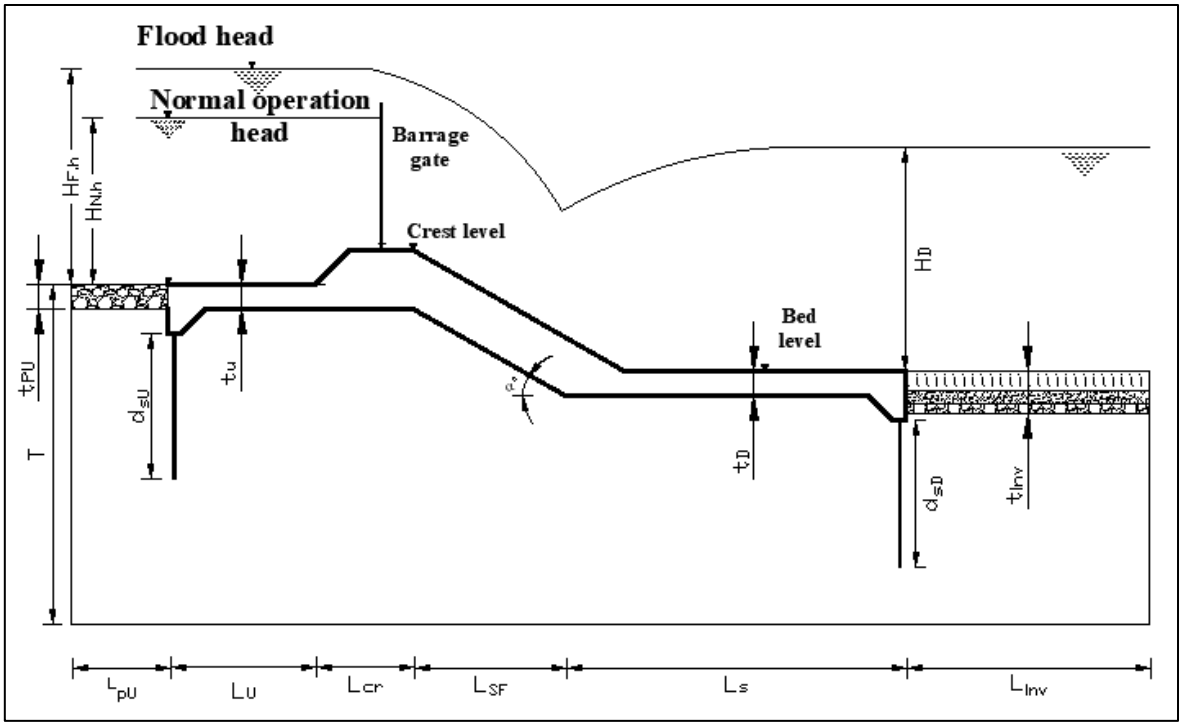


Figure (4.1): A schematic cross-section of the hypothetical case study.

The dimension of barrage components is defined as follows:

$H_{F.h}$ and $H_{N.h}$ are the high flood head and normal operation head (L) in the upstream side of the barrage, respectively.

$H_D$ is the downstream water flood head (L).

$L_{PU}$ is the length of upstream protection (L).

$L_U$ is the length of the upstream floor (L).

$L_{Cr}$ is the length of the crest (L).

$L_{SF}$ is the projection length of the inclined floor (L).

$L_S$ is the length of stilling basin (L).

$L_{Inv}$ is the length of the inverted filter (L).

$t_{PU}$ is the thickness of upstream protection (L).

$t_U$ is the thickness of the upstream floor (L).

$t_{SF}$ is the thickness of the crest (L).

$t_D$ is the thickness of the downstream floor (L).

$t_{inv.}$ is the thickness of the inverted filter (L).

$d_{SU,}$ $d_{SD}$ are the depth of sheet piles in upstream and downstream (L).

α is the angle of the inclined floor of the barrage.

$y_1$, $y_2$ are pre-jump depth and post-jump depth of water(L).

T is the depth of the soil layer beneath the barrage foundation (L).

For unsteady flow conditions, the groundwater flow in porous media for two-dimensional incompressible fluid is governed by the following equation:

$$\frac{\partial}{\partial x}\left(k_{xx}\frac{\partial h}{\partial x}\right)+\frac{\partial}{\partial y}\left(k_{yy}\frac{\partial h}{\partial y}\right)\pm q=\frac{\partial \varphi}{\partial t} \quad (4.1)$$

Where; $h$ is the flow head (L), $x$ and $y$ are the horizontal and vertical directions of flow, $k_{xx,}$ and $k_{yy}$ are the coefficient of permeability in $x$ and $y$ directions, respectively in (L/T), $q$ is the outflow/inflow rate in ($L^3$/T), $\varphi$ is the specific storage coefficient of the porous media ($L^{-1}$).

The steady seepage flow of water through homogeneous soil underneath hydraulic structure may be expressed by:

$$k_{xx}\frac{\partial^2 h}{\partial x^2}+k_{yy}\frac{\partial^2 h}{\partial y^2}\pm q=0 \quad (4.2)$$

## 4.3 Seepage Analysis

The seepage flow expressed by Eq. (4.2) beneath and around the barrage floor is the primary determinant of the structure geometry and dimensions. The boundary between the barrage floor and the flow domain represented by the foundation is the critical failure plane. Hence, inadequate seepage control devices could produce the piping through soil exposed to an extreme hydraulic pressure gradient, which causes fine soil grains to boil off the flow domain at the exit regions consequent to a local excess pressure gradient (Singh, 2011).

The GeoStudio SEEP/W module was used to conduct the numerical solution of the seepage problem by finite element method in this study.

## 4.4 GeoStudio SEEP/W Module

GeoStudio SEEP/W is a powerful software module for analyzing and simulating subsurface water flow and contaminant transport in the subsurface environment. It is a part of the GeoStudio suite, which is a comprehensive suite of geotechnical and geo-environmental engineering software tools. The SEEP/W module offers advanced capabilities for modeling groundwater flow, unsaturated and saturated flow, and heat and mass transport. The user interface is intuitive and user-friendly, making it easy to set up and run models, visualize results, and perform post-processing. One of the key features of the SEEP/W module is its robust numerical solver, which can handle complex geometries and boundary conditions, and produce accurate and reliable results. It also supports various types of finite element and finite difference meshes and can be integrated with other GeoStudio modules for multi-disciplinary analysis. An additional important feature of SEEP/W is its ability to perform sensitivity analysis, uncertainty analysis, and optimization, which can help to identify key parameters and design optimal solutions.

A series of runs of (200) have been conducted in this study for the foundation of the barrage at various dimension configurations. All sections were analyzed for fully closed gates, and isotopic soil.

## 4.5 Governing Parameters of Seepage Problem

The soil parameters were considered in this study as a linear elastic model for soil, the saturated coefficient of permeability for the higher gypsum content gypsiferous sample (i.e., $\chi$=35%), the material of the model, and the isotropic characteristics regarding soil, that are shown in table (4.1).

Table (4.1): Properties of the soil in the barrage foundation.

| Soil type | Gypsum Content % | Permeability, K (m/sec) | Material model | Anisotropy ratio |
|---|---|---|---|---|
| Gypsiferous Soil | 35 | $9.54\times10^{-08}$ | Saturated | $K_y/k_x=1$ |

### 4.5.1 Boundary Conditions

Figure (4.2) shows a schematic diagram of a barrage found on an isotropic layer. The various boundary conditions of the barrage section are as follows:

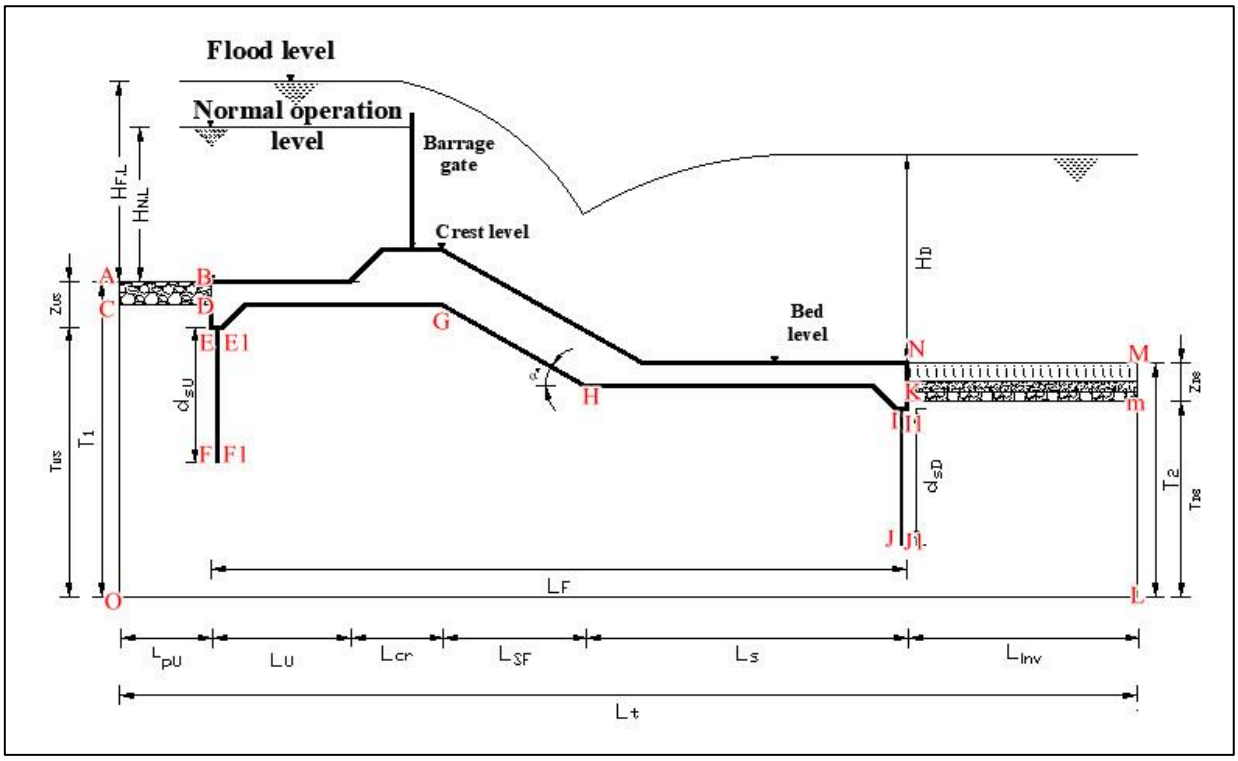


Figure (4.2): The Boundary Condition of the Barrage cross section.

$$\frac{\partial h}{\partial y}(x,0,t)=0 \qquad 0 \le x \le L_t \quad on\ OL \qquad (4.3)$$

$$h(x,T_2,t)=H_D \qquad (L_{PU}+L_F) \le x \le L_t \quad on\ NM \qquad (4.4)$$

$$\frac{\partial h}{\partial x}(L_{PU}+L_F,z,t)=0 \qquad T_{SD} \le z \le T_2 \quad on\ NK \qquad (4.5)$$

$$\frac{\partial h}{\partial y}(x, T_{DS}, t) = 0 \qquad \left(L_{PU} + L_U + L_{cr} + \frac{L_{SF}}{COS\beta}\right) \leq x \leq (L_{PU} + L_U + NL_{cr} + \frac{L_{SF}}{COS\beta} + L_S) \quad on\ HI \qquad (4.6)$$

$$\frac{\partial h}{\partial y}(x, T_{US}, t) = 0 \qquad (L_{PU} + L_U + L_{cr}) \leq x \leq (L_{PU} + L_U + L_{cr} + \frac{L_{SF}}{COS\beta}) \quad on\ GH \qquad (4.7)$$

$$\frac{\partial h}{\partial y}(x, T_{US}, t) = 0 \qquad L_{PU} \leq x \leq (L_{PU} + L_U + L_{cr}) \quad on\ EG \qquad (4.8)$$

$$\frac{\partial h}{\partial x}(L_{PU}, z, t) = 0 \qquad T_{SU} \leq x \leq T_1 \quad on\ BE \qquad (4.9)$$

$$\frac{\partial h}{\partial y}\left(x, \frac{t_s}{2}, t\right) = \frac{\partial h}{\partial y}\left(x, -\frac{t_s}{2}, t\right) \qquad 0 \leq x \leq d_{SU} \quad on\ EF\ and\ E_1F_1 \qquad (4.10)$$

$$\frac{\partial h}{\partial y}\left(x, \frac{t_s}{2}, t\right) = \frac{\partial h}{\partial y}\left(x, -\frac{t_s}{2}, t\right) \qquad 0 \leq x \leq d_{SD} \quad on\ IJ\ and\ I_1J_1 \qquad (4.11)$$

For the boundary AB, if the upstream water level is constant at level $H_{F.L}$, then

$$h(T_1, t) = H_{F.L} \qquad 0 \leq x \leq L_{PU} \quad on\ AB \qquad (4.12)$$

For the boundaries AO and ML, they are considered the constant head

$$h(o, z, t) = H_{F.L} \qquad 0 \leq z \leq T_1 \quad on\ AO \qquad (4.13)$$

$$\frac{\partial h}{\partial x}(L_t, z, t) = H_D \qquad 0 \leq z \leq T_1 \quad on\ ML \qquad (4.14)$$

### 4.5.2 Barrages in Lower Reach of Euphrates River

The present study focuses on the barrages built on the Euphrates River and its lower branches downstream of the Hindiya barrage. Accordingly, Kifil-Shinafiyah Barrages, which includes Shamiya regulators that consist of the Abbasiyah Regulator, Shamiya Regulator, and Khawarnaq Regulator. On other hand, Kufa Branch Barrages. AL-Simawi, (2010) and Abdullah et al., (2019) presented a comprehensive review covering this subject. The dimensions of the hypothetical barrage were investigated by surveying the barrages profiles

constructed on the Euphrates River in Iraq from Al-Hindiya Barrage to Abu-Sukhair Barrage, including four barrages (Al-hindiya, Al-kufa, AL-Shamiya, and Abu-Sukhair). Table (4.2) summarized the main hydraulic characteristics, dimensions, and components for the above-mentioned barrages.

Table (4.2): Barrages' main hydraulic characteristics, dimensions, and components.

| **Description** | **Barrages** | | | |
|---|---|---|---|---|
| | **Al-Hindiya** | **Al-Kufa** | **AL-Shamiya** | **Abu-Sukhair** |
| References | AL-Abbas et al., (2019) | Ministry of Irrigation General Establish-ment of Study and Design | Maatooq et al., (2015) | Ministry of Water Resources Commission for Dams and Reservoir |
| High flood level | 32.55 | 26.30 | 23.5 | 21.85 |
| Normal water level | 31.80 | 25.70 | 21 | 20.5 |
| Total length of barrage (m) | 33.5 | 32.80 | 33 | 42.7 |
| length of the launching apron and protection in upstream (m) | 25 | 13 | 21 | 30 |
| length of upstream floor (m) | 24.05 | 8.80 | 9 | 10.10 |
| length of crest (m) | 6.5 | 5.80 | 6 | 7.2 |

Table (4.2): Continue.

| | | | | |
|---|---|---|---|---|
| length of stilling basin (m) | 19.5 | 24 | 17 | 27.5 |
| length of inverted filter drain (m) | 75 | 55 | 74 | 76.5 |
| thickness of the launching apron and protection layers in upstream (m) | 1.9 | 1.5 | 1.5 | 1.5 |
| depth of the upstream cutoff wall (m) | 10.9 | 18.6 | 11 | 12 |
| depth of the downstream cutoff wall (m) | Not found | Not found | Not found | 12 |
| thickness of upstream floor (m) | 3 | 3.10 | 3 | 3 |
| Thickness of downstream floor (m) | 2.5 | 2 | 2.5 | 2.5 |
| thickness of the inverted filter drains (m) | 1.9 | 2.5 | 1.9 | 1.9 |
| High flood discharge ($m^3$/sec) | 2500 | 1400 | 1100 | 1400 |

### 4.5.3 Bounds for Dimensions of the Barrage

Based upon the previous discussion, it was obvious that almost the constructed barrages have dimensions that can be limited to a range given in table (4.3).

Table (4.3): Dimension range of barrage component dimensions (collected from different references).

| Description | Design variable | Lower bound (m) | Upper bound (m) |
|---|---|---|---|
| length of the launching apron and protection in upstream | $L_{pU}$ | 13.0 | 30 |
| Length of upstream floor | $L_U$ | 8.80 | 11.30 |
| Projection length of inclined floor | $L_{SF}$ | 4.2 | 5.0 |
| Length of stilling basin | $L_S$ | 19.5 | 27.5 |
| Length of inverted filter layer | $L_{inv}$ | 55.0 | 76.5 |
| Length of crest | $L_{cr.}$ | 5.8 | 7.2 |
| Thickness of the launching apron and protection in upstream | $t_{pU}$ | 1.5 | 1.9 |
| Depth of upstream cutoff | $d_{sU}$ | 10.94 | 18.60 |
| Thickness of upstream floor | $t_U$ | 3.0 | 3.10 |
| Depth of downstream cutoff | $d_{sD}$ | 12.0 | 18.60 |
| Thickness of inverted filter layer | $t_{inv}$ | 1.9 | 2.5 |
| Pre-jump depth | $y_1$ | 3.16 | 3.48 |
| Post-jump depth | $y_2$ | 6.72 | 7.61 |

The slope of the inclined floor ($L_{SF}$) ranged from (1:3-1:5) ( Novak et al., 2008), however, the inclination of the floor was considered to be (1:3).

## 4.6 Normalization of the Design Variables

The transformation of a regular dimension into a non-dimensional form is a mathematical process that involves dividing a physical quantity by a reference value to obtain a dimensionless quantity. This was done in order to simplify the analysis of a problem or to compare results between different

systems with different units. The resulting dimensionless quantity, also known as a dimensionless parameter, has no units and was only dependent on the ratios of the physical quantities involved. Accordingly:

Let the horizontal dimension to be denoted as $\mathbf{X_N}$ in which;

$$X_N = \frac{x}{H_{F.h}} \tag{4.15}$$

Where *x* is the horizontal distance in (m) and $H_{F.h}$ is the high flood head in (m).

Similarly, if the vertical dimension is to be denoted as $\mathbf{Z_N}$, thus;

$$Z_N = \frac{z}{H_{F.h}} \tag{4.16}$$

Where *z* is the vertical distance in (m).

The typical barrage profile section in the normalized plane is shown in Figure (4.3). Consequently, the design variable in normalized form is defined in table (4.4).

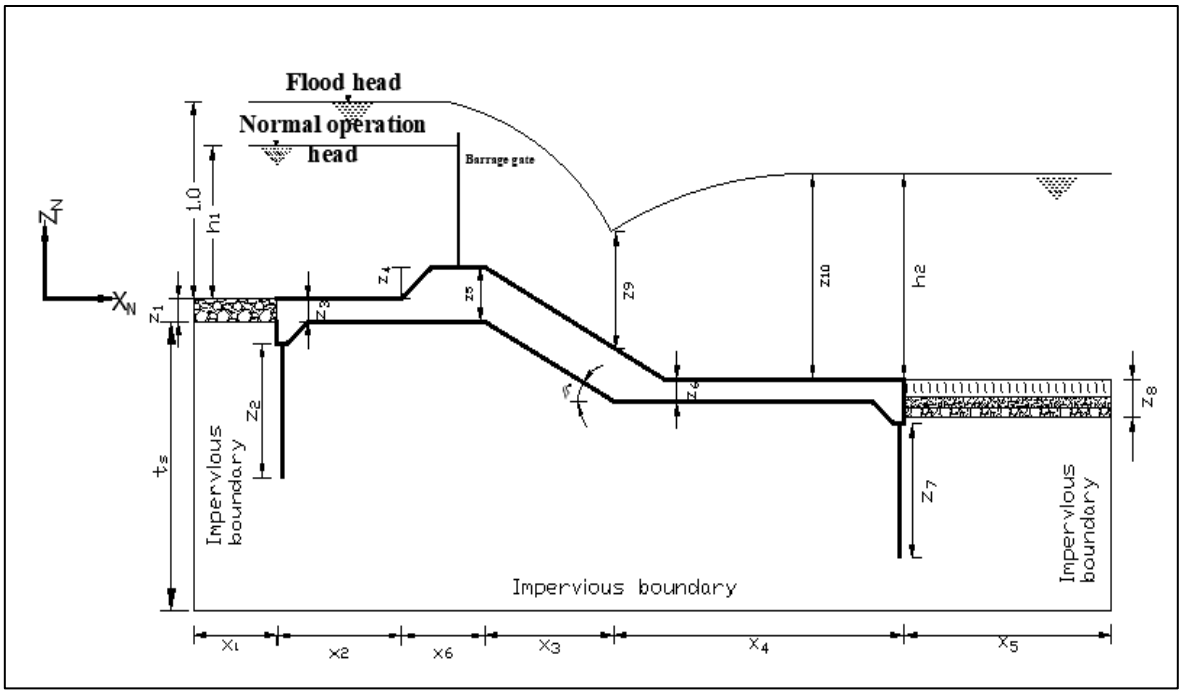


Figure (4.3): Typical profile of the hypothetical case study of barrage in normalized form.

Table (4.4): Transformation of design variable in non-dimensionlized form.

| Design Variable | Normalized Variable | Transformation | Definition |
|---|---|---|---|
| $L_{pU}$ | $\boldsymbol{x_1}$ | $x_1 = \frac{L_{PU}}{H_{F.h}}$ | $x_1$ is the non-dimensionlized length of the launching apron and protection in upstream. |
| $L_U$ | $\boldsymbol{x_2}$ | $x_2 = \frac{L_U}{H_{F.h}}$ | $x_2$ is the non-dimensionlized the length of upstream floor. |
| $L_{SF}$ | $\boldsymbol{x_3}$ | $x_3 = \frac{L_{SF}}{H_{F.h}}$ | $x_3$ is the non-dimensionlized projection length of inclined floor. |
| $L_S$ | $\boldsymbol{x_4}$ | $x_4 = \frac{L_S}{H_{F.h}}$ | $x_4$ is the non-dimensionlized length of stilling basin. |
| $L_{inv}$ | $\boldsymbol{x_5}$ | $x_5 = \frac{L_{inv}}{H_{F.h}}$ | $x_5$ is the non-dimensionlized length of inverted filter drain. |
| $L_{cr.}$ | $\boldsymbol{x}_6$ | $x_c = \frac{L_{cr}}{H_{F.h}}$ | $x$c is the non-dimensionlized length of crest. |
| $t_{pU}$ | $\boldsymbol{z_1}$ | $z_1 = \frac{t_{pU}}{H_{F.h}}$ | $z_1$ is the non-dimensionlized thickness of the launching apron and protection layers. |
| $d_{sU}$ | $\boldsymbol{z_2}$ | $z_2 = \frac{d_{sU}}{H_{F.h}}$ | $z_2$ is the non-dimensionlized depth of the upstream cutoff wall. |
| $t_U$ | $\boldsymbol{z_3}$ | $z_3 = \frac{t_u}{H_{F.h}}$ | $z_3$ is the non-dimensionlized thickness of upstream floor. |
| $d_{sD}$ | $\boldsymbol{z_7}$ | $z_7 = \frac{d_{sD}}{H_{F.h}}$ | $z_7$ is the non-dimensionlized depth of the downstream cutoff wall. |
| $t_{inv}$ | $\boldsymbol{z_8}$ | $z_8 = \frac{t_{inv}}{H_{F.h}}$ | $z_8$ is the non-dimensionlized thickness of the inverted filter drains. |
| $y_1$ | $\boldsymbol{z_9}$ | $z_9 = \frac{y_1}{H_{F.h}}$ | $Z_9$ is the non-dimensionlized pre-jump depth of water. |

Table (4.4): Continue.

| | | | |
|---|---|---|---|
| $y_2$ | $\mathbf{z_{10}}$ | $z_{10} = \frac{y_2}{H_{F.h}}$ | $Z_{10}$ is the non-dimensionlized post-jump depth of water. |
| α | β | $\beta = \alpha$ | β is the non-dimensionlized angle of inclined floor of barrage. |
| $H_{N.L}$ | $h_1$ | $h_1 = \frac{H_{N..h}}{H_{F.h}}$ | $h_1$ is the non-dimensionlized normal operation head. |
| $H_D$ | $h_2$ | $h_2 = \frac{H_D}{H_{F.h}}$ | $h_2$ is the non-dimensionlized high flood head in downstream. |

Hence; for simplicity, the dimensions of all the design variables introduced in table (4.4) have been transformed in normalization form by dividing all dimensions of the design variable on high flood level ($H_{F.L}$) as shown in table (4.5).

Table (4.5): Dimension ranges for design variables in normalized form.

| **Design variables** | **Lower bound** | **Upper bound** |
|---|---|---|
| $X_1$ | 1.6 | 3.76 |
| $X_2$ | 1.09 | 1.45 |
| $X_3$ | 0.48 | 0.57 |
| $X_4$ | 2.41 | 3.31 |
| $X_5$ | 6.79 | 9.26 |
| $X_6$ | 0.72 | 0.88 |
| $Z_1$ | 0.19 | 0.23 |
| $Z_2$ | 1.35 | 2.25 |
| $Z_3$ | 0.37 | 0.38 |
| $Z_7$ | 1.48 | 2.38 |

Table (4.5): Continue.

| | | |
|---|---|---|
| $Z_8$ | 0.23 | 0.31 |
| $Z_9$ | 0.39 | 0.43 |
| $Z_{10}$ | 0.83 | 0.94 |

The barrage structure adopted in this study was designed to be constructed on gypsiferous soil with properties involved in SEEP/W model as listed priory in the table (4.1).

## 4.7 Verification of Numerical Solutions

Verifying numerical solutions involves checking the accuracy and reliability of the calculated solution obtained from numerical methods. It is an important step in the numerical solution process as it helps to ensure that the solution obtained is reliable. In this study, a comparing the results with solutions for the specified problem taken from the literature has been carried out. The study performed by AL-Abbas et al., (2019) was considered a case study for verification. Al-Hindya barrage was analyzed to check the safety aspects, uplift pressures, and seepage ratio with the variation of discharge and water levels. Figure (4.4) shows AL-Hindiya Barrage profile.

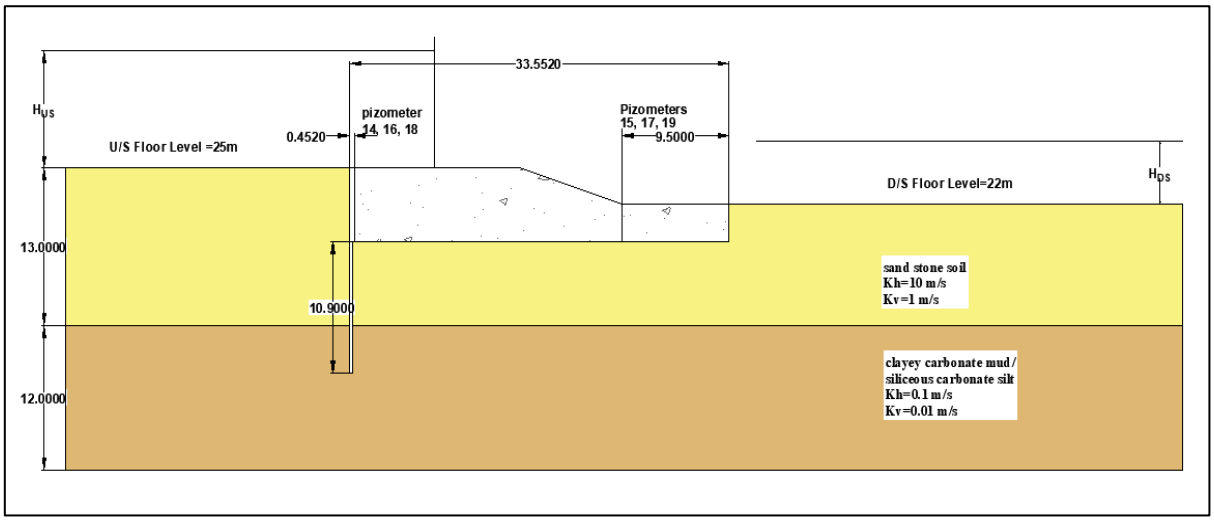


Figure (4.4): AL-Hindiya Barrage profile.

Table (4.6) presents a summary of the data used in the verification process of the measured uplift pressures of piezometers No.14 and No.15, which were located upstream and downstream of the main barrage at the location of the maximum water level observed in February 2018.

Table (4.6): The properties of soil layers and the boundary conditions for the actual operation state of AL-Hindiya barrage.

| **Description** | **Value** |
|---|---|
| upstream water level a.s.l | 31.8 |
| downstream water level a.s.l | 27.15 |
| Cut off depth (m) | 10.90 |
| Type of first soil foundation layer | sandstone soil |
| the thickness of the first layer of soil foundation (m) | 13 |
| Coefficient of permeability in the horizontal direction, $k_{x1}$ (m/sec) | 10 |
| Coefficient of permeability in the vertical direction, $k_{y1}$ (m/sec) | 1 |
| Saturation weight density of first layer $\gamma_{sat}$ ($kN/m^2$) | 20 |
| Type of second soil foundation layer | clayey carbonate mud/ siliceous carbonate silt |
| thickness of second layer of soil foundation (m) | 12 |
| Coefficient of permeability in horizontal direction, $k_{x2}$ (m/sec) | 0.1 |
| Coefficient of permeability in vertical direction, $k_{y2}$ (m/sec) | 0.01 |
| Saturation weight density of second layer $\gamma_{sat}$ ($kN/m^2$) | 18.5 |

Table (4.7), presents the field measurements of total water level in piezometers 14,15 in U/D and D/S, uplift pressure, and seepage ratio of main barrage at date 25/2/2018.

Table (4.7): Total water level of piezometers of main barrage at date 25/2/2018.

| **Piezometers** | **Total water level** | **Uplift pressure (ton/m$^2$)** |
|---|---|---|
| Piezometer 14 in u/s | 31.80 | 8.53 |
| Piezometer 15 in d/s | 27.15 | |

In this study, the results of numerical analysis under the SEEP/W 2D module (see figure 4.5) for the case study quoted from AL-Abbas et al., (2019) were shown in table (4.8).

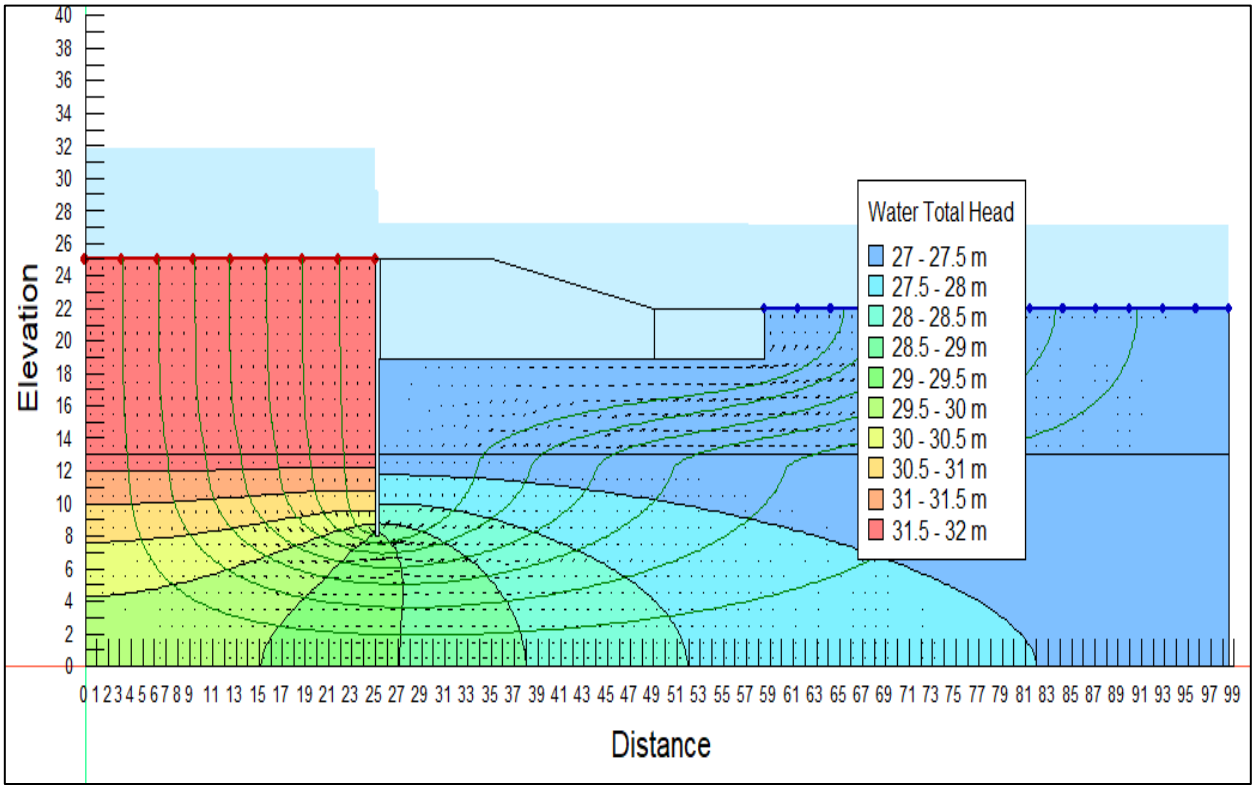


Figure (4.5): Seepage analysis for AL-Hindiya barrage in this study.

Table (4.8): Result of numerical analysis from geo-studio seep/w.

| piezometers | Water total level | Water pressure head H (m) |
|---|---|---|
| U/S | 31.78 | 12.88 |
| 14 | 27.18 | 8.28 |
| 15 | 27.17 | 8.27 |
| D/S | 27.16 | 8.26 |

To calculate the maximum force of uplift pressure $P_{max}$, figure (4.6) shows the uplift pressure distribution beneath the barrage.

$$P_{max} = p_1 + p_2 + p_3 \quad (4.17)$$

$$p_1 = \frac{h_1 + h_2}{2} * l_1 * \gamma * 1 \quad (4.18)$$

Where;

P uplift pressure force in (ton), and h is the head of water in piezometer in (m).

($\gamma$ = 1 ton/m$^3$) (Water unite weight)

$$p_1 = \frac{12.88 + 8.28}{2} * 0.452 * 1 * 1 = 4.78\ ton$$

$$p_2 = \frac{h_2 + h_3}{2} * l_2 * \gamma * 1$$

$$p_2 = \frac{8.28+8.27}{2} * 23.60 * 1 * 1 = 195.29\ ton$$

$$p_3 = \frac{h_3 + h_4}{2} * l_3 * \gamma * 1$$

$$p_3 = \frac{8.27 + 8.26}{2} * 9.5 * 1 * 1 = 78.52\ ton$$

Max. force of uplift pressure $P_{max}$ =4.78+ 195.29 + 78.52 = 278.59 ton.

Max. uplift pressure = (278.59/33.552) = 8.30 ton/m$^2$.

Mean percentage error = $\frac{8.53-8.30}{8.30} x100 = 2.77\%$

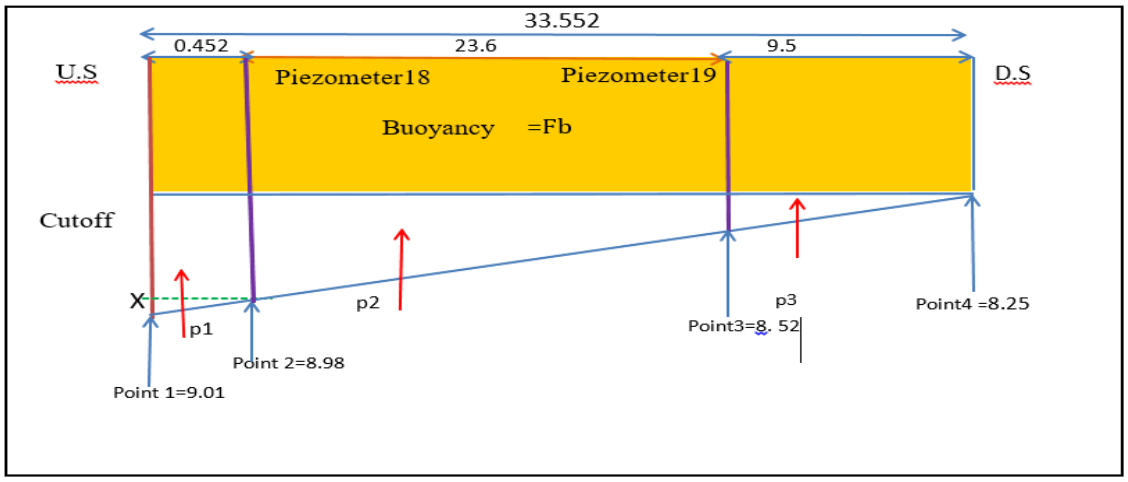


Figure (4.6): Uplift pressure distribution beneath AL-Hindiya barrage foundation from (AL-Abbas et al., 2019).

From the results of numerical analysis, it's obvious that a decrease in water total head upstream leads to a decrease in the maximum uplift pressure on a barrage floor. Thus, the mean percentage error between the calculated uplift pressure from field measurements and the uplift pressure from the numerical analysis was computed. The results showed an acceptable percentage error.

## 4.8 Scenario for investigating the Role of Gypsum Soil in AL-Hindiya Barrage Soil Foundation

To investigate the role of gypsum soil in the foundation of AL-Hindiya barrage the seepage analyses by SEEP / W were made to compute seepage properties beneath the barrage and find how such soil affects it. The seepage flux, uplift pressure, and exit gradient were computed. The boundary condition for the present state is the same as for the natural state except that the foundation soil layer is one layer containing gypsum soil of a gypsum content of 35% and with a hydraulic conductivity of $9.540 \times 10^{-8}$(m/sec). Figure (4.7) shows the seepage analyses of the barrage in presence of gypsiferous soil in its foundation.

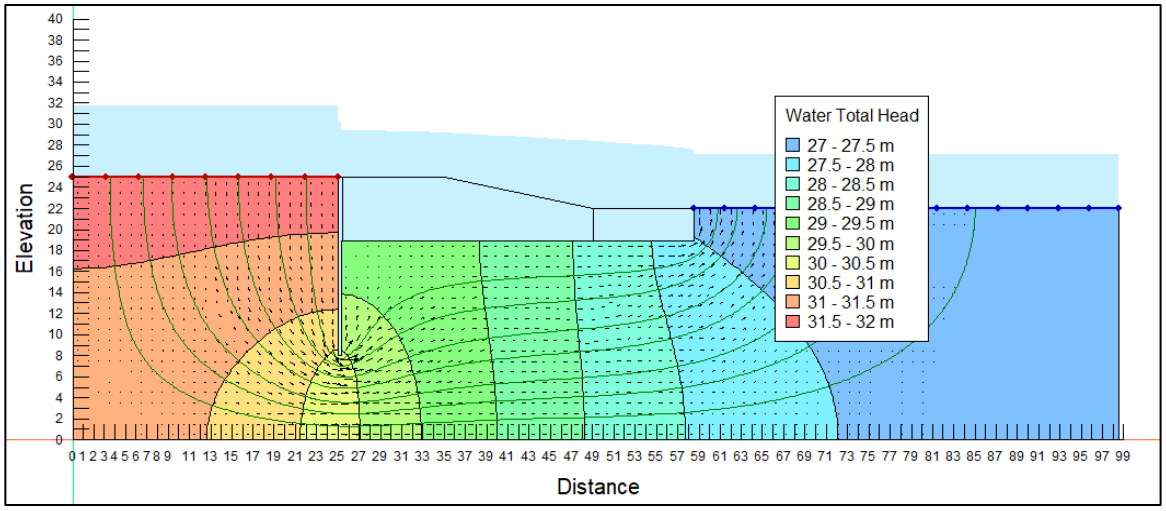


Figure (4.7): Seepage analyses for AL-Hindiya barrage in presence of gypsiferous soil beneath the foundation.

Tables (4.9) and (4.10), show the seepage properties of AL-Hindiya barrage by Seep/W model in the case of the natural state and in the case of the presence of gypsum soil in the soil foundation layer.

Table (4.9): Seepage analyses of Al-Hindiya barrage at actual state.

| **Seepage properties** | **value** |
|---|---|
| Maximum uplift pressure (ton/m$^2$/m) | 8.30 |
| Exit gradient | 0.0042 |
| Seepage flux (m$^3$/sec/m) | 0.00163 |

Table (4.10): Seepage Properties of AL-Hindiya barrage at the state of presence of gypsum soil in the soil foundation layer (hypothetical case).

| **Seepage properties** | **value** |
|---|---|
| Maximum uplift pressure (ton/m$^2$/m) | 9.75 |
| Exit gradient | 0.171 |
| Seepage flux (m$^3$/sec/m) | 1.638x10$^{-9}$ |

From the results of table (4.9), and (4.10), it is obvious that for the case of soil foundation of AL-Hindiya barrage contain gypsum soil (hypothetical case) the uplift pressure increases by 14.87% from the actual state, and the exit gradient also increased but it remained within the safe value. While for seepage flux beneath barrage when the soil foundation contain gypsum soil is less than the actual state (soil foundation free from gypsum soil) because the coefficient of permeability of gypsum soil of the present study is less than the coefficient of permeability of the soil layer beneath of AL-Hindiya barrage.

## 4.9 Investigating the Effect of Gypsum Soil in the Foundation of the hypothetical Barrage of the present study

To investigate the effect of gypsum soil in the foundation of the barrage in present study a comparison between the analyses of seepage beneath barrage in case of presence natural soil (free from gypsum), and in case of presence of gypsiferous soil. Table (4.11) shows seepage properties of the barrage foundation when the soil is free from gypsum.

Table (4.11): Seepage properties of the barrage at state of presence natural soil in the foundation.

| **Seepage properties** | **value** |
|---|---|
| Maximum uplift pressure ($kN/m^2/m$) | 65.76 |
| Exit gradient | 0.080 |
| Seepage flux ($m^3/sec/m$) | $1.382x10^{-8}$ |

An analysis of the seepage problem when the barrage contains gypsum soil in its foundation was done. Table (4.12), shows the results of seepage properties when the barrage foundation contains gypsiferous soil.

Table (4.12): Seepage properties of the barrage at the state of presence of gypsiferous soil in the foundation.

| Seepage properties | value |
|---|---|
| Maximum uplift pressure ($kN/m^2/m$) | 65.76 |
| Exit gradient | 0.080 |
| Seepage flux ($m^3/sec/m$) | $2.799x10^{-9}$ |

From the results of table (4.11), and (4.12), it's obvious that the uplift pressure and exit gradient are the same when the barrage foundation contains natural soil and when contains gypsiferous soil, while seepage flux decreased in gypsiferous soil and this is because of the coefficient of permeability of the gypsiferous soil is less than the coefficient of permeability of the natural soil.

## 4.10 Parametric Analysis for Seepage beneath Barrage Floor

Parametric analysis is a method used to study the behavior of a system as a function of its input parameters to understand the relationship between the inputs and outputs of a system and to identify the parameters that have a higher effect on the system's behavior.

### 4.10.1 Effect of Changes in Seepage Rate

Figures (4.8) and (4.9) show the variation of the seepage rate ratio ($q/KH_{F.h}$), versus the depth of the U/S cutoff wall ($z_2$) and for different cases for total length of the floor ($L_T$) and D/S cutoff wall depth in non-dimensionlized form.

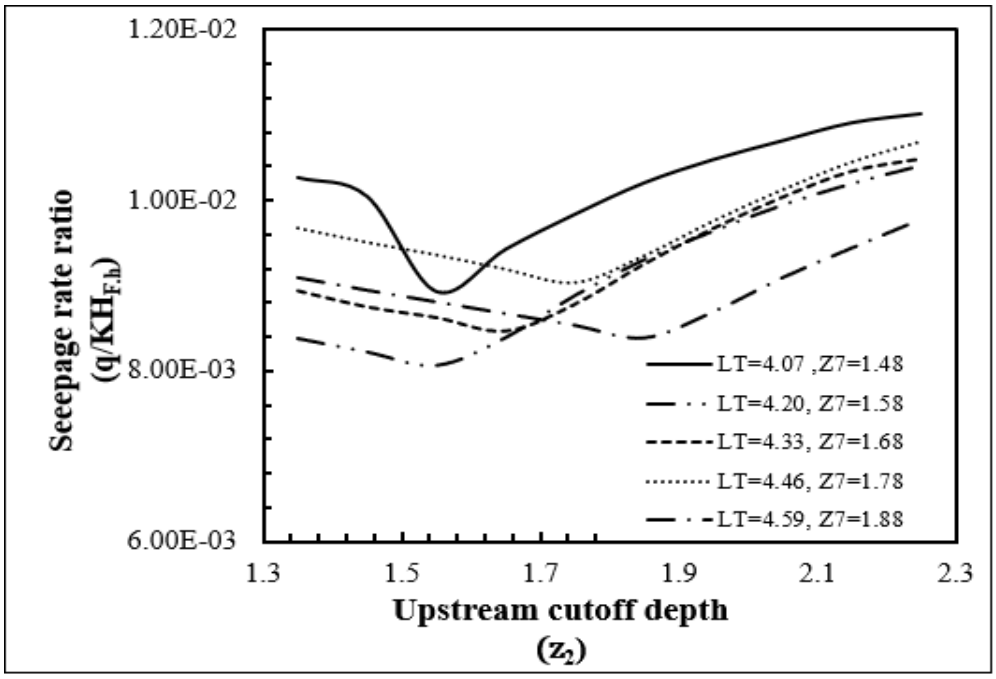


Figure (4.8): The variation of the seepage rate ratio ($q/KH_{F.h}$) with U/S cut off depth and for total length of floor ($L_T$) from (4.07 to 4.59), and ($z_7$) from (1.48 to 1.88).

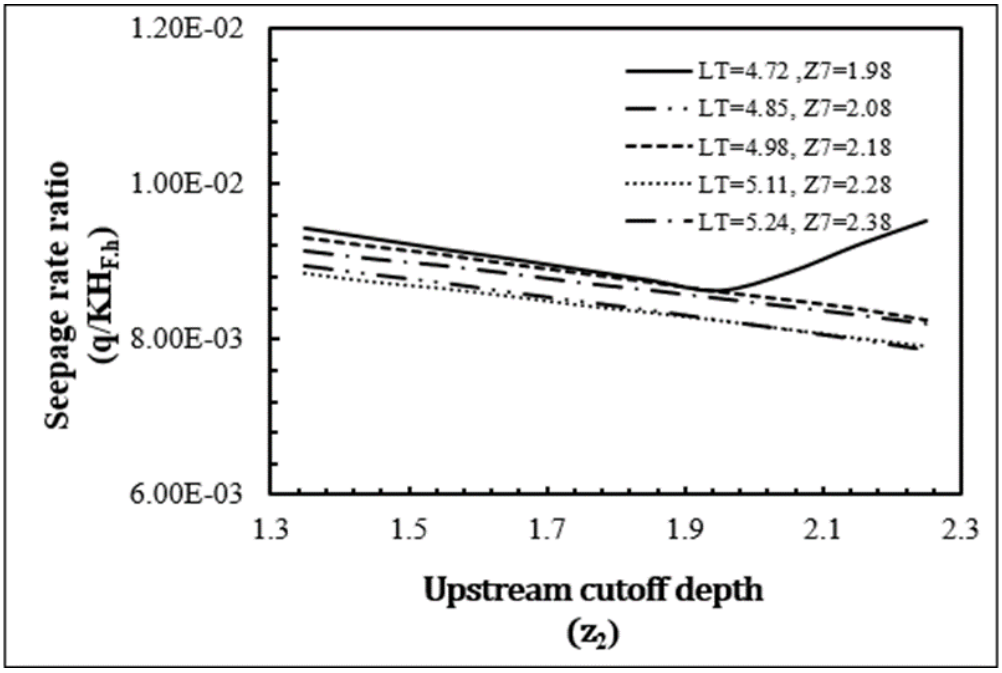


Figure (4.9): The variation of the seepage rate ratio ($q/KH_{F.h}$) with U/S cut off depth and for ($L_T$) from (4.72 to 5.24), and ($z_7$) from (1.98 to 2.38).

From figures (4.8) and (4.9), the effects of increasing the depth of the cutoff wall at U/S lead at the beginning to decrease the seepage rate with increase the total length ($L_T$) of the impervious floor and the minimum decreasing in seepage rate when $L_T$ equal to 5.11. Also, the seepage rate value is decreases when the D/S cutoff wall increase and that because of the increase in creep line length of water beneath barrage with the increase in the length of floor. It is found that the minimum decreasing in seepage rate when the D/S cutoff wall depth is equal to 2.28.

Figures (4.10) and (4.11) show the variation of the seepage rate ratio ($q/KH_{F.h}$), versus the depth of D/S cutoff wall ($z_7$) and for different cases for total length of the floor $L_T$ and U/S cutoff wall depth ($z_2$) in non-dimensionlized form.

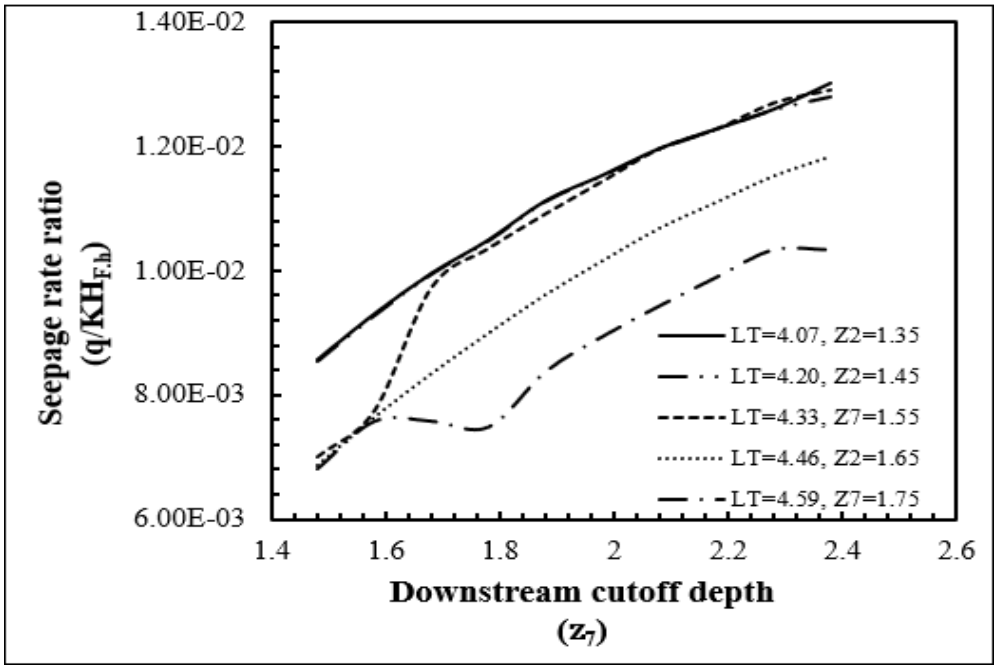


Figure (4.10): The variation of the seepage rate ratio ($q/KH_{F.h}$) with D/S cut off depth ($z_7$) and for ($L_T$) from (4.07 to 4.59), and $Z_2$ from (1.35 to1.75).

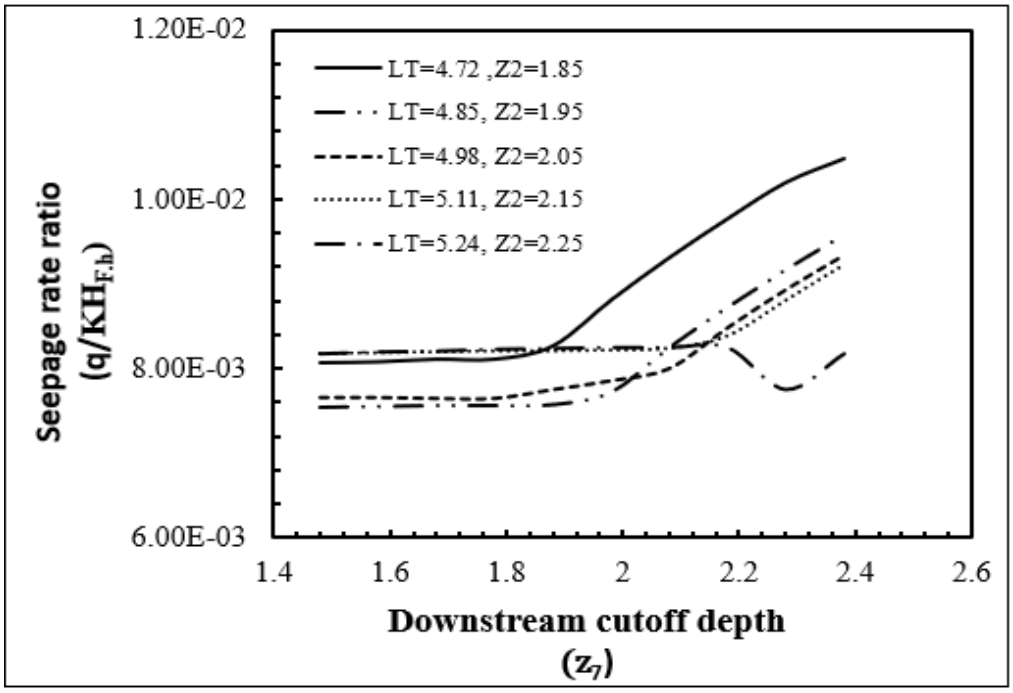


Figure (4.11): The variation of the seepage rate ratio ($q/KH_{F.h}$) with D/S cut off the wall ($z_7$), and for $L_T$ from (4.72 to 5.24), and $z_2$ from (1.85 to 2.25).

The relationship between the seepage rate ratio ($q/KH_{F.h}$) with D/S cutoff wall depth ($z_7$), as shown in figures (4.10) and (4.11), show that the increase in depth of D/S cutoff wall leads to an increase in seepage rate when U/S cutoff depth is small. But this increase decrease gradually when the total length of the impervious floor and U/S cutoff wall depth increase. For the value of $z_2$ equal to 2.25, and LT equal to 5.25 which is the maximum depth of U/S cutoff and length of the barrage floor at this study the rate seepage at minimum depths of $z_2$ value is maximum but its value begins to decrease when $z_7$ increase in depth until reach minimum value at maximum depth about 2.38.

### 4.10.2 Effect of Exit Gradient

Figure (4.12) and (4.13) show the variation of exit gradient ($i_{xy}$), versus the depth of the upstream cutoff wall ($z_2$) and for different cases for total length of the floor $L_T$ and D/S cutoff wall depth ($z_7$) in non-dimensionlized form.

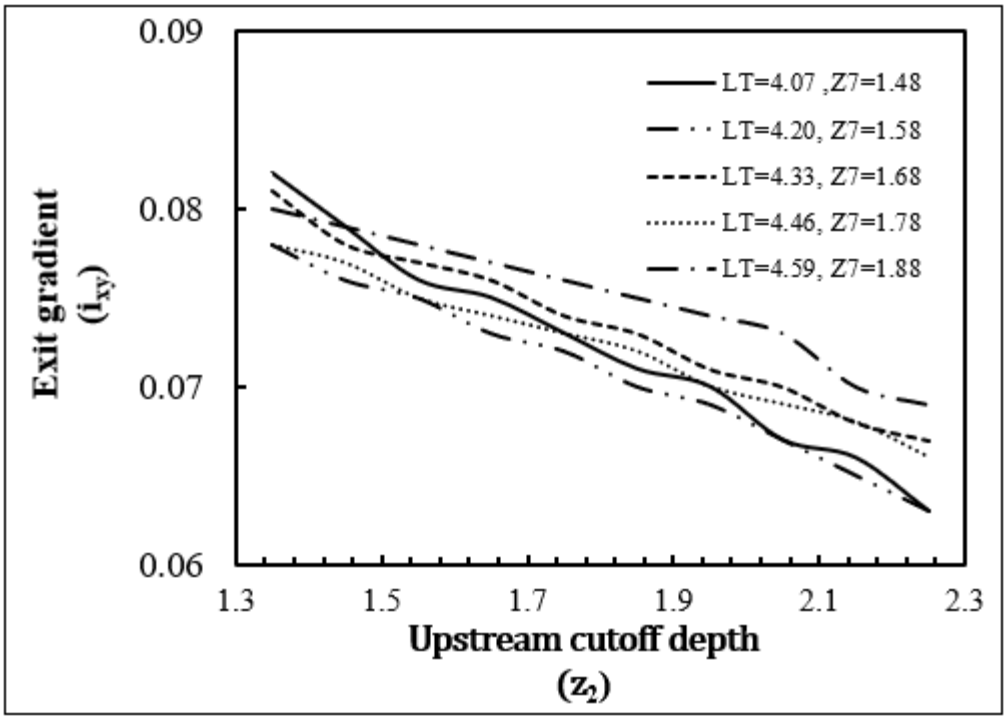


Figure (4.12): The variation of exit gradient ($i_{xy}$) with U/S cutoff wall ($z_2$) and for ($L_T$) from (4.07 to 4.59), and $z_7$ from (1.48 to1.88).

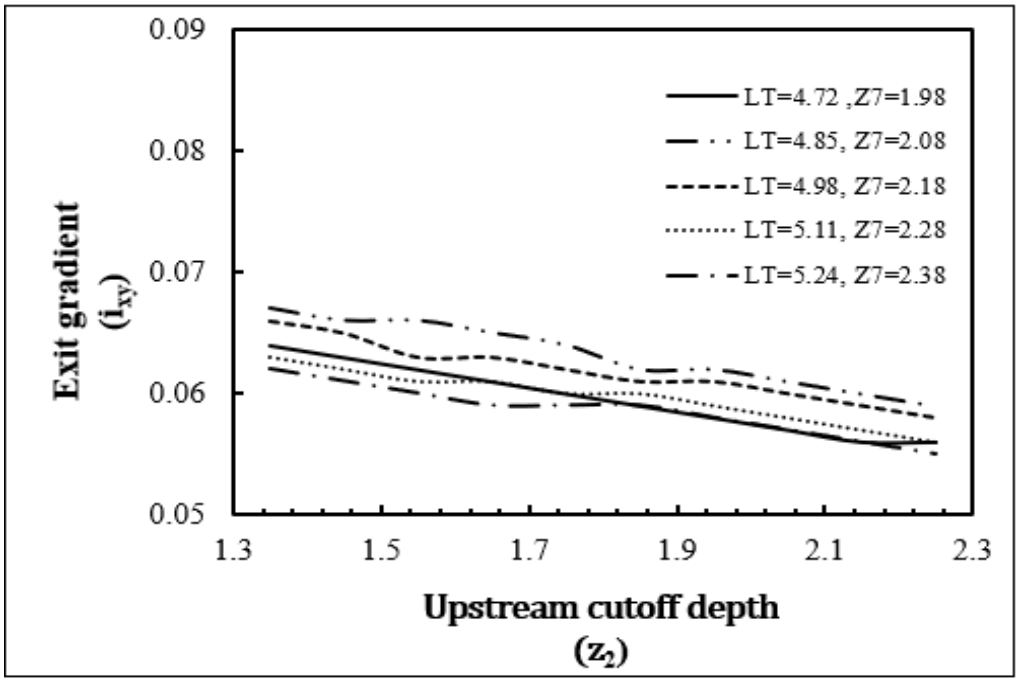


Figure (4.13): The variation of exit gradient ($i_{xy}$) with U/S cutoff wall ($z_2$) and for $L_T$ from (4.72 to 5.24), and $z_7$ from (1.98 to 2.38).

Figure (4.12) and (4.13), illustrate the relationship between the exit gradient with the U/S cutoff wall ($z_2$) for different cases of ($L_T$) and ($z_7$). The variation of the exit gradient with the depth of the u/s cutoff wall ($z_2$) indicated that an increase in the cutoff depth leads to decrease in the exit gradient value. Also, when the total floor length increase leads to decrease the exit gradient with increase the depth of the D/S cutoff wall. The minimum value of exit gradient when total floor length ($L_T$) and depth of cutoff wall in D/S ($z_7$) are at maximum range value at this study (i.e., $L_T$= 5.24, $z_7$= 2.38).

Figure (4.14) and (4.15) show the variation of the exit gradient ($I_{xy}$), versus the depth of the downstream cutoff wall ($z_7$) and for different cases of total length of the floor $L_T$ and U/S cutoff wall depth ($z_2$) in non-dimensionlized form.

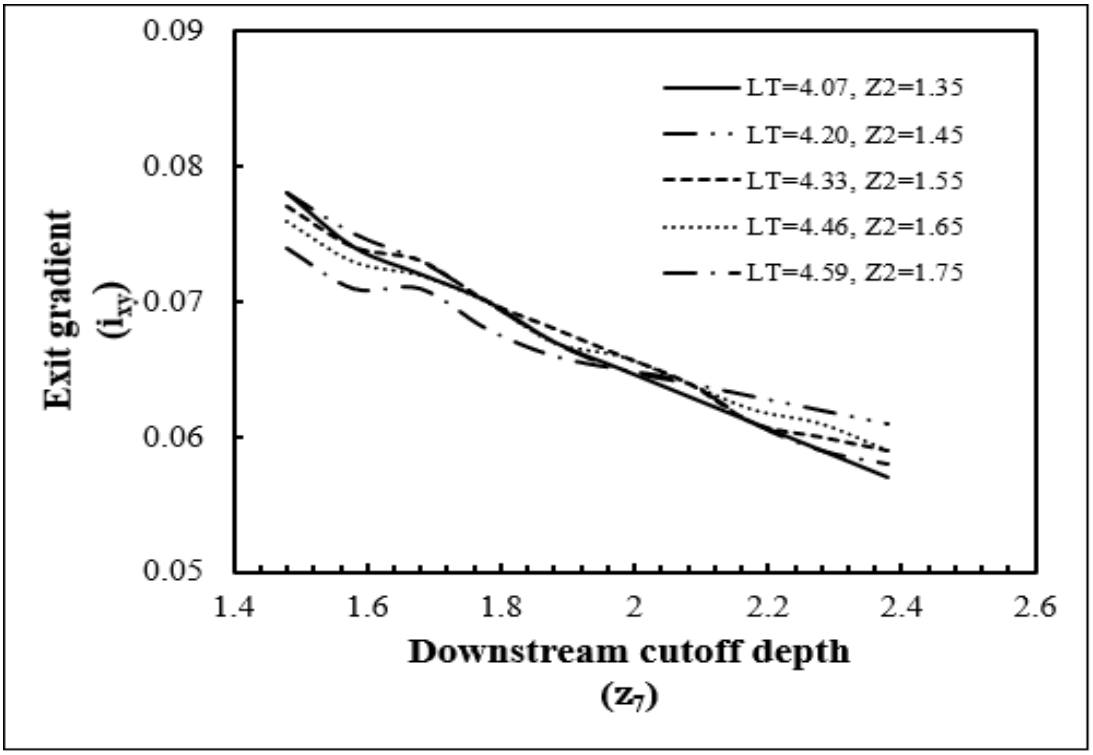


Figure (4.14): The variation of exit gradient ($i_{.xy}$) with D/S cutoff wall ($z_7$) and for $L_T$ from (4.07 to 4.59), and $z_2$ from (1.35 to 1.75).

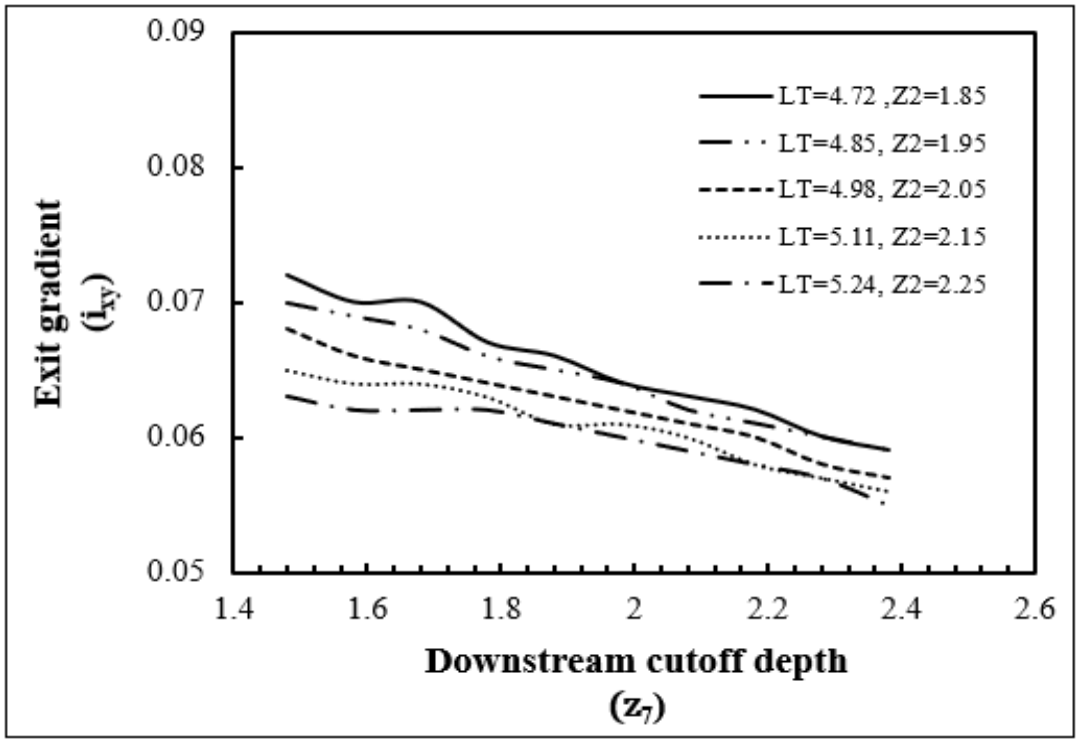


Figure (4.15): The variation of exit gradient ($i_{.xy}$) with D/S/s cutoff wall ($z_7$) and for $L_T$ from (4.72 to 5.24), and $z_2$ from (1.85 to 2.25).

Figures (4.14) and (4.15), illustrate the relationship between the exit gradient ($i_{xy}$) with D/S cutoff wall ($z_7$); it is obvious that increase in the depth of the D/S cutoff wall with increase in the total length of the floor and U/S cutoff depth leads to a decrease in the exit gradient value. The minimum value of the exit gradient is at $L_T$ equal to 5.24 and U/S cutoff depth equal to 2.25.

### 4.10.3 Effect of Uplift Pressures

Figure (4.16) and (4.17), shows the variation of uplift pressure ratio ($P/\gamma H_{F.h}$) versus the depth of the upstream cutoff wall ($z_2$), and for different cases for total length of the floor $L_T$ and D/S cutoff wall depth ($z_7$) in non-dimensionlized form.

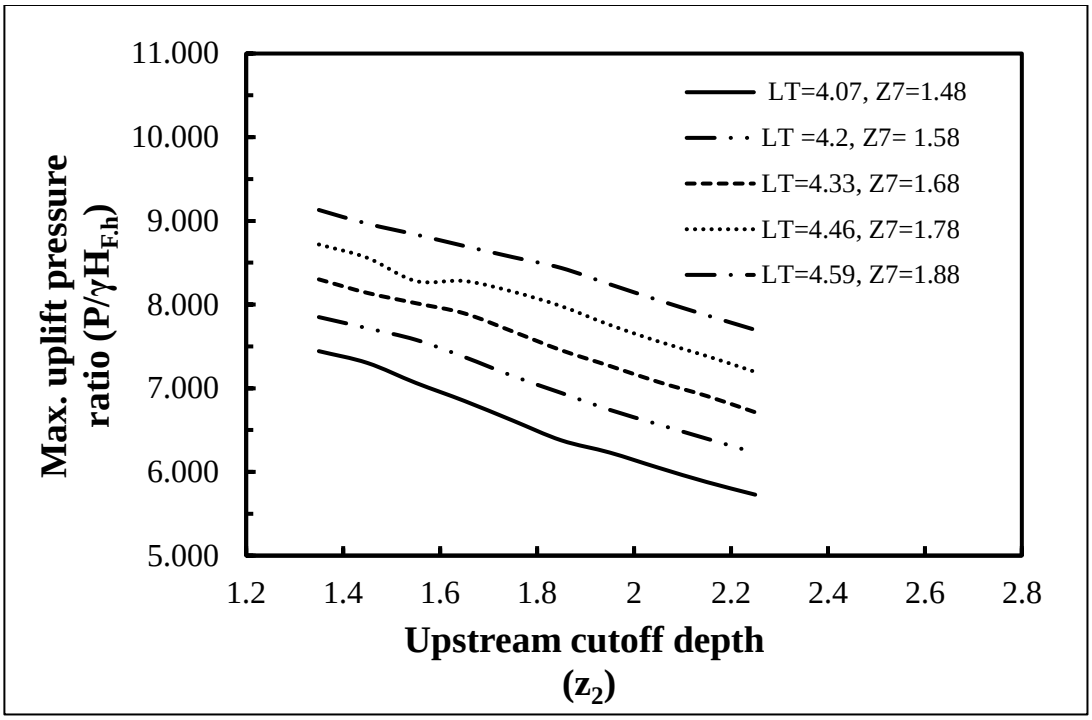


Figure (4.16): The variation of max. Uplift pressure ratio ($P/\gamma H_{F.h}$) with U/S cutoff wall ($z_2$) and for $L_T$ from (4.07 to 4.59), and $z_7$ from (1.48 to 1.88).

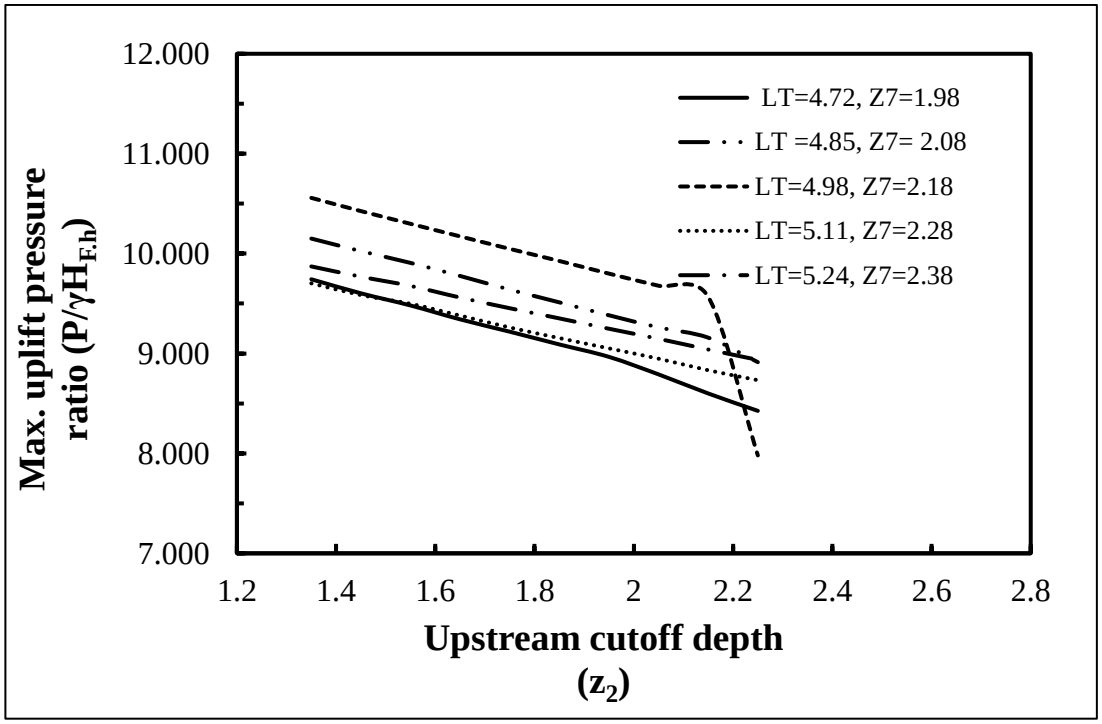


Figure (4.17): The variation of max. Uplift pressure force with U/S cutoff wall ($z_2$) and for $L_T$ from (4.72 to 5.24), and $z_7$ from (1.98 to 2.38).

Figures (4.16) and (4.17), illustrate the variation of maximum uplift pressure beneath the barrage floor with an upstream cutoff wall. It indicated that the uplift pressure values decrease with increasing the depth of the u/s cutoff wall. In contrast, this decrease varies with the increase in the total floor length and downstream cutoff wall depth.

Figure (4.18) and (4.19) show the variation of uplift pressure ratio ($P/\gamma H_{F.h}$) versus the depth of the downstream cutoff wall ($z_7$), and for different cases for total length of the floor $L_T$ and u/S cutoff wall depth ($z_2$) in non-dimensionlized form.

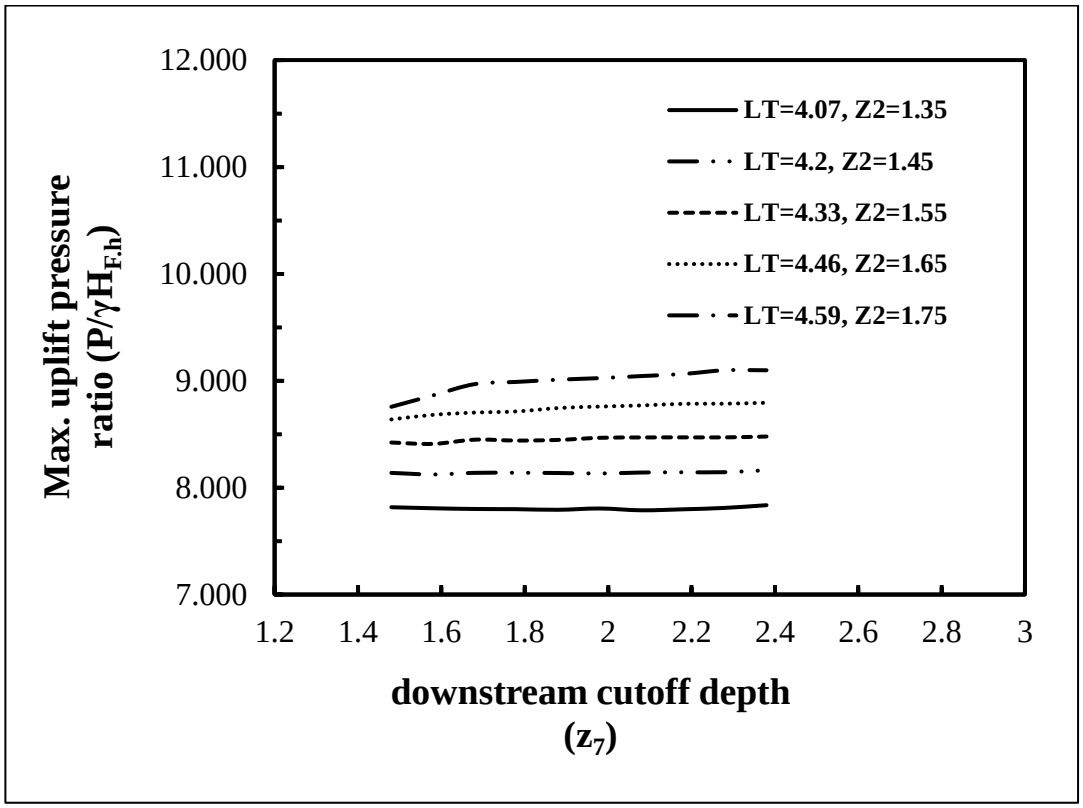


Figure (4.18): The variation of max. Uplift pressure ratio ($P/\gamma H_{F.h}$) with D/S cutoff wall ($z_7$) and for $L_T$ from (4.07 to 4.59), and $z_2$ from (1.35 -1.75).

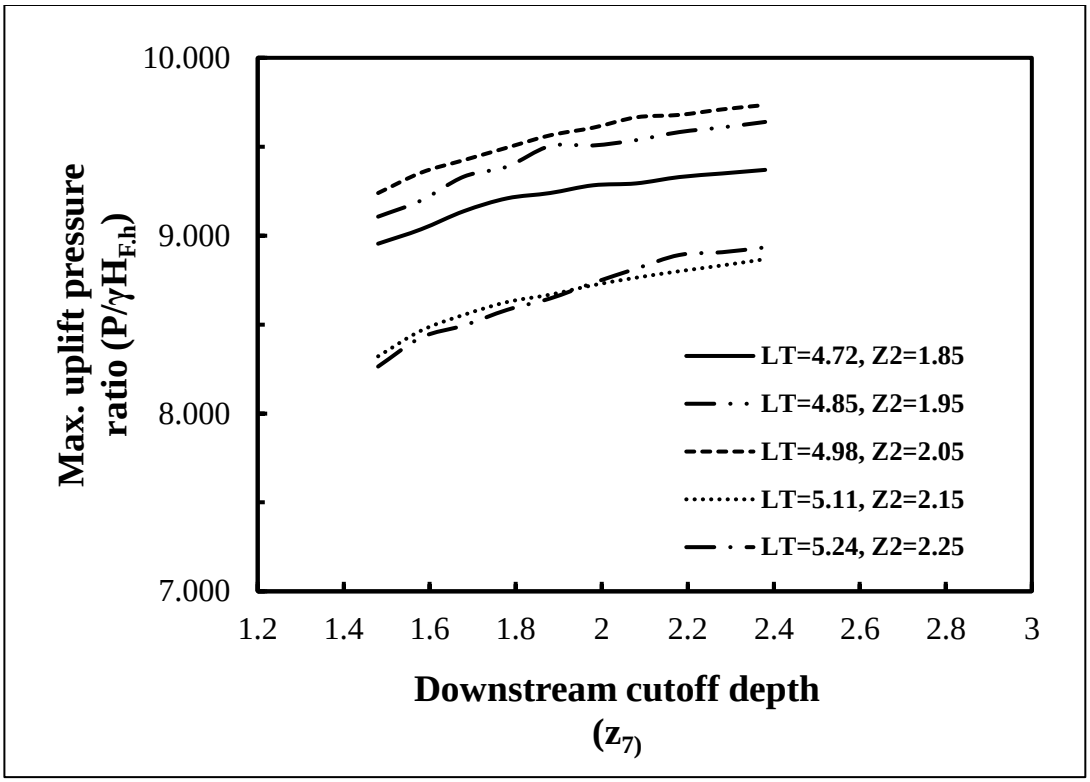


Figure (4.19): The variation of max. Uplift pressure force with D/S cutoff wall ($z_7$) and for $L_T$ from (4.72 to 5.24), and $z_2$ from (1.98 -2.38).

Figures (4.18) and (4.19), illustrate the variation of maximum uplift pressure beneath the floor foundation of the barrage with downstream cutoff wall depth; the relationship indicated that the uplift pressure increased with increasing the cutoff depth and varies for different values of floor length and cutoff depth upstream. But this variation in uplift pressure value decreased when the floor length reached its (5.11- 5.24) value.

## 4.11 The Flow Net Distribution Beneath Barrage Floor in Case of Max. & Min. (Seepage Discharge, Exit Gradient, And Uplift Pressure).

The flow net beneath the foundation of the barrage in case of maximum and minimum seepage flow, exit gradient, and uplift pressure is shown in figures (4.20), (4.21), (4.22), (4.23), (4.24), and (4.2), respectively.

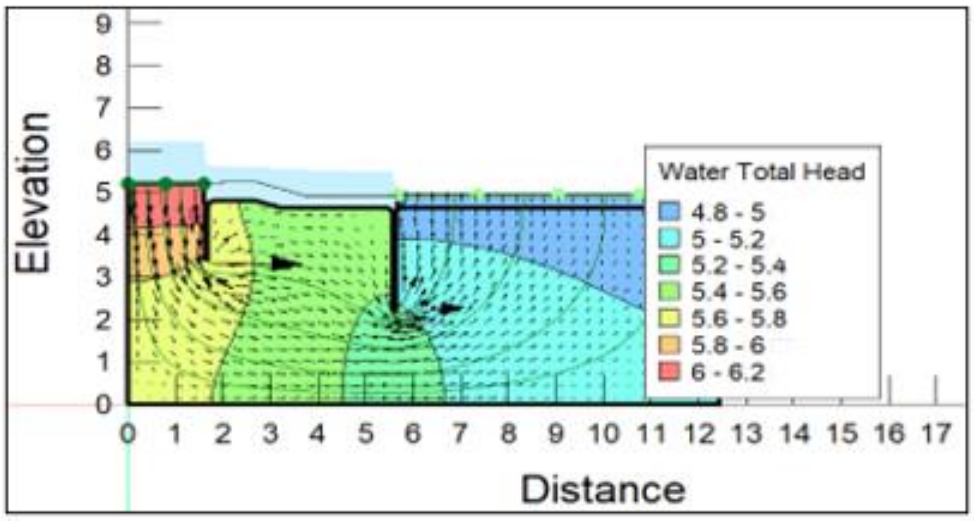


Figure (4.20): Flow net beneath barrage in case of max seepage rate.

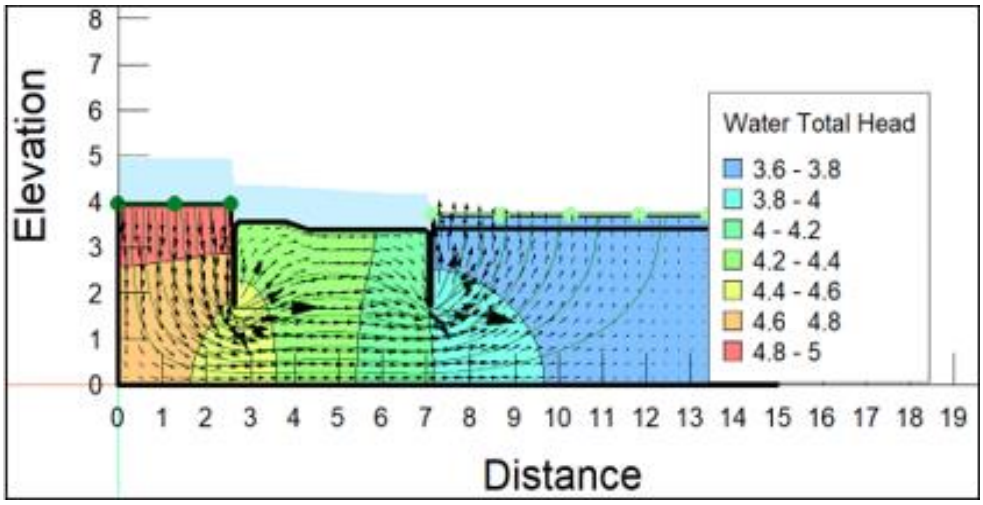


Figure (4.21): Flow net beneath barrage in case of min. seepage rate.

Figures (4.20), and (4.21), show the flow net distribution beneath the barrage in case of maximum and minimum seepage rates. Figure 4.20 shows that the maximum seepage flux beneath the barrage occurs at water total head ranging from (4.8 – 6.2), in this case the upstream cutoff depth is less than the downstream cutoff depth and the barrage dimension at minimum range. While for figure (4.21) shows that the seepage flux is at a minimum when the water total head ranged from (3.6 – 5) in which the upstream cutoff depth is larger than the downstream cutoff depth.

Figures (4.22), and (4.23), show the flow net distribution beneath the barrage in case of maximum and minimum exit gradient values.

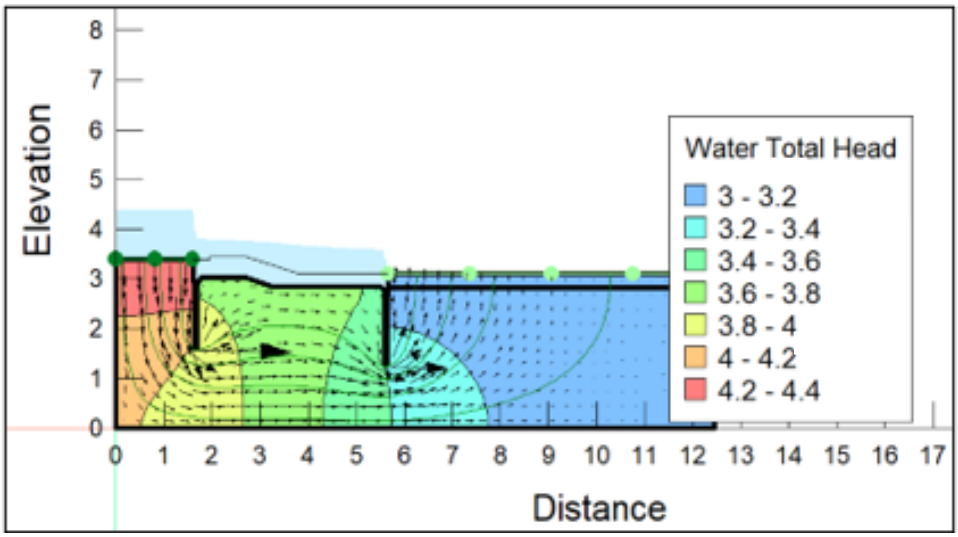


Figure (4.22): Flow net beneath barrage in case of max. Exit Gradient.

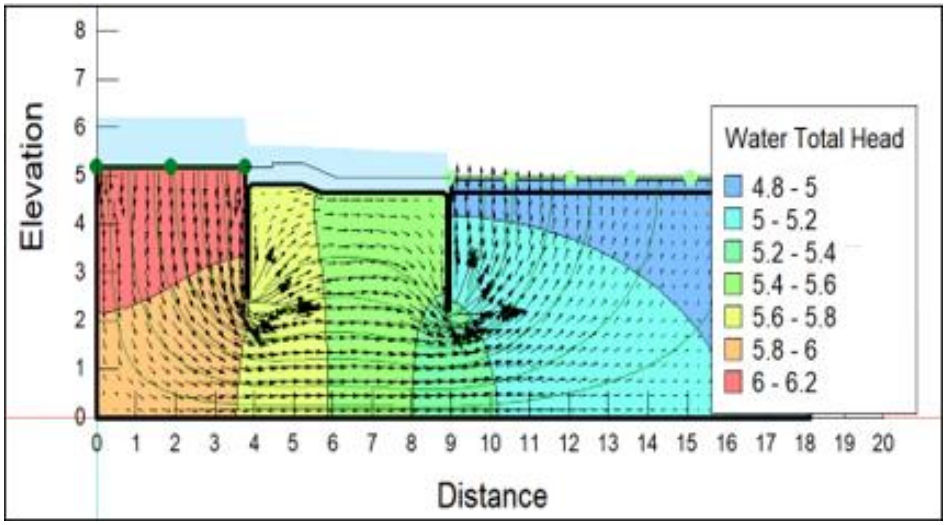


Figure (4.23): Flow net beneath barrage in case of min. Exit Gradient.

Figure (4.22), shows the maximum exit gradient that occurs at the water total head ranging from (3 - 4.4), in this case, the downstream cutoff depths are higher than the upstream cutoff depths. while in the case of distribution flow net at minimum exit gradient, as shown in figure (4.23), the water total head occurs at (4.8 -6.2), this case occurs when the upstream cutoff and downstream cutoff depth are at maximum value taken at this study.

Figures (4.24), and (4.25), show the flow net distribution in case of maximum and minimum uplift pressure.

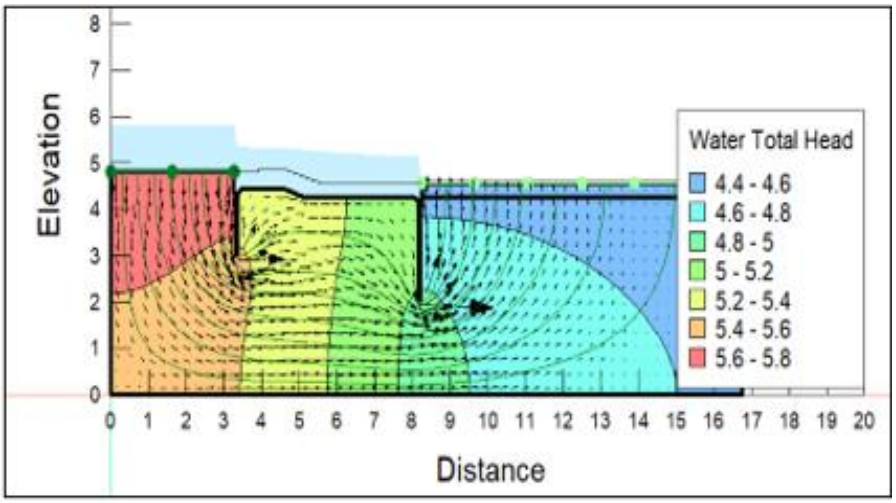


Figure (4.24): Flow net beneath barrage in case of max. uplift pressure.

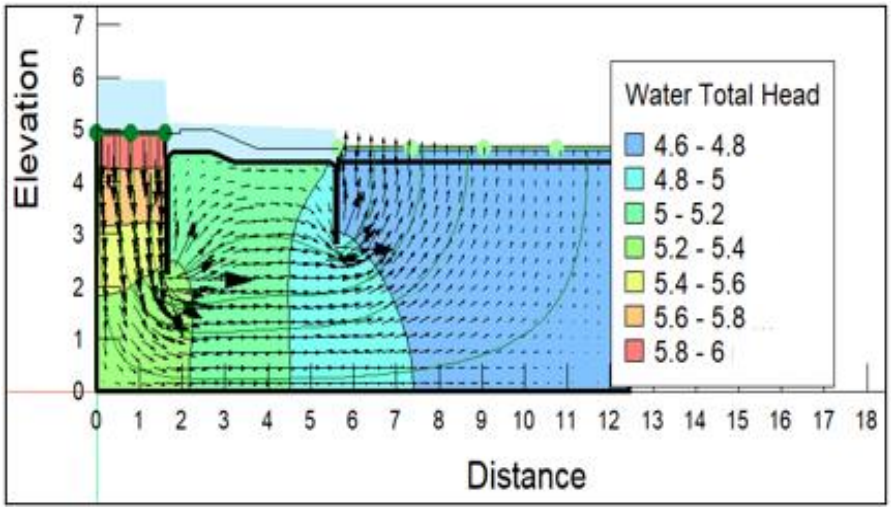


Figure (4.25): Flow net beneath barrage in case of min. uplift pressure.

Figure (4.24), shows that the maximum uplift pressure occurs at the water total head ranging from (4.4 -5.6), in this case, the downstream cutoff depth is larger than the upstream cutoff depth and this is the reason behind the increase of uplift pressure. While at minimum uplift pressure the distribution of flow net as shown in figure (4.25), the water total head ranged from (4.6 - 5.8), in this case, the downstream cutoff depth is least than the upstream cutoff depth.

# CHAPTER FIVE

# OPTIMAL DESIGN OF BARRAGE PROFILE

## 5.1 Statement of Optimization Problem

The solution to the optimization problem for the safe and, eventually, the most cost-effective design of the barrage profile is attempted in this study. The barrage section is adapted to be laid on a gypsiferous soil foundation with upstream and downstream sheet piles, as well as to an inverted filter provided at the end of a barrage. The solution method for the optimization problem introduce herein consists of objective functions and constraints. This method includes optimizing an array of objective functions with the profile of a barrage section area. The optimization is carried out subject to constraints to preserve a safe exit gradient; the uplift pressures exerted by seepage; and the hydraulic adequacy of stilling basin length. The design considers minimizing the total construction material and seepage flux beneath the floor foundation of the barrage.

### 5.1.1 Construction Materials for Barrage Floor

The thickness of the floor of barrage depends upon the residual pressure head attributed to uplift pressures exerted on the floor( Garg et al., 2002).Therefore, the volume of concrete between points (B) and (E) has been calculated by following two steps, Initially, provide concrete for a minimum thickness of floor between points (B) and (E), Then provide floor thickness in excess of the minimum wherever required depending upon the excess pressure head. However, for key points (B), (C), (D), and (E), the distribution of uplift pressures for the condition of fully closed gates is shown in figure (5.1). The objective function for minimizing the cost involves reducing the total volume

of construction materials of the barrage floor in addition to the upstream protection layers and inverted filter materials downstream.

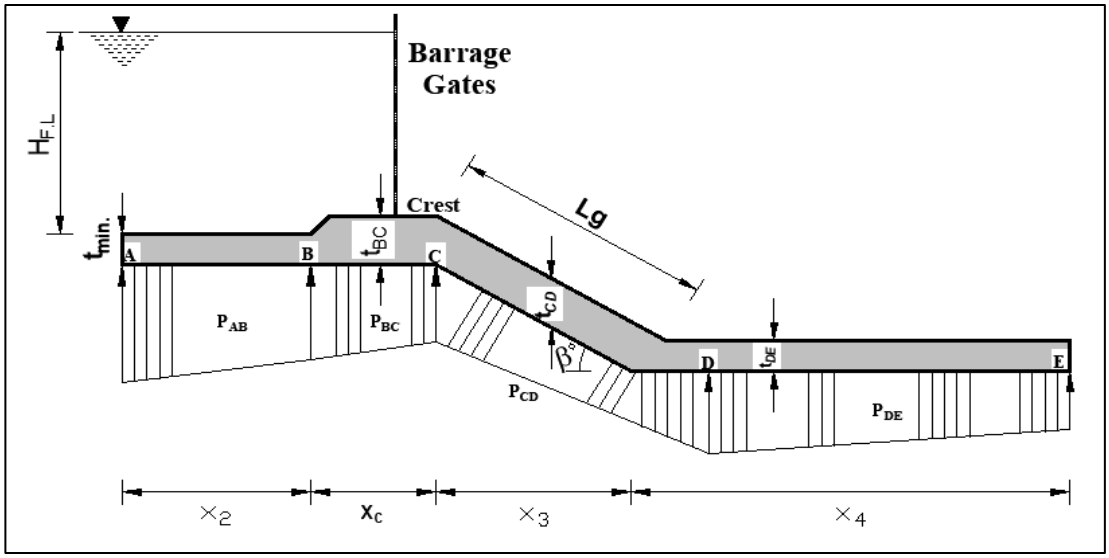


Figure (5.1): Distribution of uplift pressure beneath barrage floor.

Hence, the objective functions can be expressed by:

$$obj_1 = L_T \times t_{min.} + [(t_{BC} \times L_{cr}) + (t_{CD} \times L_G) + (t_{DE} \times L_s)] + (L_{SF} \times t_{PU}) + (L_{inv} \times t_{inv}) \quad (5.1a)$$

Where; $obj_1$ is the objective function for minimum construction material of the barrage floor ($L^3$ per meter width of the barrage), $L_T$ is the total length of concrete floor (L), $t_{min.}$ is the minimum thickness required of the barrage floor that resists the weight of water over the concrete floor corresponding to the condition of the completely closed gates, $t$ is the required thickness of the floor at any portion along the floor of the barrage. The non-dimensionlized form of Eq. (5.1a) can be written as:

$$\varphi_1 = \ell_f \times z_3 + \left[(t_{BC} \times x_6) + \left(t_{CD} \times L_g\right) + (t_{DE} \times x_4)\right] + (x_3 \times z_1) + (x_5 \times z_8) \quad (5.1b)$$

In which;

$$\ell_f = x_2 + x_6 + \frac{x_3}{\cos\beta} + x_4 \quad (5.2)$$

Where; $\varphi_1$ is the non-dimensionlized form of the total volume of construction materials of the barrage floor, $z_3$ is the non-dimensionlized form of the minimum thickness required for the barrage floor.

### 5.1.2 Total Seepage Flux Function

The total seepage discharge per unit length beneath the barrage floor across the porous flow domain can be defined in implicit form in compared with equation presented by Harr, (1998):

$$obj_2 = q_s = f(\frac{d_{su}}{T}, \frac{L_f}{T}) \quad (5.3)$$

Where; $obj_2$ is the objective function for seepage discharge, $q_s$ is the total seepage discharge in ($L^3$/sec per meter width of the barrage), $d$ is the depth of U/S cutoff walls (L), $L_f$ is the total length of the barrage floor (L), and $T$ is the depth of porous flow domain (L).

For the practical purposes, the depth of alluvium layer ($T$) that the barrage floor was proposed to be built is taken to be two times of the total floor length or the two times and a half depth of cutoff wall whichever is large (Harr, 1998). Because of the implicit nature of the seepage discharge, it was imperative that $obj_2$derived via multiple nonlinear regression technique. The non-dimensionlized form of Eq. (5.3) can be written as:

$$\varphi_2 = \frac{q_s}{KH} = f(\frac{z_2}{t_s}, \frac{\ell_f}{t_s}) \quad (5.4)$$

Where; $\varphi_2$ is the non-dimensionlized form of the objective function for seepage discharge, $K$ is the coefficient of permeability for the gypsiferous soils in the barrage foundation (L/T), $t_s$ is depth of the porous flow domain in non-dimensionlized form, and $H_{F.h}$ is the high flood head (L).

Moreover;

$$z_2 = \frac{d_{su}}{H_{F.h}} \quad (5.5\ a)$$

$$\ell_f = \frac{L_T}{H_{F.h}} \quad (5.5\ b)$$

$$t_s = \frac{T}{H_{F.h}} \qquad (5.5\ c)$$

The influence of different combinations of depth of cutoff walls ($z_2/t_s$) that located in U/S side and the barrage width as a function of ($\ell_f/t$) on the seepage discharge function ($q_s/KH$) was revealed in Figure (5.2).

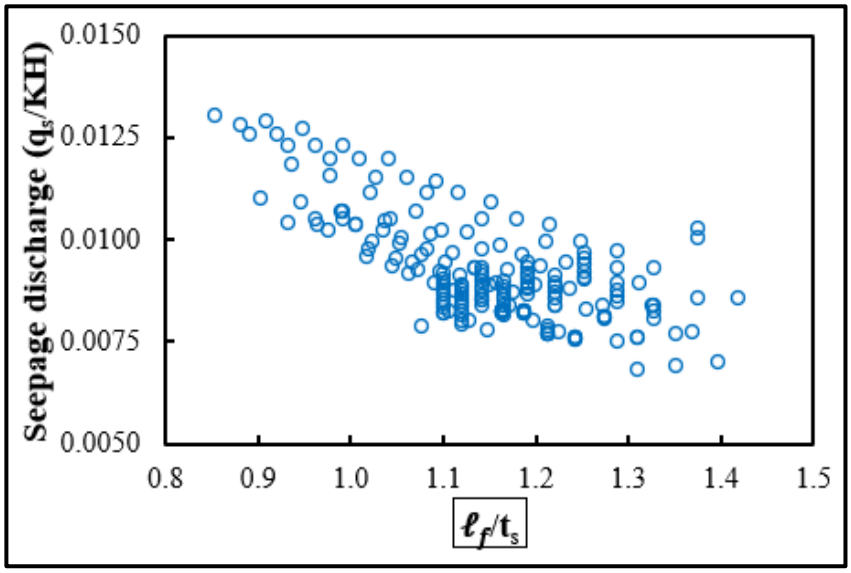


(a): ($q_s$/H) versus ($\ell_f/t_s$)

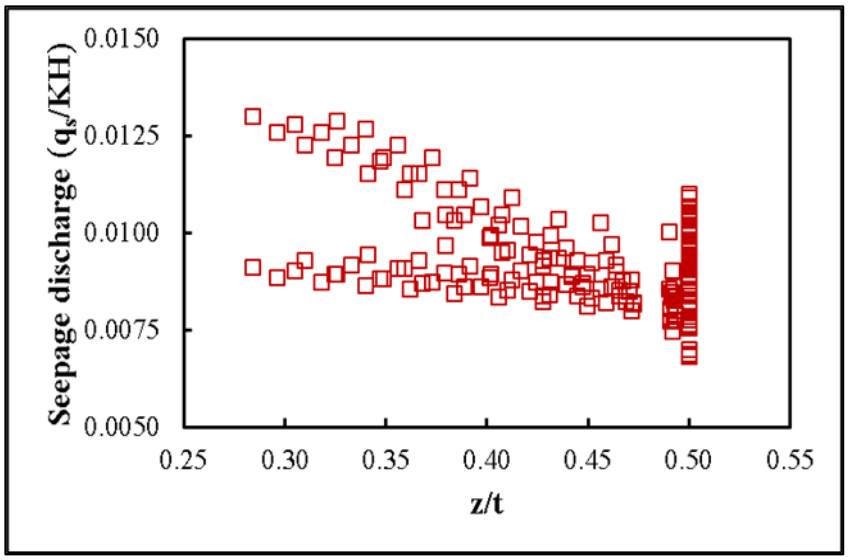


(b): ($q_s$/KH) versus ($z_2/t_s$).

Figure (5.2): Variation of ($q_s$/KH) function for various ($\ell_f/t_s$) and ($z_2/t_s$) for the investigated cases.

It is obvious from Figure (5.2a), that the seepage discharge was minimized when the floor length ratio ($\ell_f/t_s$) was ranged between (1.2-1.4), which approached the center of the barrage. On other hand, Figure (5.2b) reveals that the seepage discharge decreased slightly when the depth ratio of the cutoff walls decreased to reach a lower value when the ($z_2/t_s$) approached 0.5. As a result, the quantity of seepage discharge was evident that have a good correlation with prescribed variables. In this study, the following multiple non-linear models was proposed for the seepage flux objective function:

$$\varphi_2 = \alpha_0 \left(\frac{z_2}{t_s}\right)^{\alpha_1} \left(\frac{\ell_f}{t_s}\right)^{\alpha_2} \quad (5.6)$$

Based on multiple non-linear regression MNR analysis conducted via IBM SPSS Statistics 25 software, the ANOVA results and parameter estimates were given in Tables (5.1) and (5.2), respectively.

Table (5.1): Parameter estimates for the seepage discharge objective function $\varphi_2$.

| **Parameter** | **Estimate** | **Std. Error** | **95% Confidence Interval** | |
|---|---|---|---|---|
| | | | **Lower Bound** | **Upper Bound** |
| $\alpha_0$ | 0.008 | 0.000 | 0.008 | 0.009 |
| $\alpha_1$ | -0.244 | 0.042 | -0.326 | -0.162 |
| $\alpha_2$ | -0.872 | 0.068 | -1.006 | -0.739 |

Table (5.2): Results of ANOVA analysis for the seepage flux objective function $\varphi_2$.

| Source | Sum of Squares | df | Mean Squares |
|---|---|---|---|
| Regression | 0.017 | 3.0 | 0.006 |
| Residual | 0.0 | 197 | 0.0 |
| Uncorrected Total | 0.017 | 200 | |
| Corrected Total | 0.0 | 199 | |
| $R^2$= 0.617 | | | |

Depending on the evaluation criteria represented by the coefficient of determination ($R^2$), the derived model has a very good correlation. Accordingly; the final form for specific seepage flux function is:

$$\varphi_2 = 0.008\left(\frac{z_2}{t_s}\right)^{-0.244}\left(\frac{\ell_f}{t_s}\right)^{-0.872} \quad (5.7)$$

Likewise, the goodness of fit for Eq. (5.7) was examined graphically, as shown in Figure (5.3).

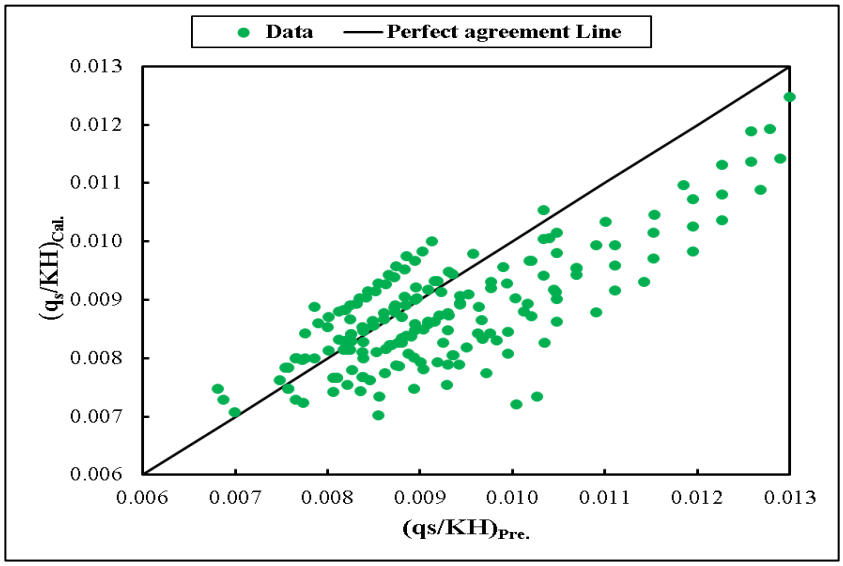


Figure (5.3): Scatter plot to reveal agreement of calculated ($q_s$/KH) versus predicted ($q_s$/KH) for predicted model.

It is evident from the results shown in Figure (5.3) that the MNR model findings were reasonable but under-estimated value.

## 5.2 Formulation of Problem Constraints

The multi-objective functions are subjected to constraints vector *C*:

$C = \{C_1, C_2, C_3\}$

### 5.2.1 Exit Gradient Constraint

The exit gradient ($i_{exit}$) around the downstream toe of the cutoff wall can be expressed in implicit form as (Harr, 1998):

$$i_{exit} = \emptyset(d_{D/S}, T, H) \quad (5.8)$$

Where; $d_{D/S}$ is the depth of downstream cutoff wall. In non-dimensionlized form, Eq. (5.8) can be written as:

$$\frac{i_{exit}}{H_{F.h}} = \psi\left(\frac{z_7}{t}, \frac{H_{F.h}}{z_7}\right) \quad (5.9)$$

A similar procedure was carried out as for Eq. (5.7); the form for the exit gradient can be proposed as:

$$\frac{i_{exit}}{H_{F.h}} = \beta_0 \left(\frac{z_7}{t}\right)^{\beta_1} \left(\frac{H_{F.h}}{z_7}\right)^{\beta_2} \quad (5.10)$$

The parameter estimates and ANOVA test statistics are given in Tables (5.3) and (5.4), respectively.

Table (5.3): Parameter estimates for exit gradient function.

| **Parameter** | **Estimate** | **Std. Error** | **95% Confidence Interval** | |
|---|---|---|---|---|
| | | | **Lower Bound** | **Upper Bound** |
| $\beta_0$ | 0.154 | 0.006 | 0.142 | 0.166 |
| $\beta_1$ | 0.694 | 0.026 | 0.642 | 0.746 |
| $\beta_2$ | 0.540 | 0.039 | 0.464 | 0.616 |

Table (5.4): Output for ANOVA analysis for exit gradient function.

| Source | Sum of Squares | df | Mean Squares |
|---|---|---|---|
| Regression | 0.867 | 3 | 0.289 |
| Residual | 0.002 | 196 | 0.0 |
| Uncorrected Total | 0.868 | 199 | |
| Corrected Total | 0.008 | 198 | |
| $R^2$= 0.777 | | | |

The final form of the exit gradient function is:

$$\frac{I_{exit}}{H} = 0.154 \left(\frac{z_7}{t}\right)^{0.694} \left(\frac{H}{z_7}\right)^{0.54} \quad (5.11)$$

Moreover, a graphical representation to reveal the goodness of fit for Eq. (5.11) was shown in Figure (5.4).

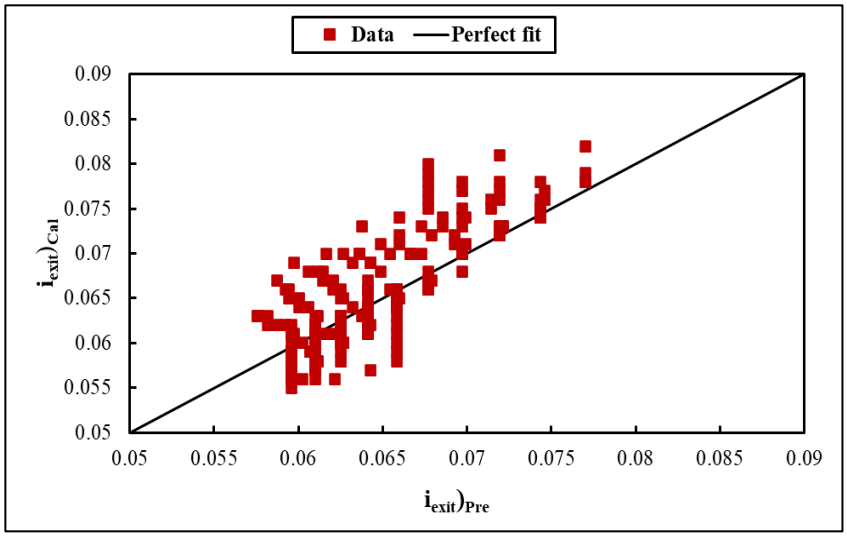


Figure (5.4): Scatter plot to reveal agreement of calculated ($i_{exit}$) versus predicted ($i_{exit}$) by the developed hydraulic model.

For safe exit gradient:

$$i_{exit} \leq i_{Critical} \quad (5.12)$$

According to Khosla theory, to maintain the structural stability against piping, the exit gradient is maintained at a level equal to 0.25 to 0.5 times the critical exit gradient. Garg, (1976), reported that at the critical condition, the critical exit gradient is:

$$\left(\frac{G_S - 1}{1 + e}\right) \tag{5.13}$$

Where; $G_S$ is the specific gravity of soil particle, *e* is the void ratio of the soil. Accordingly;

$i_{exit} \leq \frac{1}{5} \left(\frac{G_S - 1}{1 + e}\right)$

Thus, by substituting above term in Eq. (5.12); we get:

$0.154 \left(\frac{Z_7}{t}\right)^{0.694} \left(\frac{H}{Z_7}\right)^{0.54} \leq \frac{1}{5} \left(\frac{G_S - 1}{1 + e}\right)$

For the soil in the present study, $G_S$=2.63 and *e*=0.67; Eq. (5.12) become as following:

$$0.154 \left(\frac{Z_7}{t}\right)^{0.694} \left(\frac{H}{Z_7}\right)^{0.54} \leq 0.195 \tag{5.14}$$

### 5.2.2 Sufficient Length for Stilling Basin

The stilling basin length must be sufficient to withdraw the length of the hydraulic jump. The stilling basin is the most common form of energy dissipater converting the supercritical flow from the spillway into subcritical flow compatible with the downstream river regime Novak et al., (2008):

$$L_S = 6(y_2 - y_1) \tag{5.15}$$

Where; $L_S$ is the stilling basin length, $y_1$ is the pre-jump depth, and $y_2$ is the post-jump depth. In non-dimensionlized form. Now, the non-dimensional definition for design variable is: $L_S = x_4$, $y_1 = z_9$ and $y_2 = z_{10}$. Thus, Eq. (5.15) transformed into non-dimensional form as:

$$x_4 = 6(z_{10} - z_9) \tag{5.16}$$

### 5.2.3 Uplift Pressures Constraints

Referring to the Figure (5.1), $P_{BC}, P_{CD}, P_{DE}$ are the uplift pressures exerted on the upstream part of the floor (AB portion), the crest and stilling basin parts of the floor (BC and CD portions) and downstream part of the floor (DE portion), respectively. For safe design, the overall applied downward pressure from dead, live, and impact loads must resist (balanced) the uplift pressure ***P***, thus:

$$P \leq (SG - 1)\gamma_w t \tag{5.17}$$

Or; by re-arranging in term of floor thickness;

$$t \geq \frac{P}{(SG - 1)\gamma_w} \tag{5.18}$$

Where; *SG* is the specific weight of concrete. The uplift pressure zones were divided into three portions. The uplift pressures exerted on the portion (BC) can be calculated as:

$$P_{BC} = \frac{(P_B + P_C)}{2} \times x_c \tag{5.19}$$

Where; $x_c$ is the length of the crest portion from the floor. The uplift pressures that act on the inclined floor, which represents the length of the stilling basin, or portion (CD), can be derived as shown in figure (5.5):

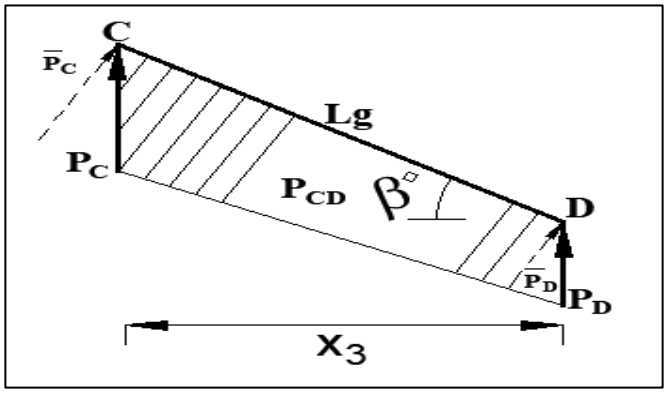


Figure (5.5): Uplift Pressure distribution along stilling basin portion.

$$L_g = \frac{x_3}{cos(\beta)} \tag{5.20}$$

Since; $\bar{P}_C = P_C cos(\beta)$ and $\bar{P}_D = P_D cos(\beta)$; therefore:

$$P_{CD} = \frac{(\bar{P}_C + \bar{P}_D)}{2} L_g \tag{5.21}$$

Thus;

$$P_{CD} = \frac{(P_C + P_D)cos(\beta)}{2}\left[\frac{x_3}{cos(\beta)}\right]$$

By simplifying and re-arrangement, we get:

$$P_{CD} = \frac{(P_C + P_D)}{2} \times x_3 \tag{5.22}$$

For the downstream portion (DE) of the barrage floor:

$$P_{DE} = \frac{(P_D + P_E)}{2} \times x_4 \tag{5.23}$$

Figure (5.6) shows the variation of uplift pressures along the floor portions of the barrage.

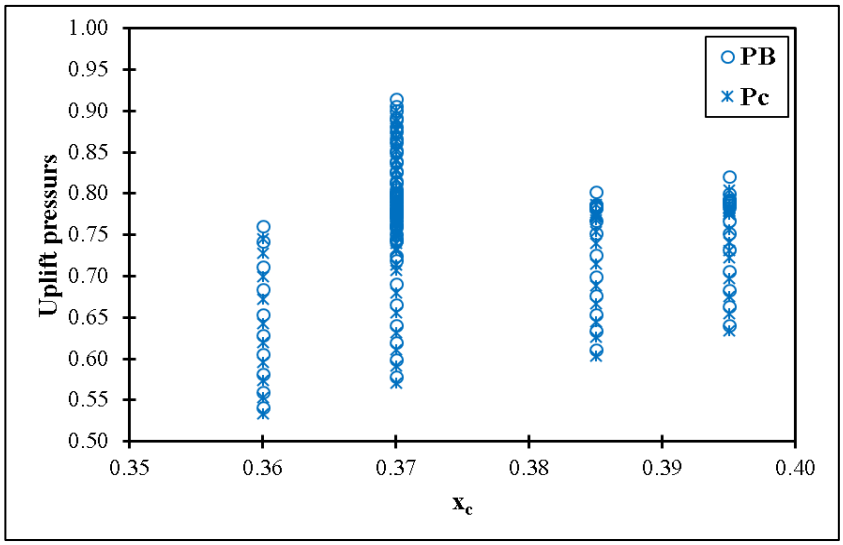


(a) For barrage crest portion.

Figure (5.6): Distribution of uplift pressures at key points along the floor portions of the barrage.

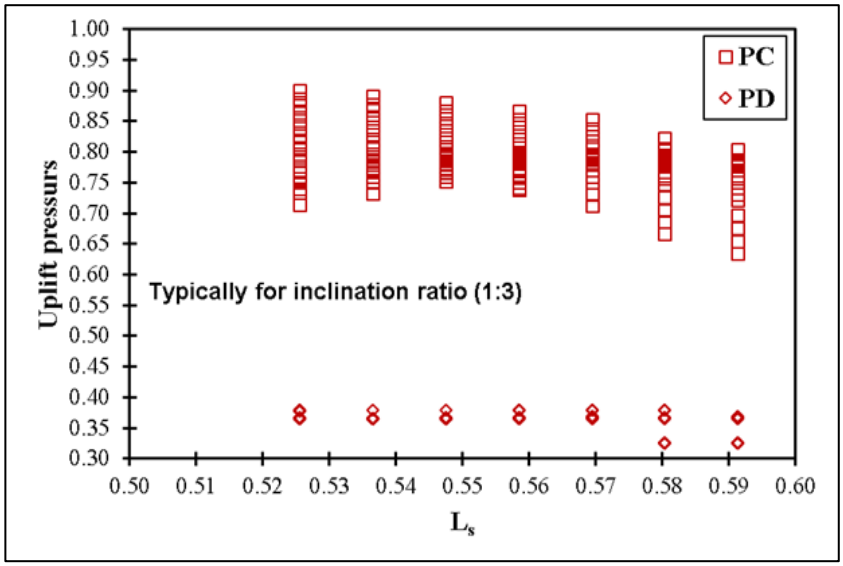


(b) For stilling basin portion.

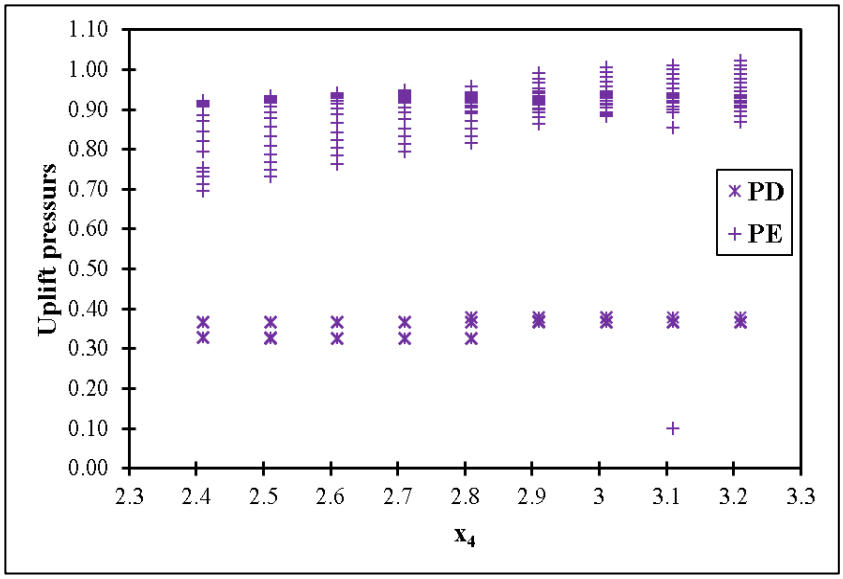


(c) For downstream portion of the floor.

Figure (5.6): continue.

By recalling Eq. (5.18), the required thickness of each portion of the barrage floor can be expressed explicitly. For the portion (BC):

$$t_{BC} \geq \frac{P_{BC}}{(SG-1)\gamma_w} \tag{5.24}$$

Similarly; for the portion (CD):

$$t_{CD} \geq \frac{P_{CD}}{(SG-1)\gamma_w} \quad (5.29)$$

Finally; for the portion (DE):

$$t_{DE} \geq \frac{P_{DE}}{(SG-1)\gamma_w} \quad (5.30)$$

Hence;

$P_{BC} = f_1(P_B, P_C, x_c)$,$P_{CD} = f_2(P_C, P_D, x_3)$and$P_{DE} = f_3(P_D, P_E, x_4)$

The multiple linear regression analysis was used to determine these relations. Table (5.5) gives the descriptive statistics for $P_{BC}$multiple linear models. On other hand, Table (5.6) presents the $P_{BC}$ model summary.

Table (5.5): Descriptive statistics for data used for deriving$P_{BC}$ model.

| Statistic / Variable | Maximum | Minimum | Mean | Std. Deviation |
|---|---|---|---|---|
| **$P_{BC}$** | 0.9075 | 0.5375 | 0.7717 | 0.0628 |
| **$P_B$** | 0.915 | 0.541 | 0.7767 | 0.0632 |
| **$P_C$** | 0.90 | 0.534 | 0.7661 | 0.0625 |
| **$x_c$** | 0.445 | 0.360 | 0.3992 | 0.0285 |

Table (5.6): Correlation summary for $P_{BC}$ model.

| Model | $R^2$ | SEE* |
|---|---|---|
| $P_{BC}$ | 1.00 | $2.52\times10^{-04}$ |

Accordingly;

$$P_{BC} = 0.502P_B + 0.498P_C - 0.01x_c \quad (5.31)$$

Figure (5.7) shows the variation of predicted uplift pressure $(P_{BC})_{Pr.}$ from Eq. (5.31) against calculated $(P_{BC})_{Cal.}$ Similarly, Tables (5.7 and 5.8) present the descriptive statistics and correlation summary for $P_{CD}$ model.

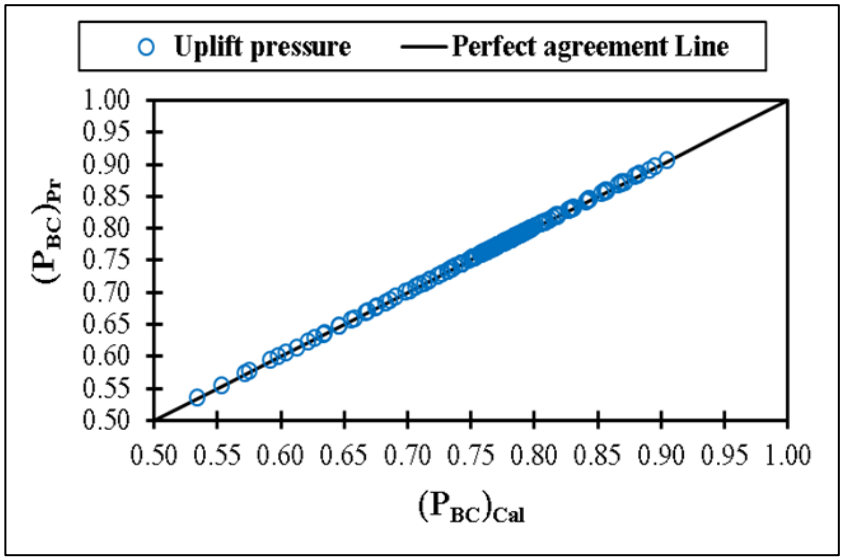


Figure (5.7): Variation of $(P_{BC})_{Pr.}$ versus $(P_{BC})_{Cal.}$ for the crest portion of the barrage floor.

Table (5.7): Descriptive statistics for data used for deriving$P_{CD}$ model.

| Statistic / Variable | Maximum | Minimum | Mean | Std. Deviation |
|---|---|---|---|---|
| **$P_{CD}$** | 0.9615 | 0.434 | 0.8370 | 0.0668 |
| **$P_C$** | 0.90 | 0.534 | 0.7661 | 0.0625 |
| **$P_D$** | 0.379 | 0.326 | 0.3579 | 0.0185 |
| **$x_3$** | 0.624 | 0.526 | 0.575 | 0.0314 |

Table (5.8): Correlation summary for $P_{CD}$ model.

| Model | $R^2$ | SEE* |
|---|---|---|
| $P_{CD}$ | 0.815 | $2.9\times10^{-02}$ |

Therefore;

$$P_{CD} = 1.005P_C - 0.029P_D + 0.139x_3 - 0.002 \quad (5.32)$$

Figure (5.8) displays the changes between the predicted uplift pressure $(P_{CD})_{Pr.}$ from Eq. (5.32) against calculated $(P_{CD})_{Cal.}$ Finally, Tables (5.9) and (5.10) gives the descriptive statistics and correlation summary for $P_{DE}$ model.

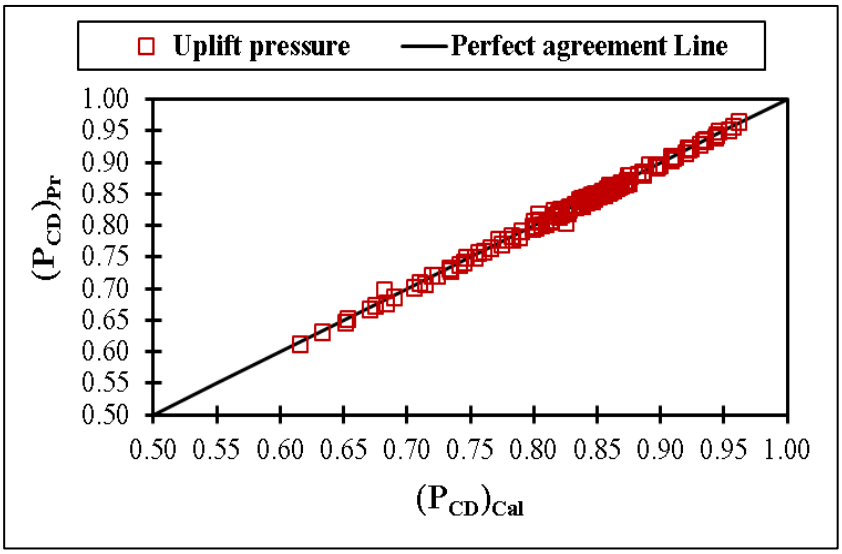


Figure (5.8): Variation of $(P_{CD})_{Pr.}$ versus $(P_{CD})_{Cal.}$ for the stilling basin portion of the barrage floor.

Table (5.9): Descriptive statistics for data used for deriving$P_{DE}$ model.

| Statistic / Variable | Maximum | Minimum | Mean | Std. Deviation |
|---|---|---|---|---|
| **$P_{DE}$** | 0.6945 | 0.233 | 0.6329 | 0.0454 |
| **$P_D$** | 0.379 | 0.326 | 0.3579 | 0.0185 |
| **$P_E$** | 0.943 | 0.10 | 0.9073 | 0.0818 |
| **$x_4$** | 3.31 | 2.41 | 2.860 | 0.2880 |

Table (5.10): Correlation summary for $P_{DE}$ model.

| Model | $R^2$ | SEE* |
|---|---|---|
| $P_{DE}$ | 1.00 | $2.51\times10^{-04}$ |

Consequently;

$$P_{DE} = 0.501P_D + 0.5P_E - 9.0 \times 10^{-05}x_4 \qquad (5.33)$$

Figure (5.9) shows the variations between the predicted uplift pressure $(P_{DE})_{Pr.}$ from Eq. (5.33) against calculated $(P_{CD})_{Cal.}$

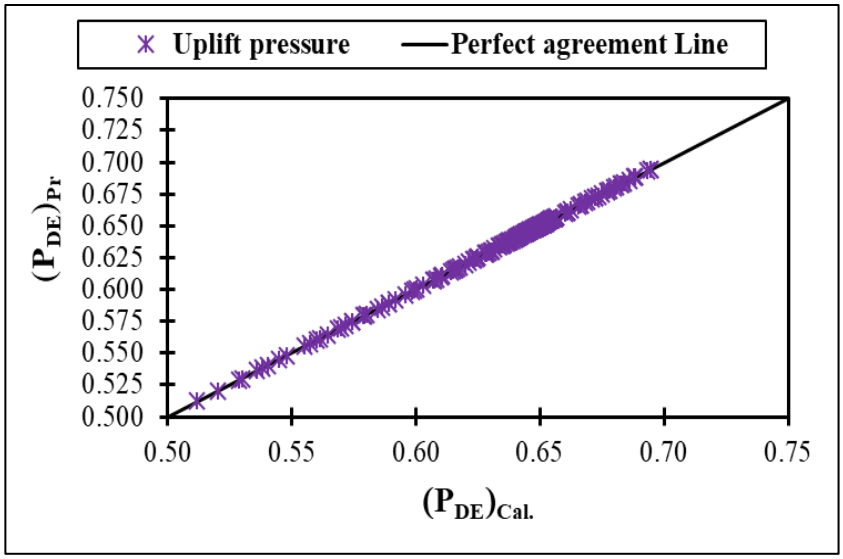


Figure (5.9): Variation of $(P_{DE})_{Pr.}$ versus $(P_{DE})_{Cal.}$ for downstream portion of the barrage floor.

Based upon the statistical analysis that was carried out formerly; relations between the calculated uplift pressures versus the derived models reveal a perfect to very good correlation. Accordingly, involving these models in the final version of Eq. (5.18) is probably substantial. Substitution of Eqs. (5.31, 5.32, and 5.33) into Eq. (5.18), yields the floor thickness per each portion along the barrage length versus the prescribed uplift pressures constraints as:

$$t_{BC} \geq \frac{(0.502P_B + 0.498P_C - 0.01x_c)}{(SG-1)\gamma_w} \tag{5.34}$$

$$t_{CD} \geq \frac{(1.005P_C - 0.029P_D + 0.139x_3 - 0.002)}{(SG-1)\gamma_w} \tag{5.35}$$

$$t_{DE} \geq \frac{(0.501P_D + 0.5P_E - 9.0 \times 10^{-05}x_4)}{(SG-1)\gamma_w} \tag{5.35}$$

## 5.3 Multi-Objectives Optimization Functions

The multi-objective optimization problem involving the minimization of barrage construction material and seepage flux underneath barrage floor. The structure of multi-objective optimization vector of the present study is:

$$\text{Find } X = \begin{Bmatrix} x_1 \\ x_2 \\ x_3 \\ x_4 \\ x_5 \\ x_6 \end{Bmatrix}, \qquad Z = \begin{Bmatrix} z_1 \\ z_2 \\ z_3 \\ z_7 \\ z_8 \\ z_9 \\ z_{10} \end{Bmatrix}$$

Which minimize:

$$\varphi = \{\varphi_1(x,z), \varphi_2(x,z)\}$$

Subject to:

$$C = \{C_1(x,z), C_2(x,z)\}$$

$$x^l \le x \le x^u$$

$$z^l \le z \le z^u$$

Hence, the final form of the multi-objective optimization problem in present study from Eqs. (5.1b), and (5.7) is:

$$\varphi 1 = \left(x_2 + x_6 + \frac{x_3}{cos\beta} + x_4\right) \times z_3 + \left[t_{BC} \times x_6 + t_{CD} \times \frac{x_3}{cos\beta} + t_{DE} \times x_4\right] + x_1.z_1 + x_5.z_8$$

$$\varphi 2 = 0.008\left(\frac{z_2}{t_s}\right)^{-0.244}\left(\frac{\ell_f}{t_s}\right)^{-0.872}$$

Subjected to the following constraints which are the Eqs. (5.14), and (5.16);

$$0.154\,(\frac{z_7}{t_s})^{0.694}(\frac{H_{F.h}}{z_7})^{0.54} - 0.195 \le 0$$

$$x_4 + 6z_9 - 6z_{10} \le 0$$

The uplift pressure constraint is implicit with the objective function of minimum construction material of barrage.

Upper and lower bound of the design variables of the optimization problem in normalized form are from table (4.5);

$1.6 \leq x_1 \leq 3.76$

$1.09 \leq x_2 \leq 1.45$

$0.48 \leq x_3 \leq 0.57$

$2.41 \leq x_4 \leq 3.41$

$6.79 \leq x_5 \leq 9.44$

$0.72 \leq x_6 \leq 0.88$

$0.19 \leq z_1 \leq 0.23$

$1.35 \leq z_2 \leq 2.25$

$0.37 \leq z_3 \leq 0.38$

$1.48 \leq z_7 \leq 2.38$

$0.27 \leq z_8 \leq 0.31$

$0.39 \leq z_9 \leq 0.43$

$0.83 \leq z_{10} \leq 0.94$

$x_1, x_2, x_3, x_4, x_5, x_6, z_1, z_2, z_3., z_7, z_8, z_9, z_{10} \geq 0$

## 5.4 Solution of Multi-Objective Optimization Problem by Genetic Algorithm

Genetic algorithms (GA) are a popular optimization method for solving multi-objective optimization problems (MOPs). The basic idea of a GA for MOPs is to evolve a population of candidate solutions that represent a trade-off between multiple objectives (Maghawry, 2021). In this study, the following steps for solving the underlying optimization problem by GA are revealed by the flowchart shown in figure (5.10).

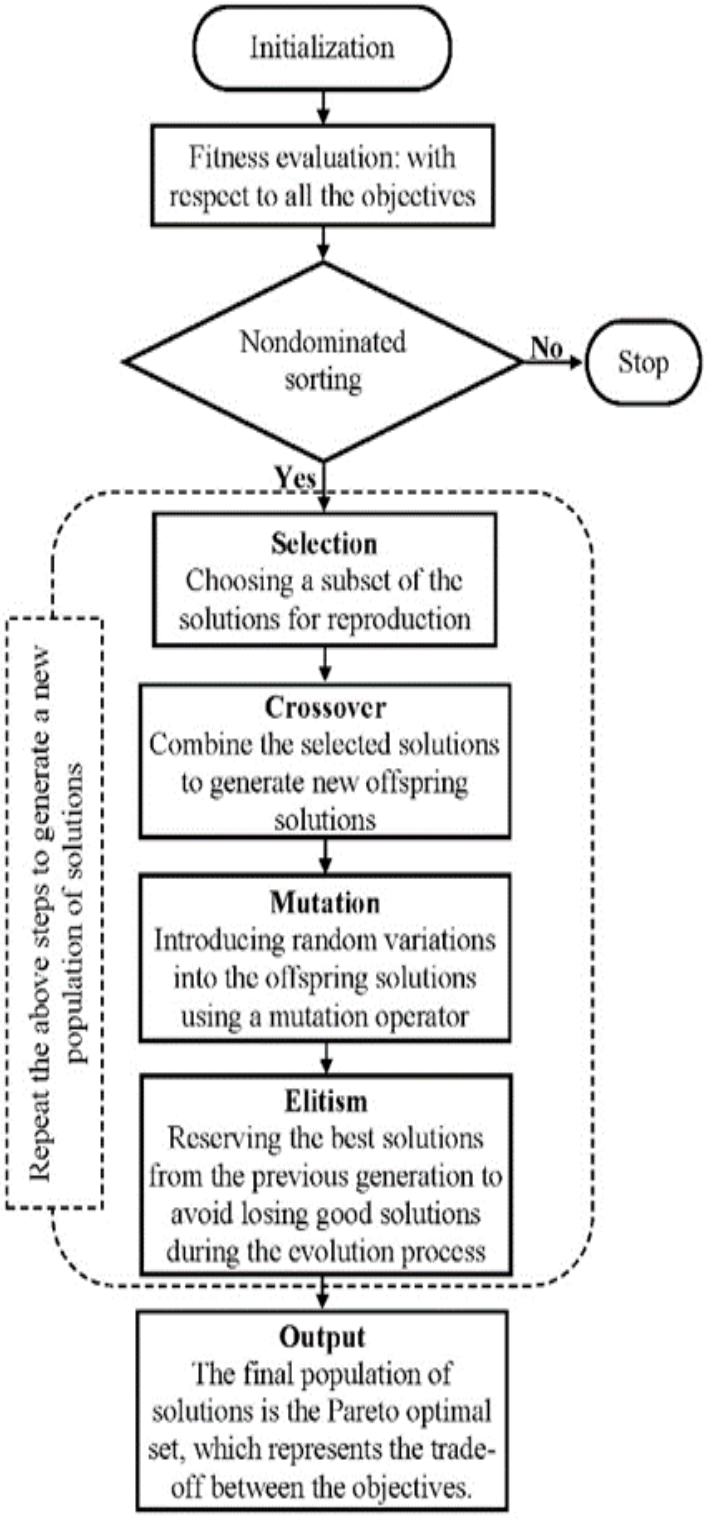


Figure (5.10): Genetic algorithm for MOPs problems.

In this study, the MOP's can be solved using a Genetic Algorithm (GA) with MATLAB software R2015a. MATLAB offers the "Genetic Algorithms and Direct Search Solvers" that provides a software-based optimization using GA. The process of GA involves continuously modifying a population or set of solutions or individuals throughout the entire run. In each step, the GA selects individuals from the current population to be the parents, based on certain criteria, and uses them to generate the next generation, known as the children. Through successive generations, the population evolves towards finding an optimal solution or a set of Pareto optimal solutions in the case of a multi-objective problem. The GA Solver within the Global Optimization Toolbox has various GA capabilities that are available in software form. The "GA" command in the syntax provides the ability to perform nonlinear optimization with constraints, while the "GAMULTIOBJ" command enables optimization of multiple objectives.

### 5.4.1 Optimum Solution of Research Problem

This research introduces an optimization technique for the hydraulic design of a barrage, which involves solving a nonlinear constrained problem. 56 runs of a GA algorithm were conducted using default settings and varying population sizes (200, 600, 1000, and 1400). The fitness and constraint functions, named "objective" (coded in MATLAB as 'obj-barrage') and "constraints" (coded as 'cons-barrage'), were identified and implemented as M-file scripts. The values of lower bounds for design variables are (1.6, 1.09, 0.48, 2.41, 6.79, 0.72, 0.19, 1.35, 0.37, 1.48, 0.23, 0.39, 0.83), and the for upper bounds are (3.76, 1.45, 0.57, 3.41, 9.44, 0.88, 0.23, 2.25, 0.38, 2.38, 0.31, 0.43, 0.94). Figure (5.11) displays the user interface windows for configuring the optimization tool settings.

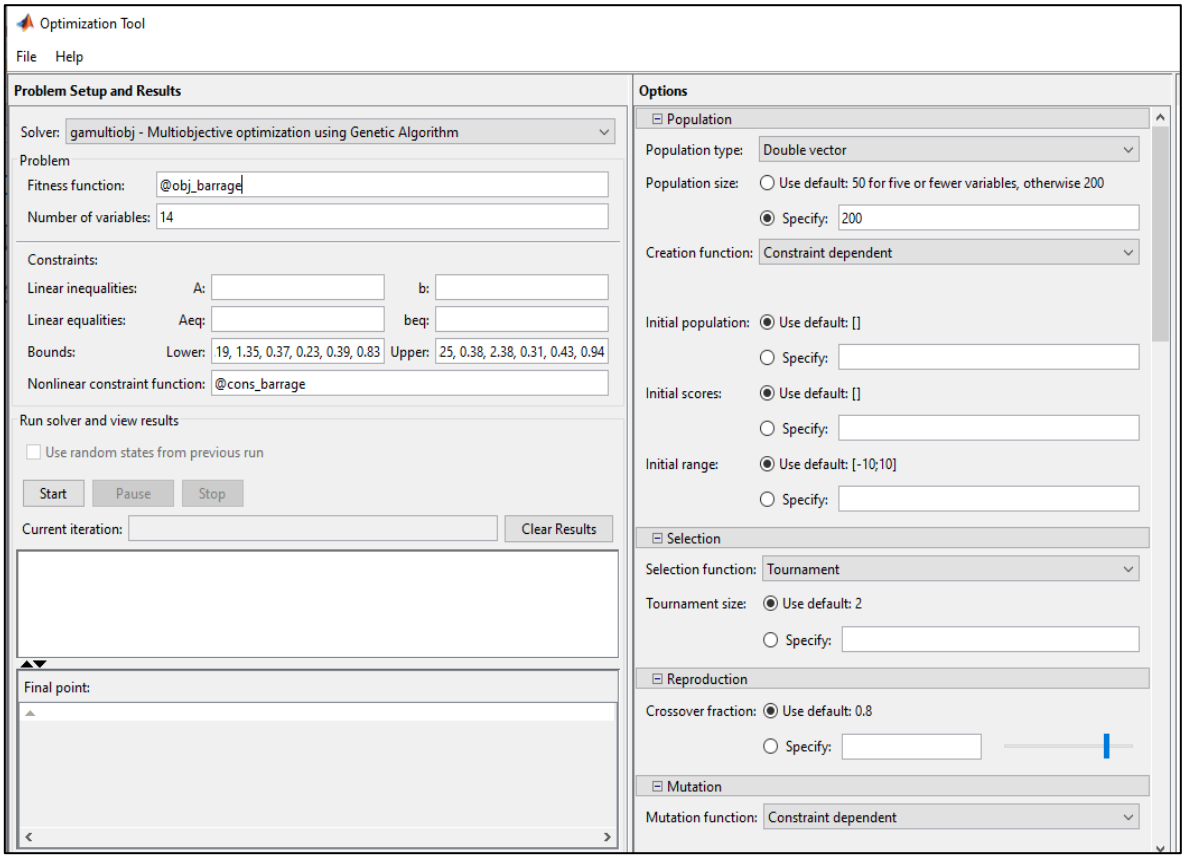


Figure (5.11): MATLAB genetic algorithm toolbox.

Table (5.13) shows the results of using the optimization problem model with the standard configuration and varying population sizes of 200, 600, 1000, and 1400.

Table (5.11): Results of optimum values of design variables result from application of GA optimization model.

| **Design Variables** | **Population Size** | | | |
|---|---|---|---|---|
| | **200** | **600** | **1000** | **1400** |
| Length of upstream protection($x_1$). | 1.60 | 1.60 | 1.60 | 1.60 |
| Length of upstream floor ($x_2$). | 1.09 | 1.09 | 1.11 | 1.09 |
| Projection length of inclined floor ($x_3$). | 0.48 | 0.48 | 0.48 | 0.48 |
| length of downstream floor ($x_4$) | 2.41 | 2.41 | 2.41 | 2.41 |
| Length of inverted filter layer ($x_5$). | 6.79 | 6.79 | 6.79 | 6.79 |
| Length of crest ($x_6$). | 0.72 | 0.72 | 0.72 | 0.72 |

Table (5.11): continue.

| | | | | |
|---|---|---|---|---|
| Thickness of upstream protection layer ($z_1$). | 0.19 | 0.19 | 0.19 | 0.19 |
| Depth of upstream cutoff wall ($z_2$). | 1.37 | 1.41 | 1.70 | 1.44 |
| Minimum thickness required ($z_3$). | 0.37 | 0.37 | 0.37 | 0.37 |
| Depth of downstream cutoff wall ($z_7$). | 1.48 | 1.48 | 1.52 | 1.48 |
| Thickness of inverted filter drain ($z_8$) | 0.27 | 0.27 | 0.27 | 0.27 |
| Pre-jump depth of water ($z_9$). | 0.39 | 0.43 | 0.39 | 0.39 |
| Post-jump depth of water ($z_{10}$). | 0.83 | 0.83 | 0.86 | 0.94 |
| Minimum construction volume ($\varphi_1$). | 4.9341 | 4.9341 | 4.9419 | 4.9341 |
| Minimum seepage flux ($\varphi_2$). | 0.0023 | 0.0021 | 0.0016 | 0.0021 |

The non-dimensional cost function and seepage flux variation for various population sizes across generations data are demonstrated in Figures (5.12) and (5.13).

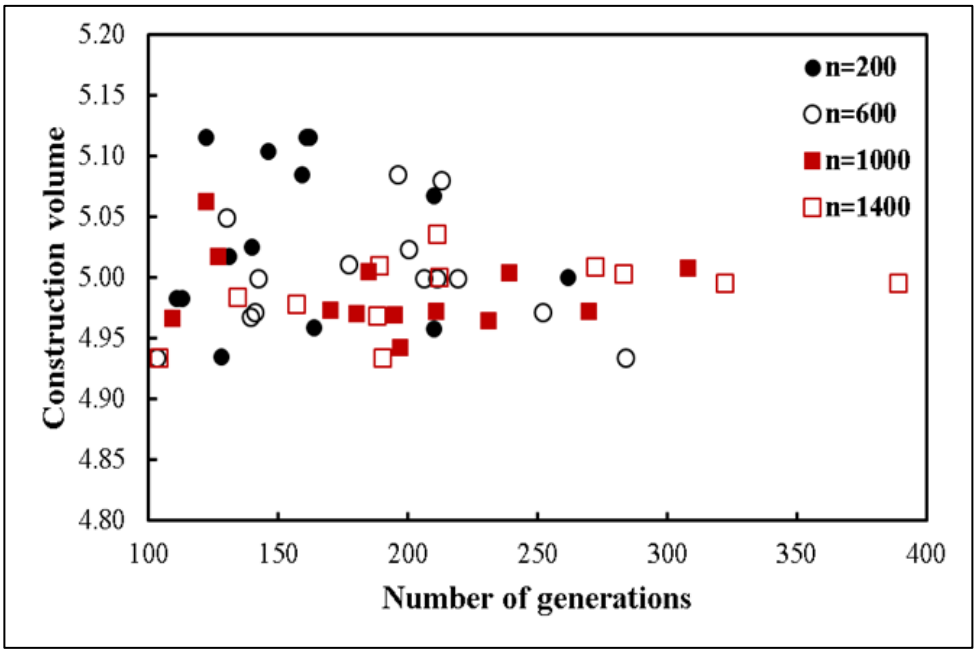


Figure (5.12): Variation of the non-dimensional construction volume versus the number of generations data for different population sizes.

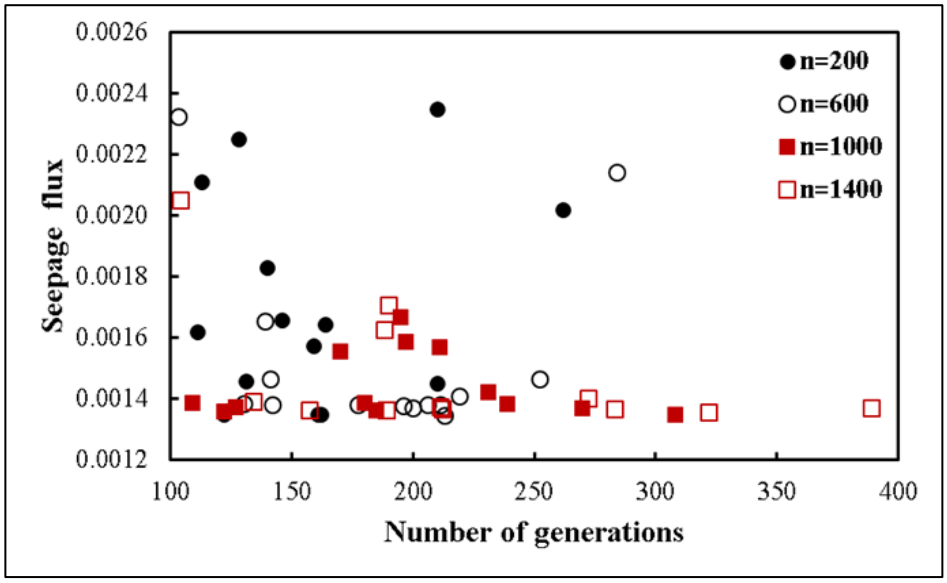


Figure (5.13): Variation of the non-dimensional seepage flux versus the generations data for different population sizes.

From figures (5.12) and (5.13), it is obvous that there are several effects in which the size of the population and the number of generations can influence the optimization solution found by genetic algorithm. First, the size of the population can affect the variety of the solutions that were explored by the algorithm. If the population size is small, the algorithm may obtain closer in a local minimum and be unable to find the global minimum. On the other hand, if the population size is large, the algorithm may take longer time to run and may be less efficient. The number of generations can also have an impact on the optimization results. If the number of generations is small, the algorithm may not have enough time to thoroughly explore the search space and find the optimal solution. On the other hand, if the number of generations is too large, the algorithm may run for an unnecessarily long time, even if it has already found the optimal solution.

It is important to find a balance between the size of the population and the number of generations in order to obtain reliable optimization results. In the

present study, 56 runs were conducted and distributed between four groups with 14 runs per group for population sizes from 200 to 1400.

Figure (5.14) shows the uplift pressure distribution beneath the barrage floor on key points along the floor corresponding to minimum non-dimensional construction volume objective function ($f_1^*$) and non-dimensional seepage flux objective function ($f_2^*$), respectively.

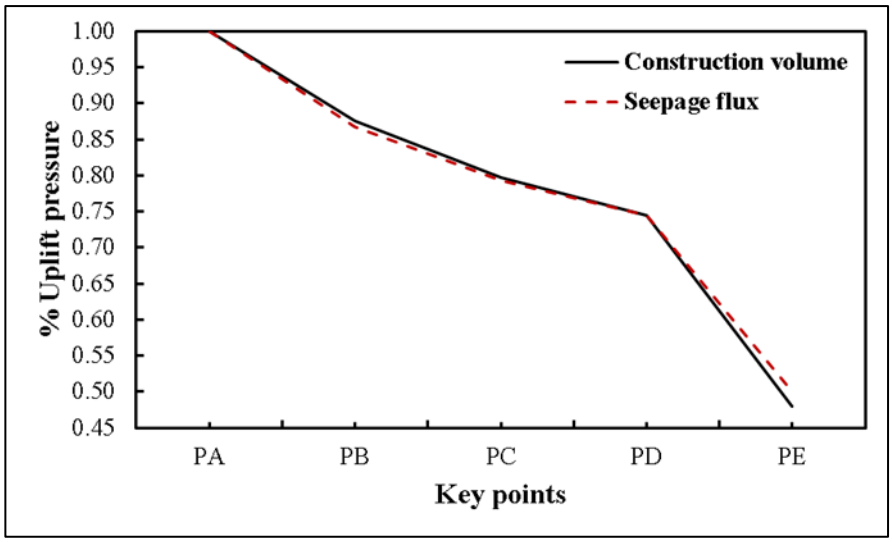


Figure (5.14): Distribution of uplift pressures on key points in the barrage floor corresponding to ($f_1^*$) and ($f_2^*$).

The results of figure (5.14) indicated that the uplift pressure distributions were close to each other. However, for ($f_1^*$), these values were accompanied by a population size (200 and 600), while for ($f_2^*$) they accompany a population size of 200. From the previous discussion, it was exhibited that the population size of 600 could be satisfactory to meet the solution of the constrained nonlinear optimization problem of optimal hydraulic design of the problem under consideration.

The following vectors present the optimal values for non-dimensional design variables:

$X^* = \{x_1^*,\ x_2^*, x_3^*, x_4^*, x_5^*, x_6^*\}$

$Z^* = \{z_1^*,\ z_2^*, z_3^*, z_7^*, z_8^*, z_9^*, z_{10}^*\}$

In order to simplify and make the design of the barrage profile and dimensions applicable, design charts were introduced in figures (5.15 to 5.24) that incorporated the optimal design variables in non-dimensionlized form. All the design charts are for population size of 600, while the design charts for population size of 200 are introduced later in appendix A.

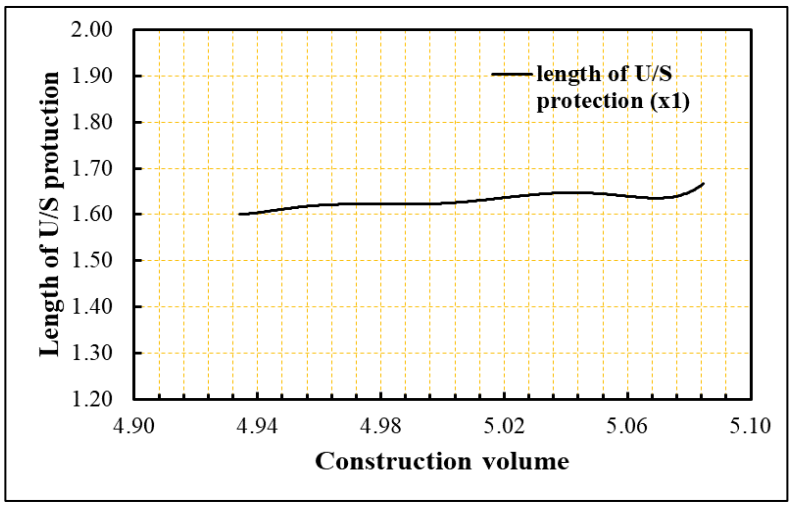


(a) Length of U/S protection versus construction volume.

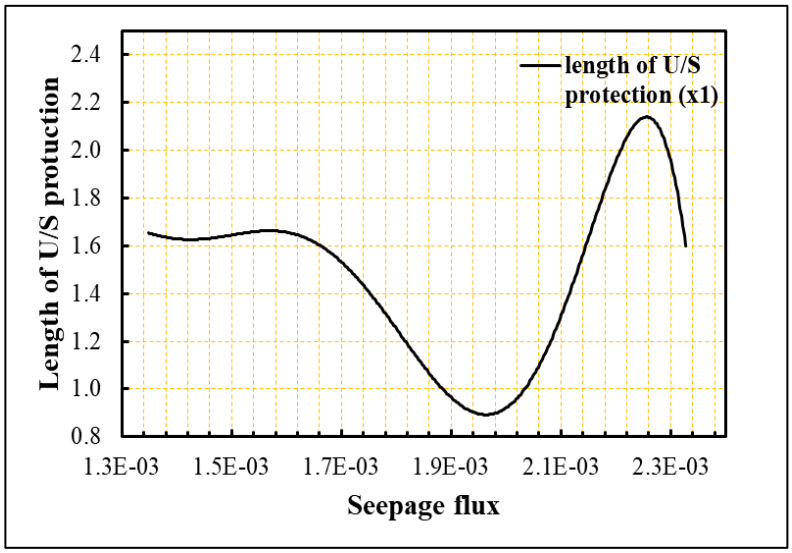


(b) Length of U/S protection versus seepage flux.

Figure (5.15): Design chart for length of U/S protection against different objectives for population size n=600.

Figures 5.15a, and 5.15b, show that as the length of upstream protection increased, there is a corresponding increase in construction volume and seepage flux.

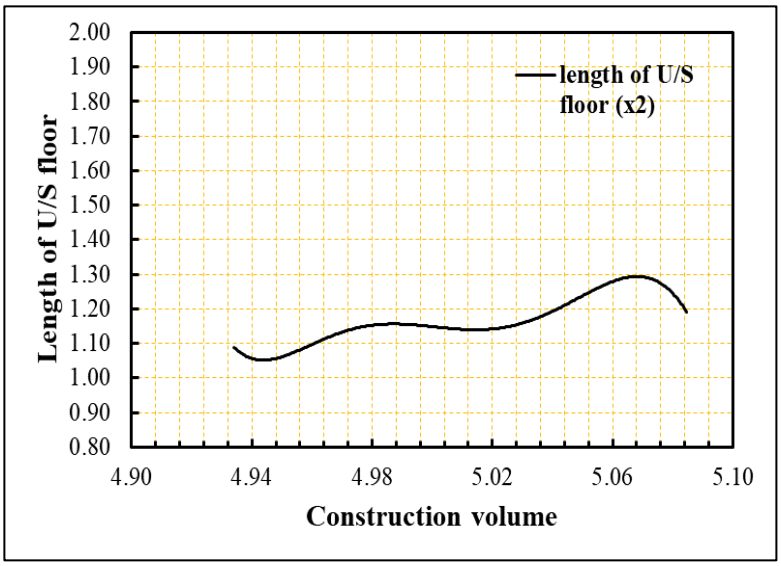


(a) Length of U/S floor versus construction volume.

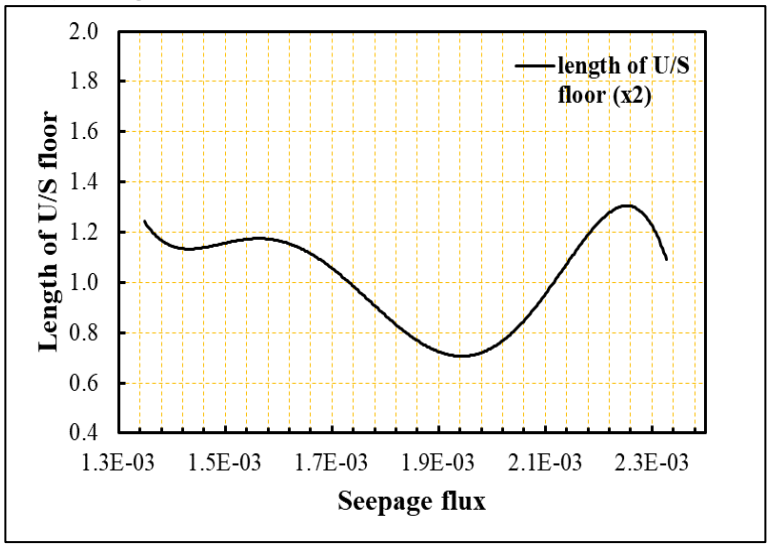


(b) Length of U/S floor versus seepage flux.

Figure (5.16): Design chart for length of U/S floor against different objectives for population size n=600.

Figures 5.16a, and 5.16b, show the relationship between the length of the upstream floor with construction volume, and seepage flux. Increasing the length

of U/S floor results in an increase in construction volume and a decrease in seepage flux.

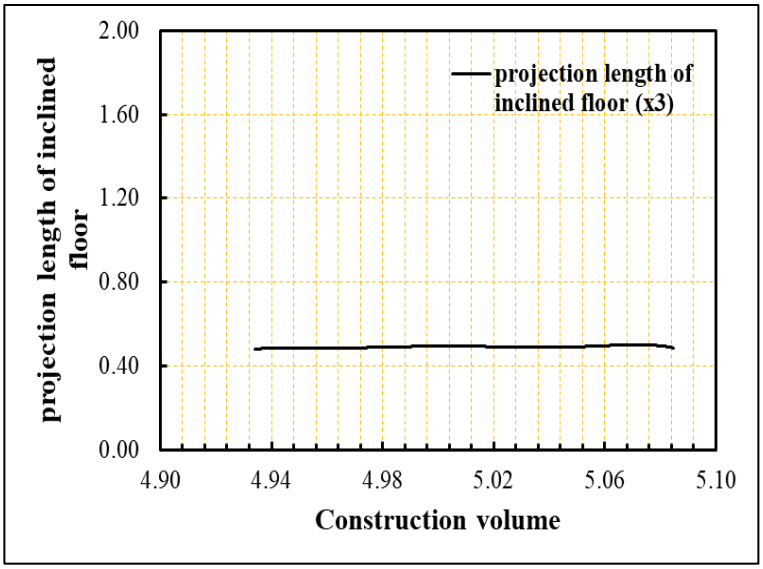


(a) Projection length of inclined floor versus construction volume.

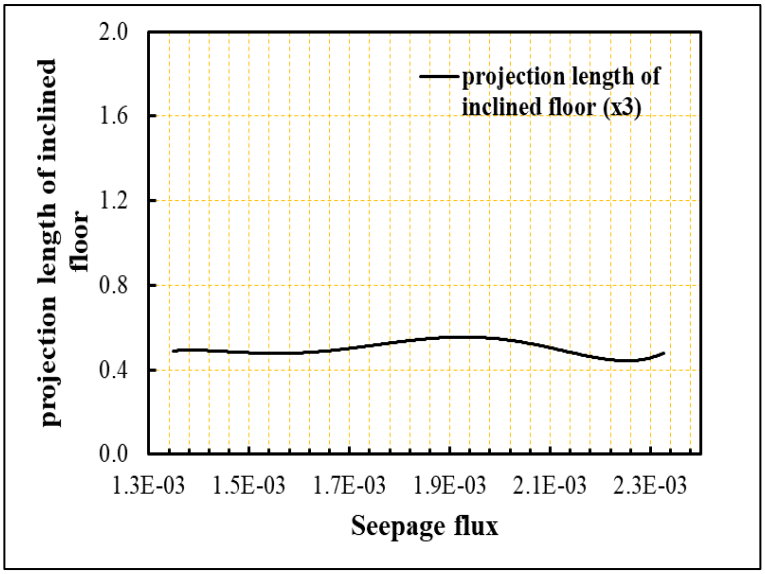


(b) Projection length of inclined floor versus seepage flux.

Figure (5.17): Design chart for length of inclined floor against different objectives for population size *n*=600.

Figures 5.17a, and 5.17b, show the relationship between the projection length of inclined floor versus construction volume, and seepage flux. From

these figures, the projection length of inclined floor has the same value at all points and ranged between 0.4 to 0.8.

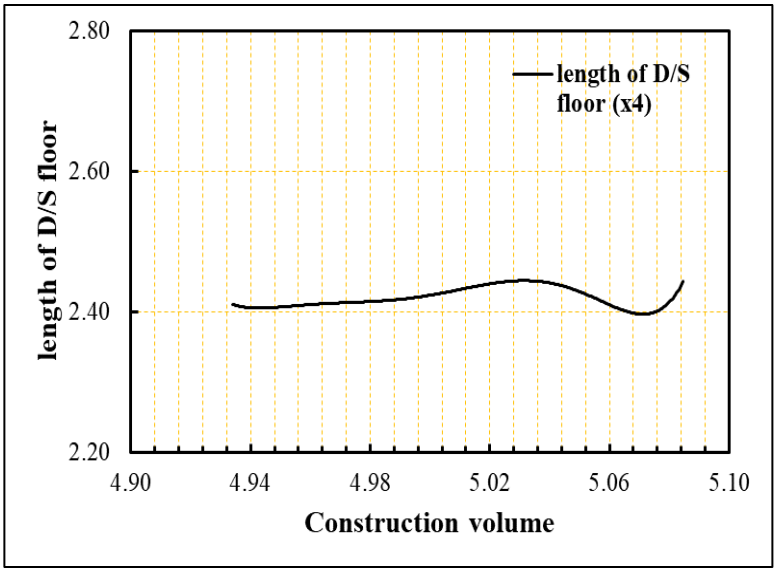


(a) Length of D/S floor versus construction volume.

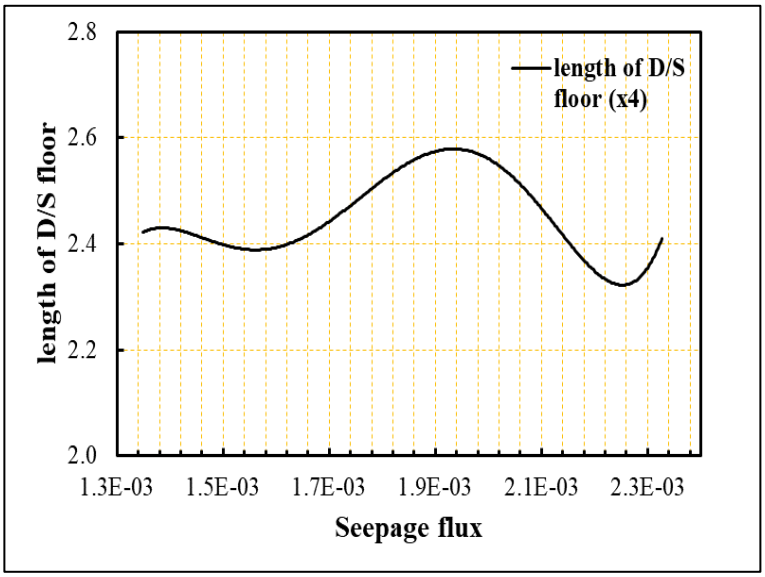


(b) Length of D/S floor versus seepage flux.

Figure (5.18): Design chart for length of D/S floor against different objectives for population size n=600.

Figures 5.18a, and 5.18b, show downstream floor length versus construction volume, and seepage flux respectively. The length value ranged between (2.4 to 2.6), for each generation the construction volume

increase with increasing downstream length. Moreover, for seepage flux increased in seepage when the length of floor decreasing.

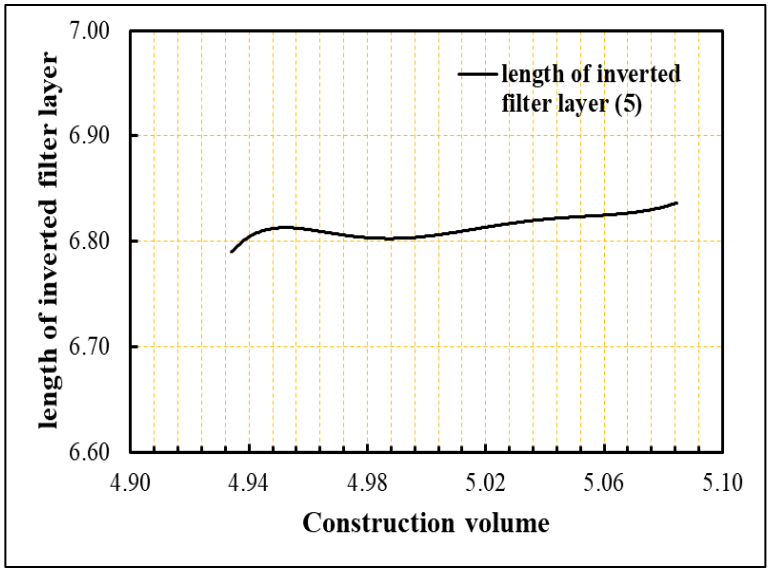


(a) Length of inverted filter layer versus construction volume.

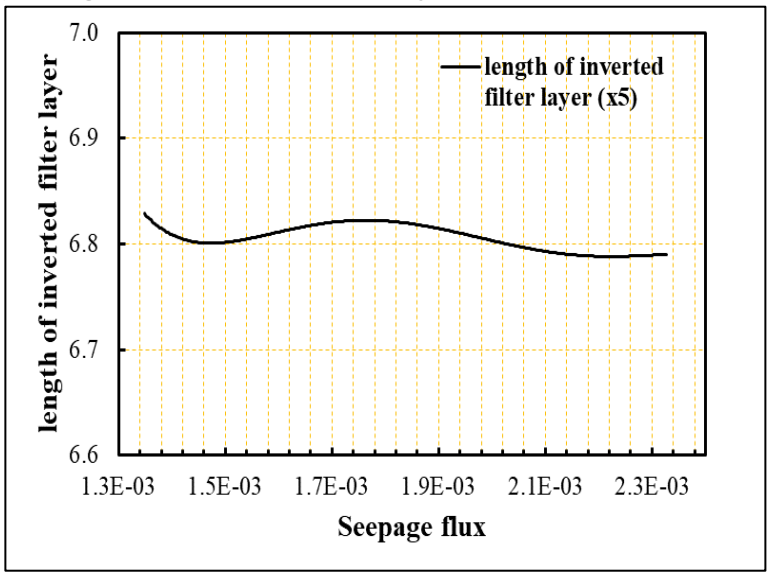


(b) Length of inverted filter layer versus seepage flux.

Figure (5.19): Design chart for the length of inverted filter layer against different objectives for population size n=600.

Figures 5.19a, and 5.19b, show length of inverted filter versus construction volume, and seepage flux respectively. The length ranged between 6.8 and 6.9

at all points and increase in the inverted filter length leads to an increase in construction volume and a decrease in seepage flux.

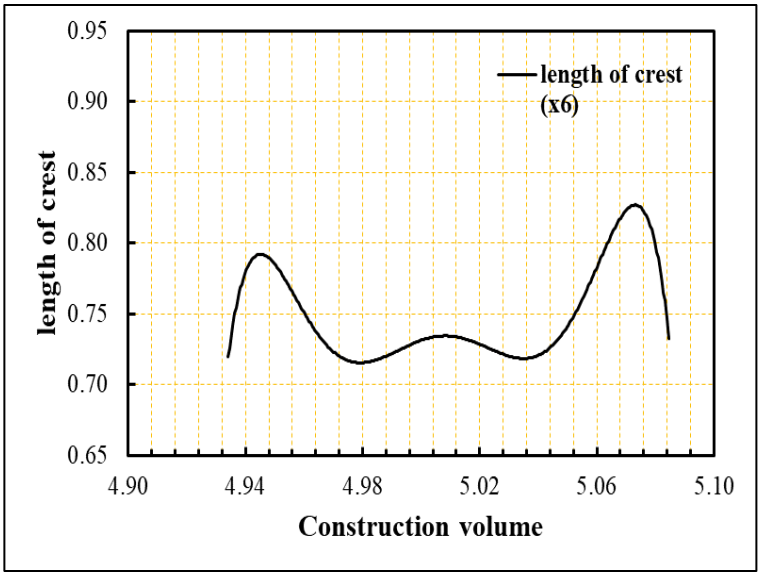


(a) Length of crest versus construction volume.

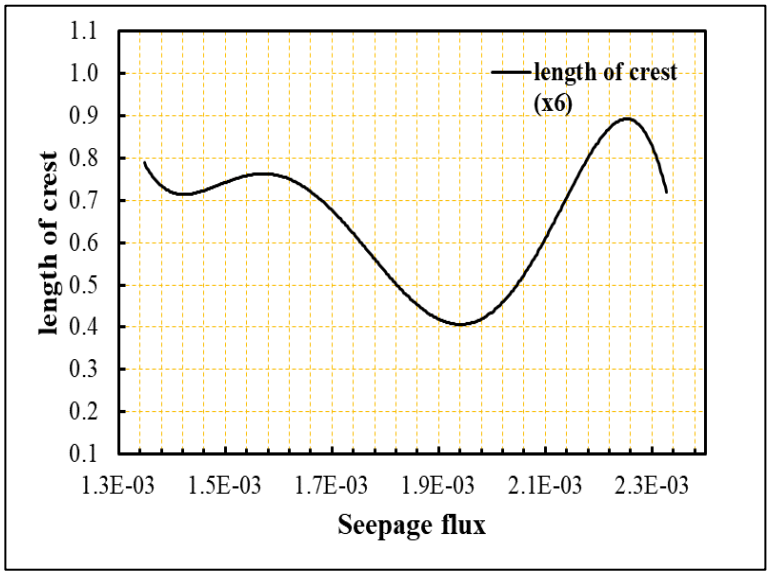


(c) Length of crest versus seepage flux.

Figure (5.20): Design chart for length of crest against different objectives for population size n=600.

Figures 5. 20a, and 5.20b, show the length of crest versus construction volume, and seepage flux respectively. From the figures the increase in length leads to an increase in construction volume, and seepage flux.

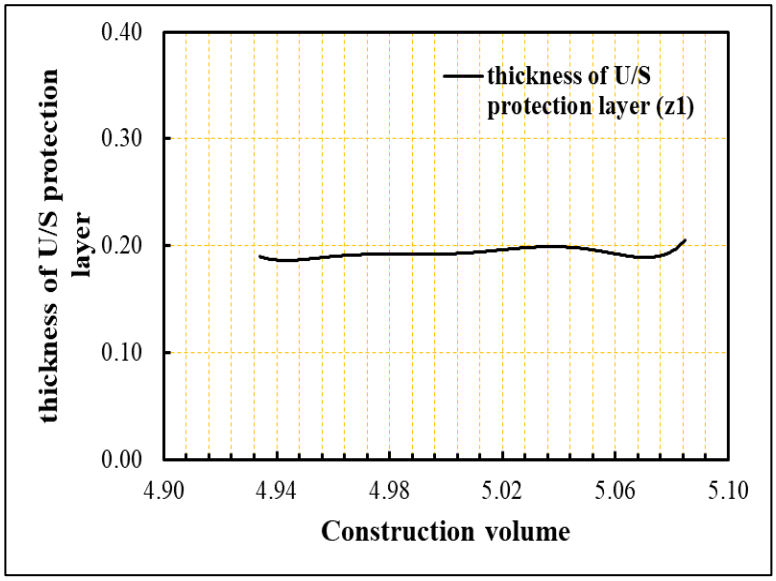


(a) Thickness of U/S protection layer versus construction volume.

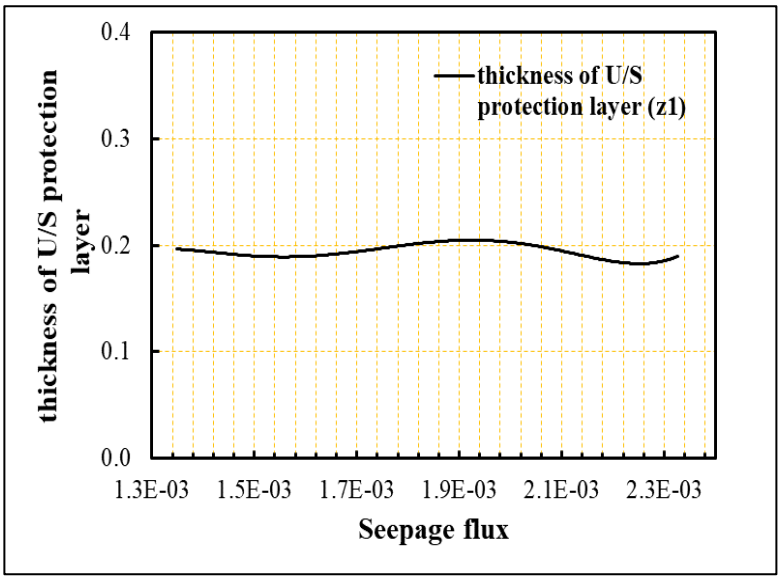


(b) Thickness of U/S protection layer versus seepage flux.

Figure (5.21): Design chart for the upstream protection layer against different objectives for population size n=600.

Figures 5.21a, and 5.21b, show the relationship between the thickness of upstream protection versus construction volume, and seepage flux in which thickness remain at same value about 0.20.

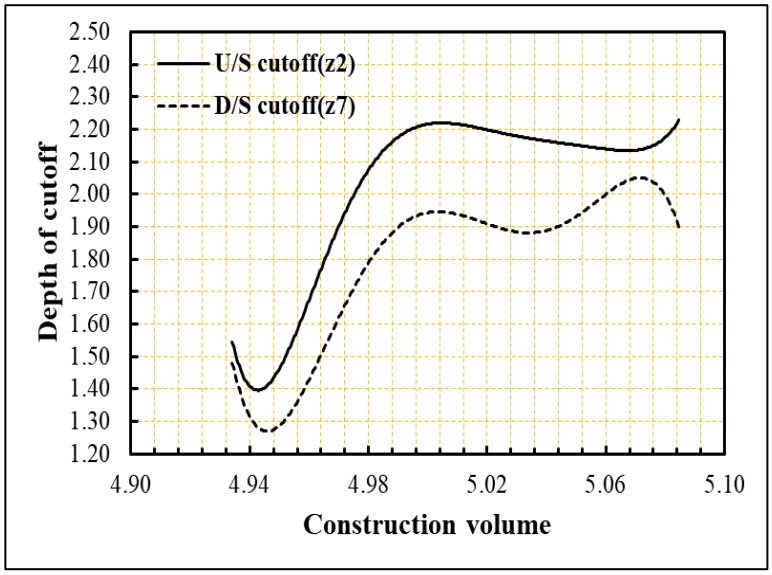


(a) Depth of cutoff versus construction volume function

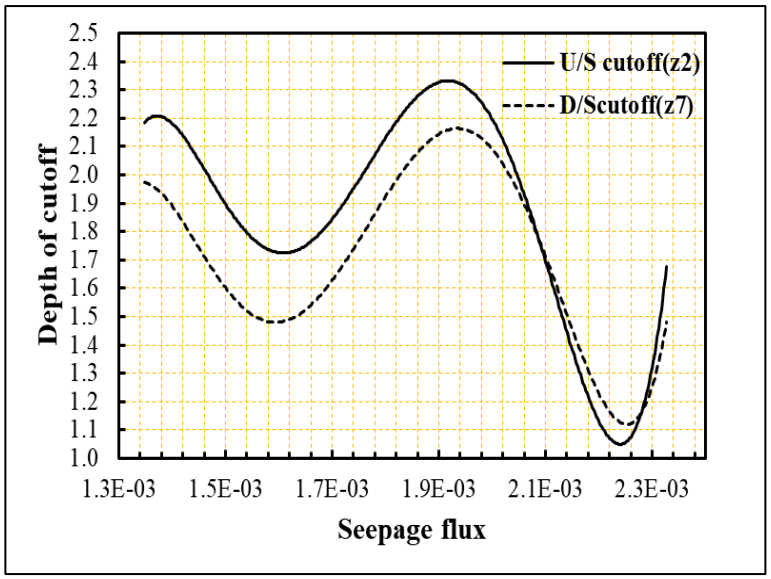


(b) Depth of cutoff versus seepage flux function.

Figure (5.22): Design chart for cutoff depth ratio against different objectives for population size n=600.

Figure 5.22a, show the relationship between cutoff depths with construction volume in which the increase in cutoff depths leads to increase of construction volume. While for figure 5.22b, depth of cutoff versus seepage flux function the seepage flux increased when cutoff depths decreased.

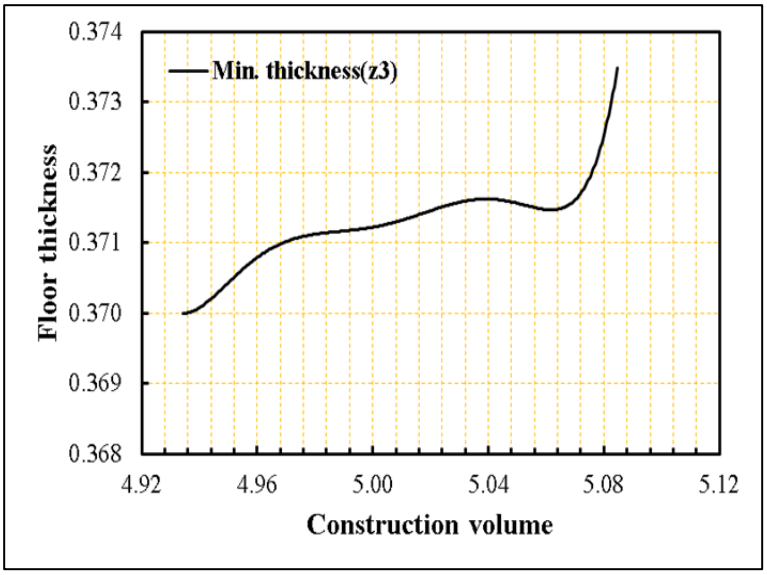


(a) Min. floor thickness versus construction volume function.

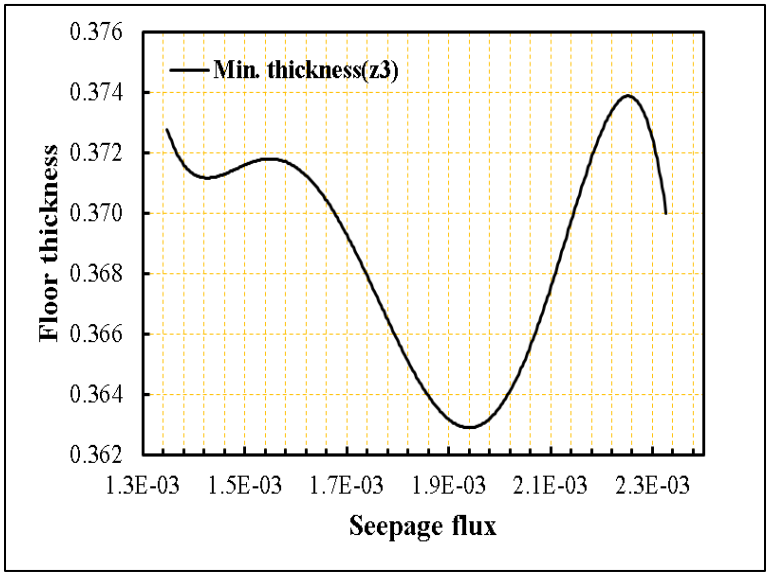


(b) Min. floor thickness versus seepage flux function.

Figure (5.23): Design chart of Min. floor thickness ratio against different objectives for population size *n*=600.

Figure 5.23a, shows the minimum floor thickness versus construction volume function in which construction volume increased when floor thickness increased. While for figure 5.23b, minimum floor thickness versus seepage flux functions that the minimum seepage flux at floor thickness was about o.363.

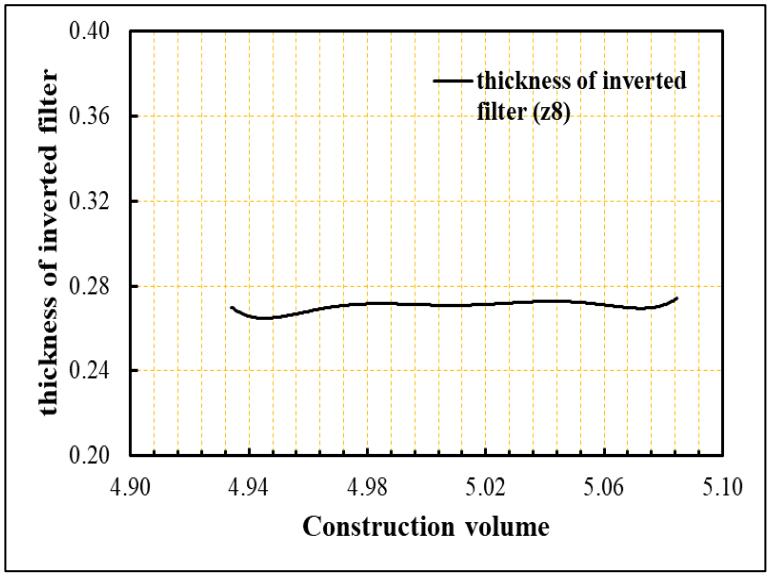


(a) Thickness of inverted filter versus construction volume.

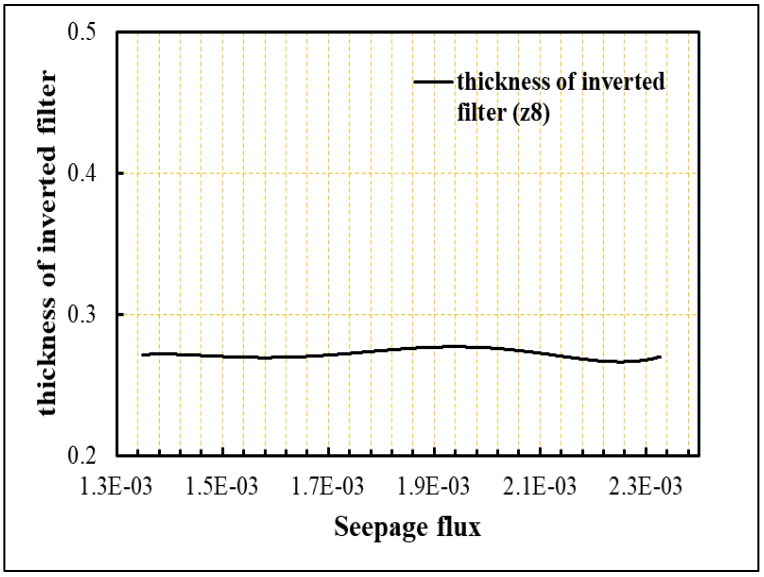


(b) Thickness of inverted filter versus seepage flux.

Figure (5.24): Design chart for the thickness of inverted filter against different objectives for population size n=600.

Figures 5.24a, and 5.24b, show the thickness of inverted filter versus construction volume, and seepage flux respectively. From these figures, the thickness ranged between 0.25 to 0.3, and there is small effect on seepage flux. While the construction volume increase.

### 5.4.2 Application Problem

In this study, the design example would be used is Abu-Sukhair barrage, as shown in figure (5.25). Table (5.14) provides the details and dimensions of its various components (Republic of Iraq, Ministry of Water Resources Commission for Dams and Reservoir).

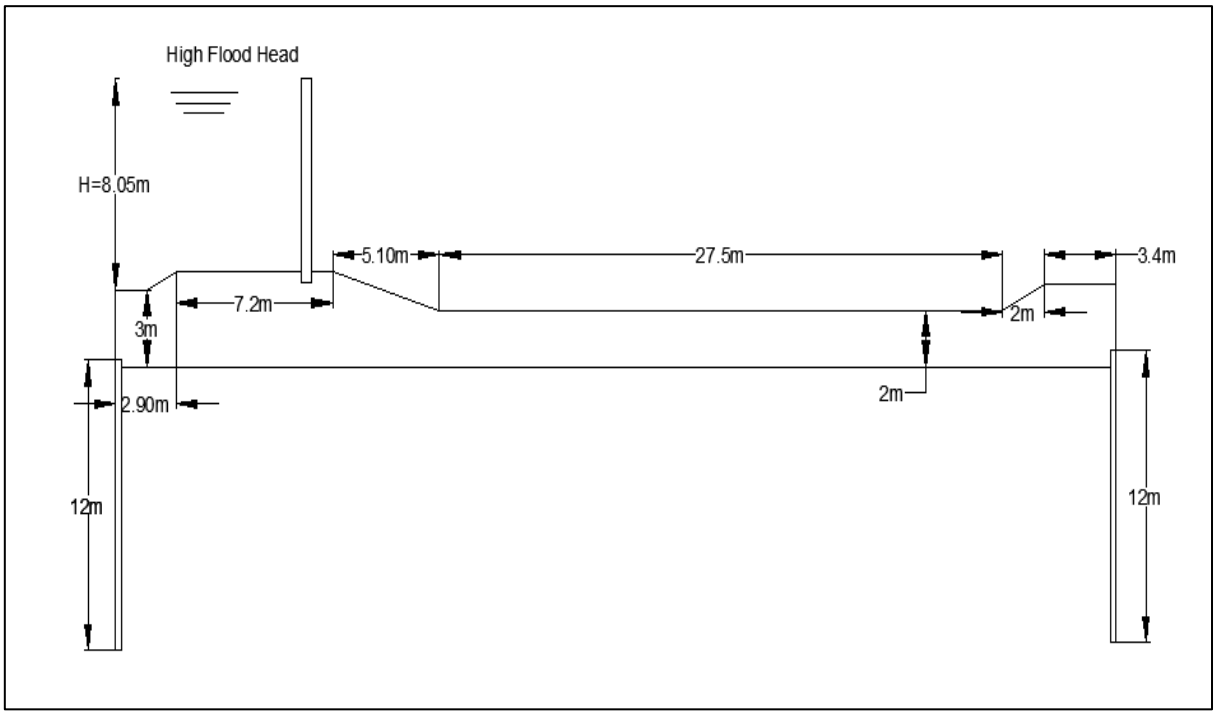


Figure (5.25): Profile of Abu-Sukhair barrage.

Tabel (5.12): Geometric charactrisitcs for Abu-Sukhair barrage(Republic of Iraq, Ministry of Water Resources Commission for Dams and Reservoir).

| **Component parts of barrage** | **Dimensions, (m)** |
|---|---|
| High flood head | 8.05 |
| Normal water head | 6.7 |
| Length of U/S protuction | 30 |

Table (5.12): Continue.

| | |
|---|---|
| Length of U/S floor | 10.1 |
| projection length of inclined floor | 5.10 |
| Length of D/S floor | 27.5 |
| Length of inverted filter | 76.5 |
| Length of crest | 7.2 |
| Thickness of U/S protection | 1.5 |
| Depth of U/S cutoff | 12.0 |
| Thickness of U/S floor | 3.0 |
| Depth of D/S cutoff | 12.0 |
| Thickness of inverted filter | 1.9 |

In this study, GeoStudio SEEP/W was utilized to investigate the seepage characteristics underneath the barrage floor. This involved calculating the uplift pressure, exit gradient, and seepage flux beneath the barrage. The properties of the soil foundation of the barrage were assumed to be identical to the gypsiferous soil properties employed in the study, with the soil being isotropic and possessing a coefficient of permeability of $9.540 \times 10^{-8}$ m/sec. The results of the seepage analysis for Abu-Sukhair barrage are presented in figure (5.26), with the mesh properties consisting of an element size of 1m, 3921 elements, and 4117 nodes.

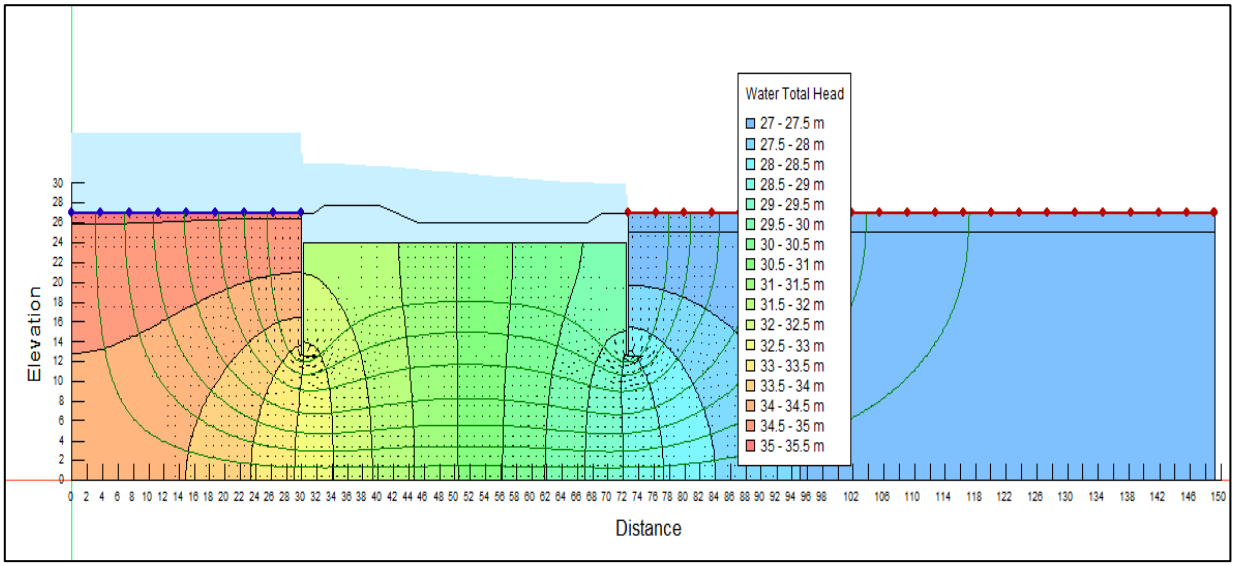


Figure (5.26): Seepage Analysis of Abu-Sukhair Barrage by SEEP/W.

Based on the results of the present analysis, which are presented in figure (5.26), it is evident that the seepage flow beneath the barrage occurred at a water total head ranging from 27m to 35.5m. Table (5.13) shows the results of the SEEP/W seepage analyses of the barrage.

Table (5.13): Results of seepage analysis for Abu-Sukhair barrage.

| **Seepage characteristics** | **Value** |
|---|---|
| Maximum uplift pressure force (ton) | 295.49 |
| Actual exit gradient | 0.0445 |
| Seepage flux ($m^3$/sec/m) | $1.206\times10^{-9}$ |

By using the seepage flux beneath the barrage obtained from both its actual dimensions and the design chart correlating seepage flux with design variables, it was possible to calculate the dimensions of the individual component parts of Abu-Sukhair barrage. The dimensions derived from the design chart were in a normalized form, which allowed the calculation of the actual dimensions in meters by multiplying each value by the high flood head

of the barrage. The resulting calculated dimensions were then compared to other values for validation. However; the results were shown in table (5.14).

Table (5.14): The actual and calculated dimension of abu-sukhair barrage.

| **Abu-Sukhair barrage component** | **Optimal dimensions* in non-dimensional form** | **Optimal dimension in (m)** | **Actual dimension in (m)** |
|---|---|---|---|
| Length of u/s protection | 1.7 | 13.69 | 30 |
| Length of u/s floor | 1.18 | 9.50 | 10.1 |
| projection length of inclined floor | 0.48 | 3.86 | 5.10 |
| Length of d/s floor | 2.41 | 19.40 | 27.5 |
| Length of inverted filter | 6.82 | 54.90 | 76.5 |
| Length of crest | 0.75 | 6.04 | 7.2 |
| Thickness of u/s protection | 0.18 | 1.45 | 1.5 |
| Depth of u/s cutoff | 1.76 | 14.17 | 12 |
| Thickness of u/s floor | 0.3719 | 3 | 3 |
| Depth of d/s cutoff | 1.49 | 12 | 12 |
| Thickness of inverted filter | 0.2707 | 2.18 | 1.9 |
| * Based on present study design charts. | | | |

Table 5.14 gives the dimensions of the barrage obtained through the use of design charts. Upon comparing the results in Table 5.14 with those in Table 5.12, it is apparent that all of the dimensions of the barrage decreased, except for the depth of the upstream cutoff and the thickness of the inverted filter.

In order to confirm the method's applicability and effectiveness, the seepage problem beneath Abu-Sukhair barrage was re-analyzed using the optimal dimensions obtained from the current design charts as shown in figure (5.27).

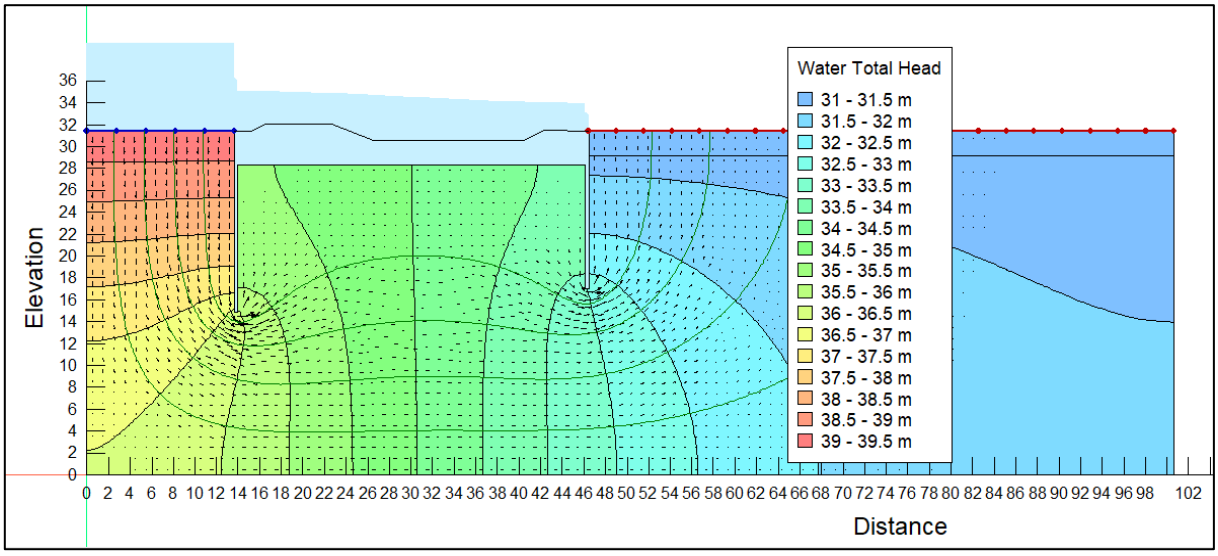


Figure (5.27): Seepage analysis of Abu-Sukhair barrage based on the obtained optimal dimensions.

In Figure 5.27, the seepage analyses underneath the barrage are displayed using dimensions calculated from design charts. The soil properties utilized in the analysis match those of the actual state. The water total head varied between 31m and 39.5m due to the foundation layer's increasing depth, which is dependent on the maximum cutoff depths. The mesh properties used were an element size of 1m, a total of 3101 elements, and 3254 nodes. Consequently, the results of the previous analysis are shown in table (5.15).

Table (5.15): Results of optimal design of Abu-Sukhair barrage.

| **Seepage properties** | **value** |
|---|---|
| Maximum uplift pressure (Ton) | 201.52 |
| Exit gradient | 0.0433 |
| Seepage flux ($m^3$/sec/m) | $2.206\times10^{-9}$ |

### 5.4.3 Verification by Design criteria

The predictions of this study in term of safety can be verified by comparing some important design criteria in this aspect, including:

1. **Factor of Safety against Piping:** It is a measure of the stability of a soil or earthen structure against internal erosion due to seepage. It is defined as the ratio of the soil's shear strength to the hydraulic gradient driving the seepage flow. A higher factor of safety indicates a greater resistance to piping, while a lower factor of safety indicates a higher risk of soil failure due to piping. In general, a factor of safety against piping of at least 1.3 is considered to be a minimum acceptable value for many engineering applications. However, the exact required factor of safety depends on the specific soil and site conditions, as well as the consequences of failure.
2. **Critical Exit Gradient of Seepage Water in a Soil**: The maximum hydraulic gradient that can exist in soil without causing piping-induced soil erosion is known as the critical exit gradient of seepage water. At this hydraulic gradient, soil particles start to move, and piping can occur. If the hydraulic gradient exceeds this limit, it can result in the formation of piping channels within the soil, which can lead to the failure and instability of earthen structures such as dams or embankments. As such, this parameter is a crucial consideration in the design and analysis of earthen structures to ensure their safety and stability.

$$i_{critical} = \frac{(G_s - 1)}{(e + 1)} \tag{5.44}$$

3. **Factor of Safety against Sliding**: The factor of safety against sliding for barrage is a measure of the safety and stability of a barrage against sliding failures, which can result from inadequate shear strength or excessive shear stresses in the foundation soils or underlying rock. It is calculated as the ratio of the available shear strength to the shear stress acting on the potential sliding plane. A factor of safety against sliding of greater than one indicates that the available shear strength is greater than the shear stress acting on the

potential sliding plane, indicating that the barrage is stable against sliding. This can be expressed as:

$$F_{sliding} = \frac{Restraining\ force}{Sliding\ force} \quad (5.36)$$

Table (5.16) illustrates the differences in design criteria between the conventional design method (as it is) and the present optimal approach.

Table (5.16): The design criteria for Abu-sukhair barrage.

| Design criteria | Conventional design method | Optimal design method |
|---|---|---|
| $i_{actual}$ | 0.0445 | 0.0433 |
| $i_{critical}$ | 0.976 | 0.976 |
| $F_{sliding}$ | 8.86 | 7.23 |

To calculate the required creep length underneath Abu-Sukhair barrage from conventional design method and optimal design method the hydraulic gradient equal to H/L in which H, the seepage head, is the head difference between the upstream and downstream water level (L), and $L$ is the total creep line length (L). for fully closed gate and in case of high flood head H=8.05 m

$$i_{actual} = \frac{H}{L} \quad (5.37)$$

From conventional design method, $L = \frac{8.05}{0.0445} = 180.89\ m$

From optimal design method, $L = \frac{8.05}{0.0433} = 185.91\ m$

Based on the prior discussions and analysis of the results, the study presented method produces acceptable results, particularly regarding economic constraints and decreasing costs, while considering all problem limitations. Thus, it is probably safe to recommend such optimal hydraulic design charts to be considered as guide in design and analysis of optimal profile for hydraulic structures, in particular barrages.

# CHAPTER SIX

# CONCLUSION AND RECOMMENDATION

## 6.1 Conclusion

The following points can summarize the major conclusions of the present study.

1- This study focused on the hydraulic optimal design of a barrage profile on gypsiferous soil, which is a problematic soil containing soluble material. When exposed to water seepage, this soil can cause significant issues for constructions.

2- Gypsiferous soil was subjected to leaching-permeability and direct shear tests. Initially, the saturated permeability of the soil was adversely affected by its initial gypsum content. However, at the end of the leaching process, the coefficient of permeability increased due to the increase of voids in the soil mass. This allowed more infiltrated water to flow through the soil mass under the applied head.

3- Direct shear tests revealed that the gypsiferous soil sample with 20% initial gypsum content in the dry state exhibited a high increase in soil cohesion before leaching. However, soil samples with 35% initial gypsum content experienced a significant decrease in cohesion. After the leaching test, the soil sample with an initial gypsum content of 25% experienced an increase in cohesion of approximately 32%, based on the relative difference in the wet state. In contrast, soil samples with high initial gypsum content lost a significant amount of cohesion in the wet state.

4- In terms of the angle of internal friction, the gypsiferous sample with 20% initial gypsum content caused a slight reduction in the internal friction angle compared to the natural soil in both dry and wet states. On the other hand, the gypsiferous samples with a higher gypsum content of 35%

displayed an increase in the internal friction angle for all leaching and moisture conditions.

5- The analyses of steady state of seepage beneath the barrage is in non-dimensionlized form, the seepage rate decreases by 39.24% when upstream cutoff depth ($z_2$) increases from (1.35 to 2.25), and total floor length of the barrage increase from (4.07 to 5.11), this increase in total floor length leading to an increase in the creep line length of seepage beneath the barrage. In addition, the exit gradient decreased as the total floor length $L_T$ and downstream cutoff depth $z_7$ are increased, in which minimum exit gradient at $L_T$ equal to 5.25, and $z_2$ equal to 2.38.

6- The optimization technique for hydraulic design of a barrage involves solving a multi-objective optimization problem to minimize the construction volume and seepage flux under the barrage floor. Thus, in order to solve the optimization problem, a genetic algorithm method (GA) was utilized. The GA algorithm was run 56 times, with different population sizes of 200, 600, 1000, and 1400. The results indicated that a population size of 600 was sufficient to provide a satisfactory solution for the constrained nonlinear optimization problem of optimal hydraulic design.

7- The study introduced design charts for the barrage to facilitate the design of the barrage profile and dimensions. The effectiveness and applicability of the design charts were evaluated using Abu-Sukhair barrage as a design example. The design charts were used to calculate the optimal dimensions of the barrage, and the results indicated that all dimensions, except for the depth of the upstream cutoff and the thickness of the inverted filter, decreased.

## 6.2 Recommendation and Suggestion for Future Studies

1. During the process of manufacturing gypsum soil, adding gypsum to silt soil has reduced the coefficient of permeability and thus reduced the rate of seepage underneath the foundation of the barrage. It is possible to consider mixing silt soil with gypsum as one of the treatments that reduce the access of water to gypsum salts.
2. Re-designing Abu Sakhir barrage from the design charts has reduced the dimensions of the barrage and thus reduced the cost of the construction materials. Therefore, these charts can be adopted when designing similar structures.
3. Further research is needed to examine the long-term effects of seepage in steady and transient states on gypseous soil and how it may influence the performance of the barrage and seepage control measures.
4. Conduct further experimental and numerical studies to investigate the long-term behavior of the barrage and its seepage control measures under different loading and environmental conditions.
5. Extend the study to include more problematic soil types in the foundation of the barrage, such as expansive and loss soils, to assess the applicability and effectiveness of the proposed design technique and charts. This can help provide more comprehensive guidelines for hydraulic design of barrages on different soil types, and may lead to improvements in the design and construction of such structures in the future.

# REFERENCES

Al-Dabbas, M. A., Schanz, T., & Yassen, M. J. (2010). Proposed engineering of gypsiferous soil classification. *Arab J Geosci*, *5*, 111–119.

Al-Mufty, A. (1997). Effect of Gypsum Dissolution on the Mechanical Behavior of Gypseous Soils. PhD thesis, Department of civil Engineering, University of Baghdad.

Al-Damluji, O., Al-Obaidi, S., Al-Omari, A. L. M., Al-Ani, R. R., M. M., & Fattah, M. Y. (2018). Experimental and numerical investigations of dissolution of gypsum in gypsiferrous. *International Conference on Soil Mechanics and Geotechnical Engineering*. https://doi.org/10.3233/978-1-60750-031-5-820

AL-Simawi, H. (2010). Irrigation and Drainage Projects in Iraq.

Abdullah, M., Al-Ansari, N., & Jan Laue. (2019). Water Resources Projects in Iraq: Barrages. *Journal of Earth Sciences and Geotechnical Engineering*, *9*(4), 153–167.

AL-Abbas, R. A., Hommadi, A. H., Abbas, A. A., Essa, H. M., & Nheir, A. O. (2019). Checking the safety of Alhindyabarrage foundation from uplift pressure and seepage ratio with variation of discharge and water level. *Proceeding of ICCEET*, *978*(9).

AL-OBAIDI, Q. A. J. (2003). *Studies In Geotechnical And Collapsible Characteristics Of Gypseous Soil*. M.Sc thesis, Department of Civil Engineering, AL-Mustansiria University.

AL-OBAIDI, Q. A. J. (2015). *Studies In Hydro-Mechanical Behaviour of Collapsible Soils*. PhD thesis, Civil and Environmental Engineering Ruhr-University at Bochum.

Al-Gharbawi., A. S. A., Fattah., M. Y., & Mahmood., M. R. (2021). Evaluation of Leaching Behavior of Treated and Untreated Gypseous

Soil. *IOP Conf. Series: Earth and Environmental Science*, *856*(012050).

Ayadat, T. and A.M. Hanna, 2005. “Encapsulated Stone Column as A Soil Improvement Technique for Collapsible Soil.” Proc., ICE - Ground Improvement, 9(4): 137-147.

ASTMD854 (2010), `Standard test methods for specific gravity of soil solids by water pycnometer1',Annual Book of ASTM Standards,Vol.04.08, Philadelphia,PA, ASTM, USA. Copyright ,ASTM International, 100 Barr Harbor Drive, PO Box C700, West Conshohocken, PA 19428-2959, United States.

ASTMD4318 (2010), `Standard test methods for liquid limit, plastic limit, and plasticity index of soils', Annual Book of ASTM Standards,Vol.04.08, Philadelphia,PA, ASTM,USA. Copyright ,ASTM International, 100 Barr Harbor Drive, PO Box C700, West Conshohocken, PA 19428-2959, United States.

ASTMD1557 (2012), `Standard test methods for laboratory compaction characteristics of soil using modified effort (56,000 ft-lbf/ft3 (2,700 kn-m/m3))', Annual Book of ASTM Standards,Vol.04.08, Philadelphia,PA, ASTM,USA. Copyright , ASTM International, 100 Barr Harbor Drive, PO Box C700, West Conshohocken, PA 19428-2959, United States.

ASTMD2216 (2010), `Standard test methods for laboratory determination of water (moisture) content of soil and rock by mass', Annual Book of ASTM Standards,Vol.04.08, Philadelphia,PA, ASTM,USA. Copyright , ASTM International, 100 Barr Harbor Drive, PO Box C700, West Conshohocken, PA 19428-2959, United States.

Barzanji, A. (1973), Gypsiferous Soils in Iraq, PhD thesis, University of Ghent, Belgium.

British standard. (1999). Code of practice for site investigations. In *British*

*Standards Institution, London 152*.

Clemence, S.P., and Finbarr, A.O., (1981). Design considerations for collapsible soils, Journal of the Geotechnical Engineering Division, 107(3), pp.305-317.

Fattah, M. Y., Al-Ani, M. M., & Al-Lamy., M. T. A. (2014). Studying collapse potential of gypseous soil treated by grouting. *Soils and Foundations*, *3*(54), 396–404.

Fattah, M. Y., Obead, I. H., & Hassan, A. O. (2019). A study on leaching of collapsible gypseous soils. *International Journal of Geotechnical Engineering*.

https://doi.org/10.1080/19386362.2019.1647664A

Garg, N. K., Bhagat, S. K., & Asthana, B. N. (2002). Optimal Barrage Design based on Subsurface garg2002.pdf. *JOURNAL OF IRRIGATION AND DRAINAGE ENGINEERING*, *128*, 253-263.

Garg, S. K. (1976). *Irriagtion_Engineering_and_Hydraulic.pdf*.

Haestad, M., Walski, TM., Chase, DV., Savic, DA., Grayman, W., Beckwith, S., Koelle, E. (2003) Advanced water distribution modeling and management. Haestad Press, Waterbury, pp 673–677.

Hassan, Z. F. (2015). *Optimal Hydraulic Design of a Barrage Using Genetic Algorithms A*. M.Sc Thesis, Department of the Civil Engineering, University of Babylon.

Hassan, W. H. (2019). Application of a Genetic Algorithm for the Optimization of a Location and Inclination Angle of a Cut-Off Wall for Anisotropic Foundations Under Hydraulic Structures. In *Geotechnical and Geological Engineering* (Vol. 37, Issue 2, pp. 883–895).

https://doi.org/10.1007/s10706-018-0658-9

Hassan, W., Hussein, H., Khashan, H., Alshammari, H., Nile, K. (2022). *Application of the Coupled Simulation-optimization Method for the*

*Optimum Cut-off Design Under a Hydraulic Structure. Water Resources Management*, 36:4619-4636.

Harr, M. (1998). Groundwater and Seepage. In *The Handbook of GroundwaterEngineering*. https://doi.org/10.1201/9781420048582.ch4

Ismael, N. F. (1993). *Laboratory And Field Leaching Tests On Coastal Salt-Bearing Soils*. *119*(3), 453–470.

Irshayyid, E. J. (2015). *Effect of Suction on Swelling Behavior of Unsaturated Expansive Clayey Soil* . M.Sc thesis, Department of Building And Construction Engineering,University of Technology.

James, A., and I. Kirkpatrick. 1980. "Design of Foundations of Dams Containing Soluble Rocks and Soils." Quarterly Journal of Engineering Geology London 13: 189–198.

http://doi:10.1144/GSL. QJEG.1980.013.03.05

Khassaf, S. I., Al-Adili, A. S., & Rafid S. Rasheed. (2009). SEEPAGE ANALYSIS UNDERNEATH DIYALA WEIR FOUNDATION. *Thirteenth International Water Technology Conference*, *13*.

Majeed A.H. (2000). Data base for gypseous soils. PhD. Thesis University of Baghdad. Iraq.

Mohammed-Ali, W. S. (2011). The Effect of Middle Sheet Pile on the Uplift.pdf. *European Journal of Scientific Research*, *65*(3), 350–359.

Maatooq, D. J. S., HaiderAlwash, & Al-Khafaji, H. M. (2015). Al-shamiya Barrage .pdf. *Eng. &Tech.Journal.*, *33*(4).

Maghawry, A., Hodhod, R., Omar, Y. *et al.* (2021). An approach for optimizing multi-objective problems using hybrid genetic algorithms. *Soft Comput* **25**, 389–405. https://doi.org/10.1007/s00500-020-05149-3

Ministry of Irrigation General Establishment of Study and Design. Al-Kufa barrage design.

Ministry of Water Resources Commission for Dams and Reservoir. Abu-Sukhair barrage design.

Novak, P., Moffat, A. I. B., Nalluri, C., & R. Narayanan. (2008). Hydraulic structures. In *Journal of Hydraulic Research* (Vol. 46, Issue 5). https://doi.org/10.1080/00221686.2008.9521916

Nashat, I. H., (1990), "Engineering Characteristics of Some Gypseous Soils in Iraq", Ph.D. thesis, Civil Engineering Department, University of Baghdad, Baghdad, Iraq.

http://doi:10.1099/00221287-136-2-327

Nassralla, T., & Rabea, A. (2015). Seepage Characteristics under Hydraulic Structure Foundation (Supported by Sheet pile) In Multi-Layers Soil. *Egyptian Journal for Engineering Sciences and Technology*, *18*(4), 229–238. https://doi.org/10.21608/eijest.2015.97121

Obead, I. H. (2013). Effect of Position and Inclination Angle of Cutoff Wall on Seepage Control in the Foundation of Dam Structure. In *Journal of Kerbala University* (Vol. 11, Issue 4, pp. 17–32). Journal of Kerbala University.

Obead, I. H., AL-Baghdadi, H. M., & Hamad, R. (2014). *Reducing the Impact of Uplift Pressures on the Base of a Concrete Dam by Configuration of Drainage Holes (Hypothetical Case Study)*. *6*(1).

Obead, I. H., Omran, H. A., & Fattah, M. Y. (2021). Implementation of artificial neural network to predict the permeability and solubility models of gypseous soil. *Pertanika Journal of Science and Technology*, *29*(1), 107–122. https://doi.org/10.47836/pjst.29.1.06

Obead, I. H., Fattah, M. Y., & Omran., H. A. (2022). Role of Soluble Materials on the Hydro-mechanical.pdf. *Transportation Infrastructure Geotechnology Chemical*.

Petrukin. V.P, Arakelyan, EA (1985) Strength of Gypsum–day Soils and

Its Variation during the leaching of Salts. Soil Mechanics and Foundation Eng. Vol. 21, No.6, pp.23-25.

Rao, S. S. (2009). *Engineering Optimization - Theory and Practice*.

Rasool, M. H. (2018). Effect Of Mutual Interference Piles On Seepage Properties Under Hydraulic Structures. *Kufa Journal of Engineering*, *9*(4).

Sa'eed, N.K. (2006). Effective Comparison of the Shear Strength of Gypsum Soil in Iraq Desert. the ministry of Housing and Construction / AL-Fao General Engineering Company /Republic of Iraq**.**

Singh, R. M. (2011). Design_of_Barrages_with_Genetic_Algorith.pdf. *Water Resour Manage (2011)*, *25*, 409–429. https://doi.org/10.1007/s11269-010-9706-9

Schanz, T., & Karim, H. H. (2018). Geotechnical characteristics of some Iraqi gypseous soils. *MATEC Web of Conferences*, *162*(01005). https://doi.org/10.1051/matecconf/201816201005

Saleh, L. A., (2018). Studying the seepage phenomena under a concrete dam using SEEP/W and Artificial Neural Network models. *Materials Science and Engineering*, *433*(012029).

Salim, I. H., & Othman, B. S. (2021). The Effect of inclined intermediate Sheet Pile on Seepage Properties Under Hydraulic Structure Using SEEP/W Program. *IOP Conference Series: Materials Science and Engineering PAPER*, *1076*(012131).

https://doi.org/10.1088/1757-899X/1076/1/012131

Yaqoob, M., Rahil, W., F. H., & Neami, M. A. A.-. (2019). Characteristics of Artificial, Gypsified and Natural Gypseous Soils under Leaching Condition. *Engineering and Technology Journal*, *37*(8).

# Appendix (A)

## Design charts for population size *n*=200

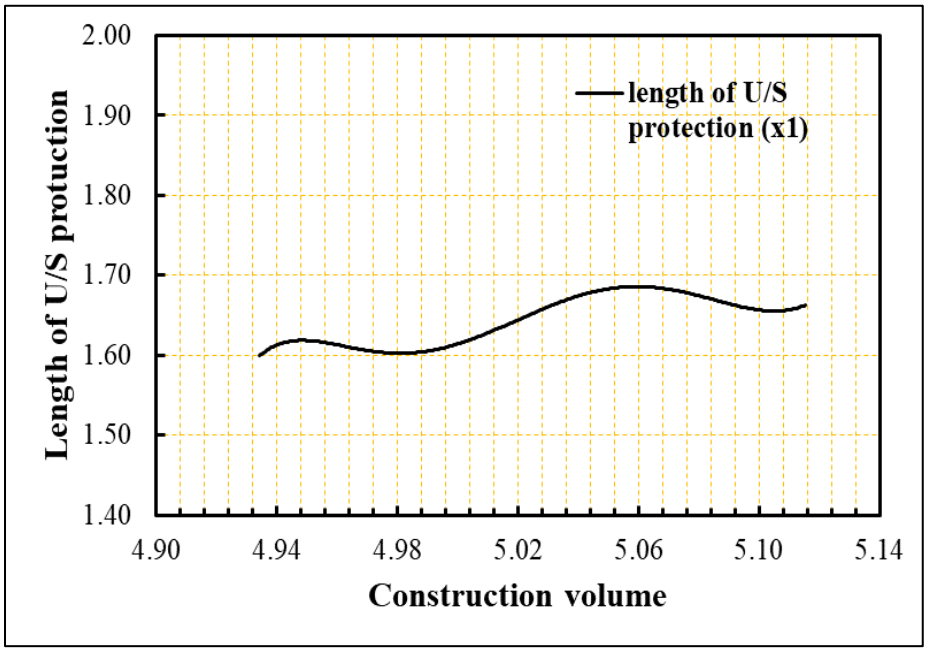


(a) Length of U/S protection versus construction volume.

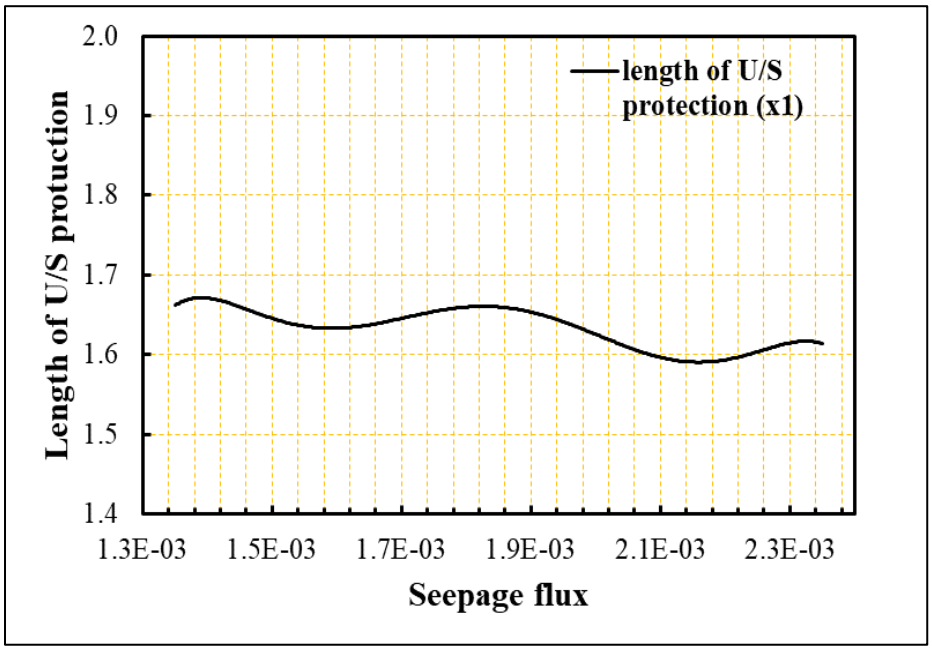


(c)Length of U/S protection versus seepage flux.

Figure (A.1): Design chart for length of U/S protection against different objectives for population size n=200.

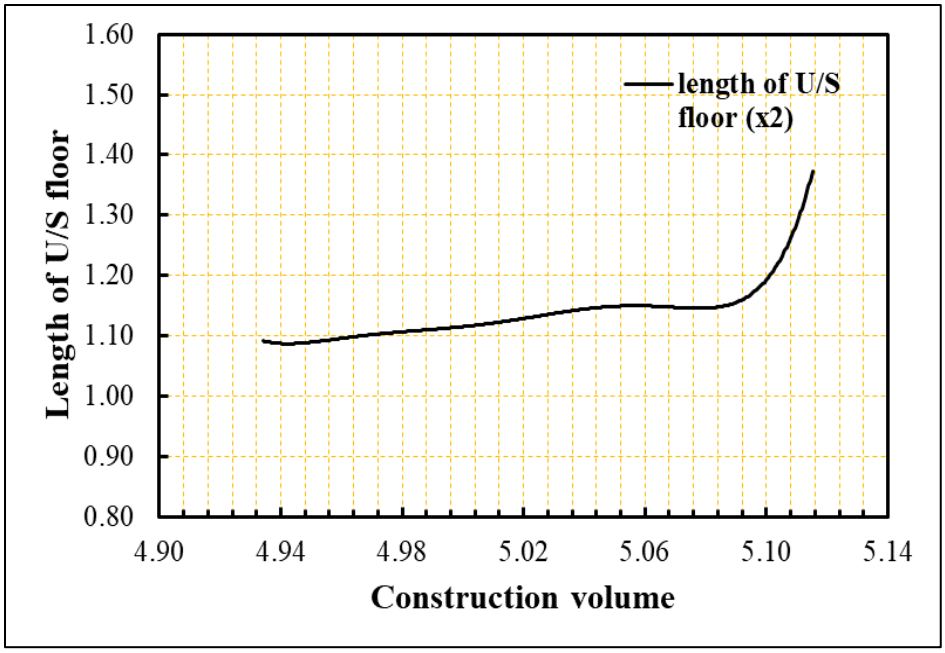


(a) Length of U/S floor versus construction volume.

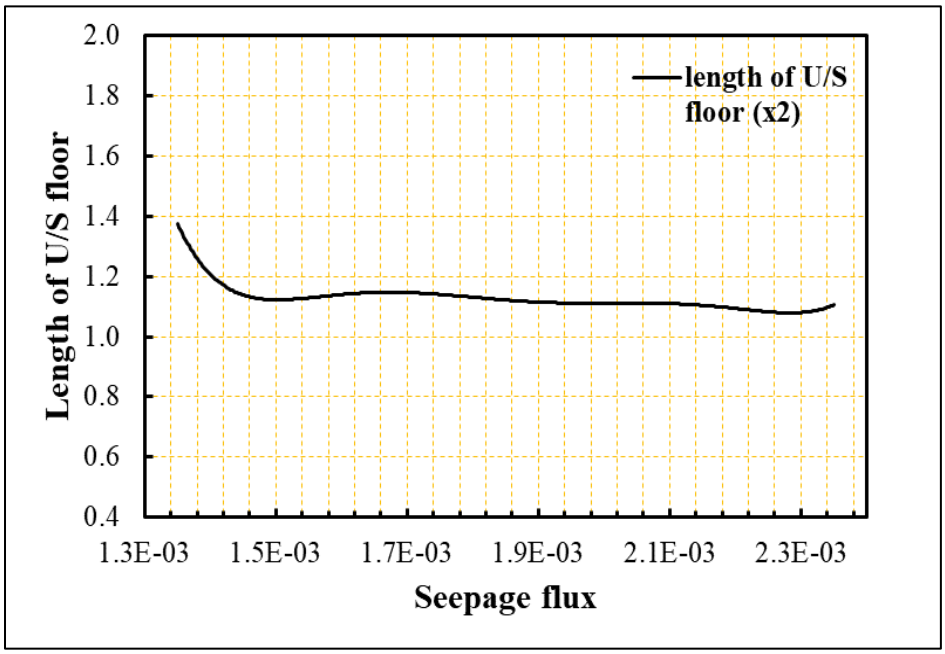


(b) Length of u/s floor versus seepage flux.

Figure (A.2): Design chart for length of U/S floor against different objectives for population size n=200.

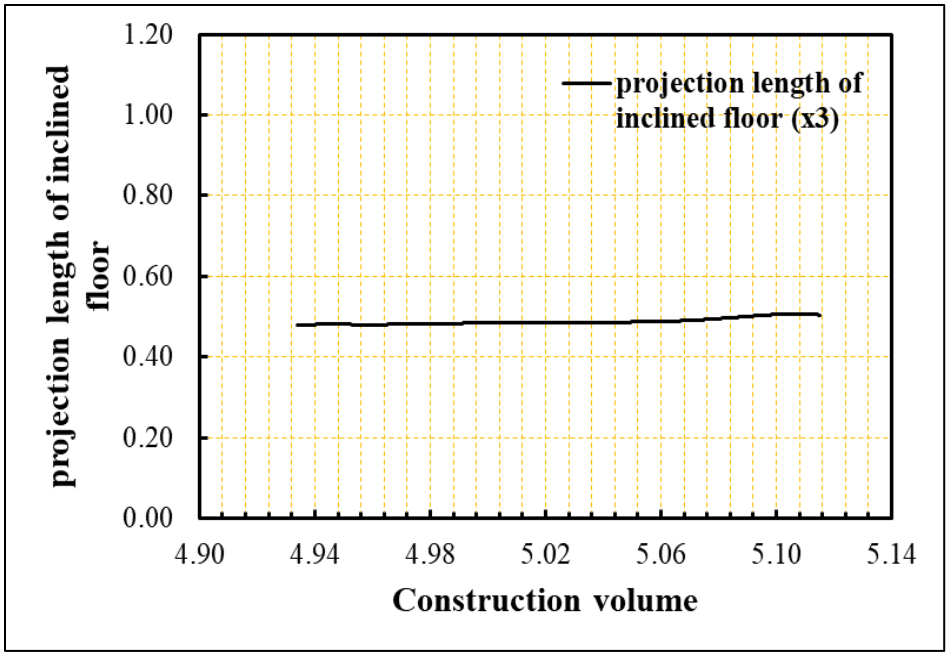


(a) Projection length of inclined floor versus construction volume.

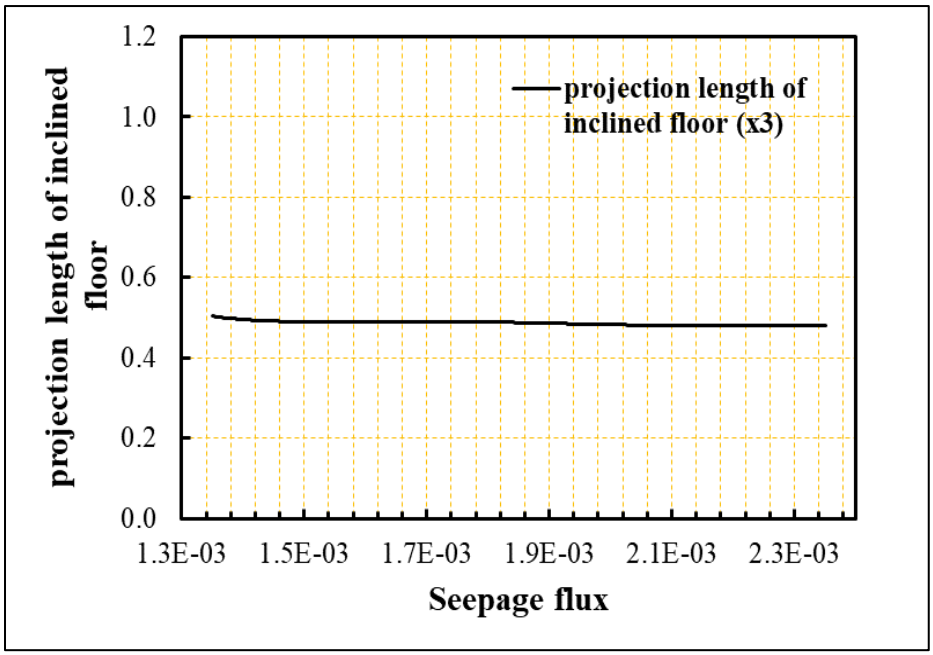


(b) Projection length of inclined floor versus seepage flux.

Figure (A.): Design chart for projection length of inclined floor against different objectives for population size n=200.

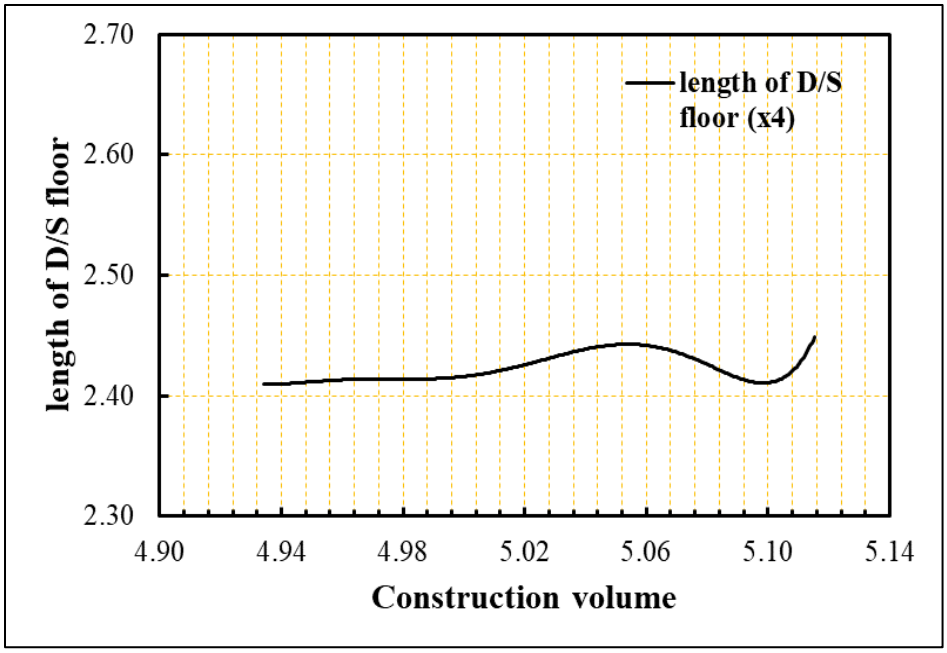


(a) Length of D/S floor versus construction volume.

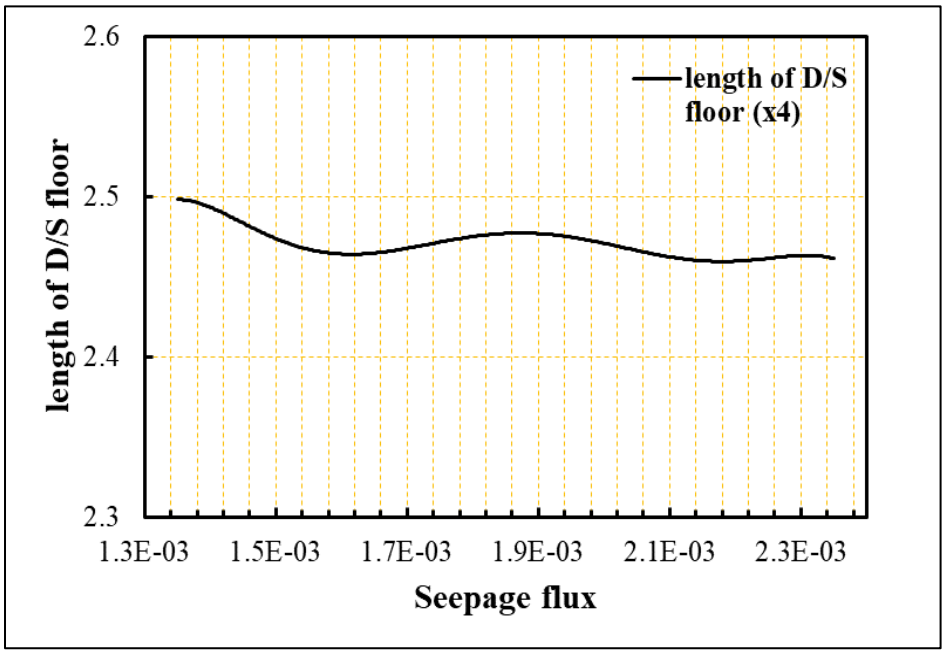


(b) Length of D/S floor versus seepage flux.

Figure (A.4): Design chart for the length of D/S floor against different objectives for population size n=200.

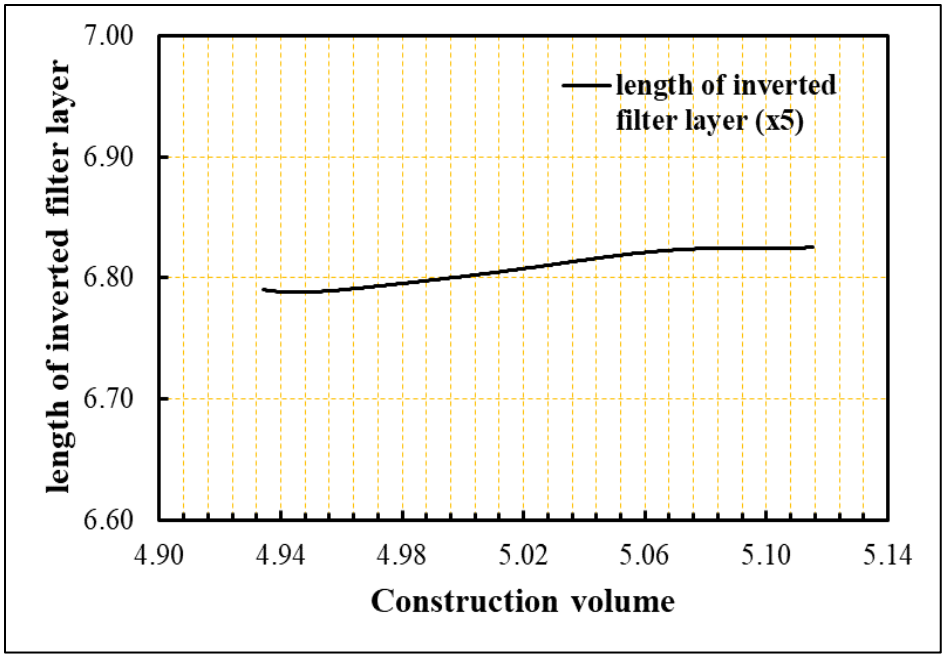


(a) Length of inverted filter layer versus construction volume.

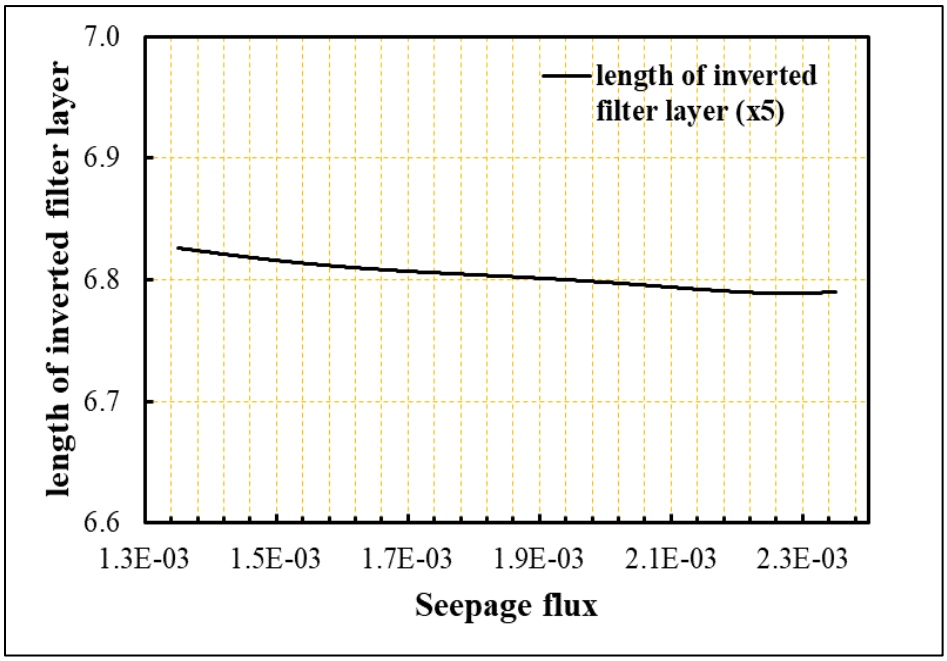


(b) Length of inverted filter layer versus seepage flux.

Figure (A.5): Design chart for length of inverted filter layer against different objectives for population size n=200.

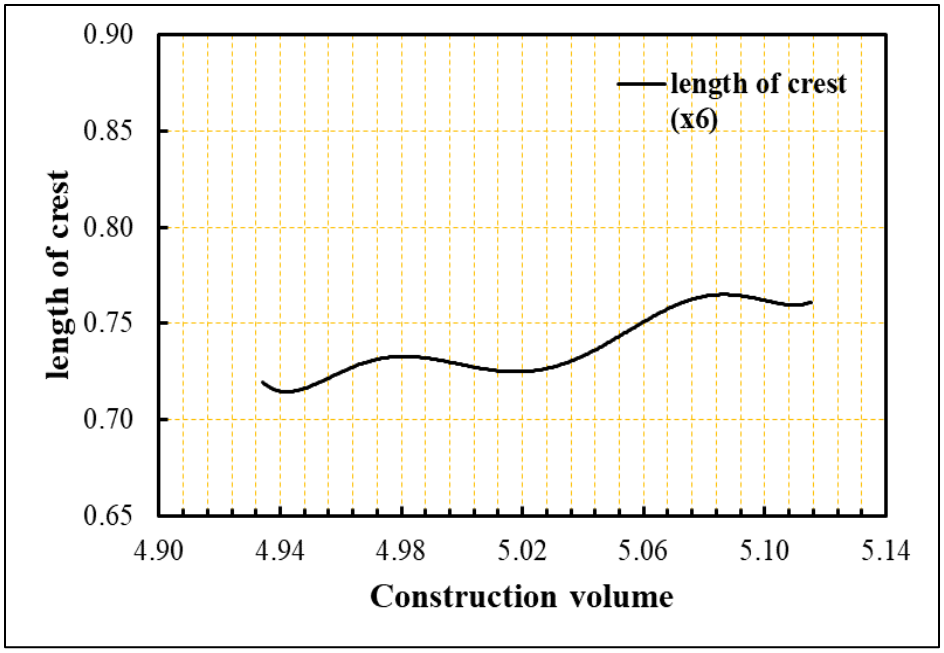


(a) Length of crest versus construction volume.

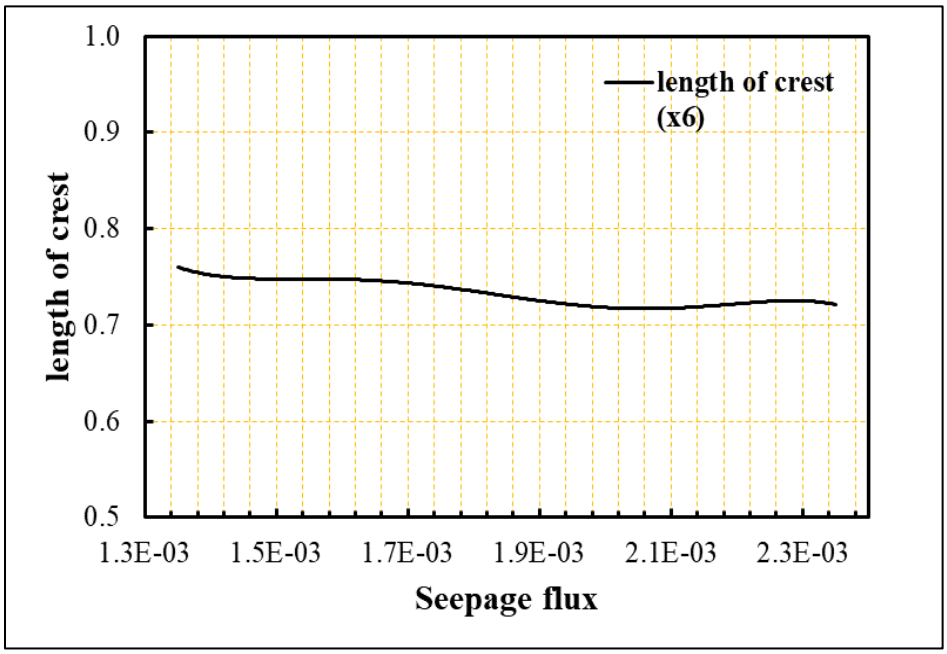


(b) Length of crest versus seepage flux.

Figure (A.6): Design chart for length of crest against different objectives for population size n=200.

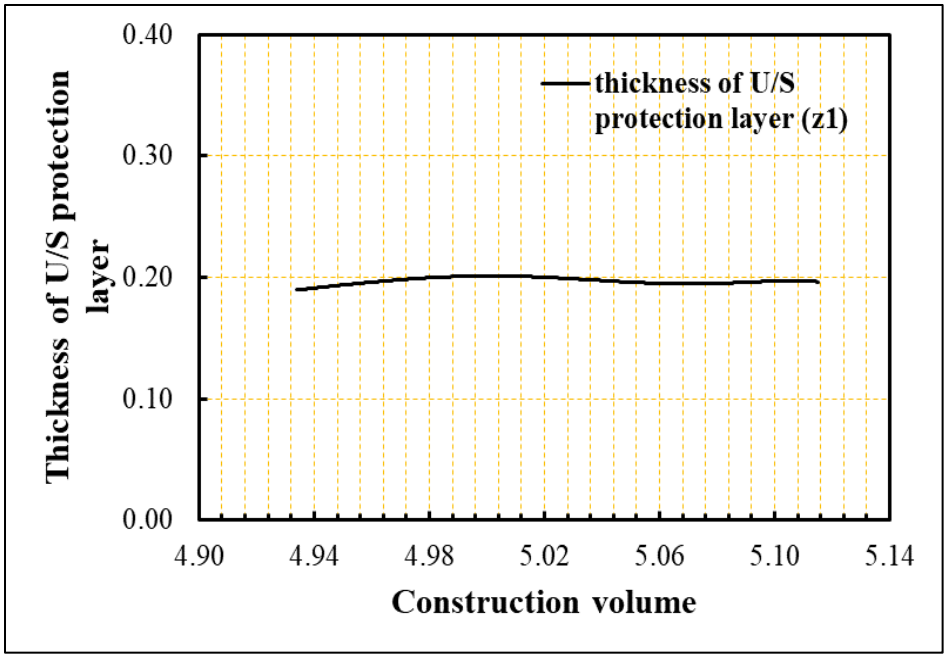


(a) Thickness of U/S protection layer versus construction volume.

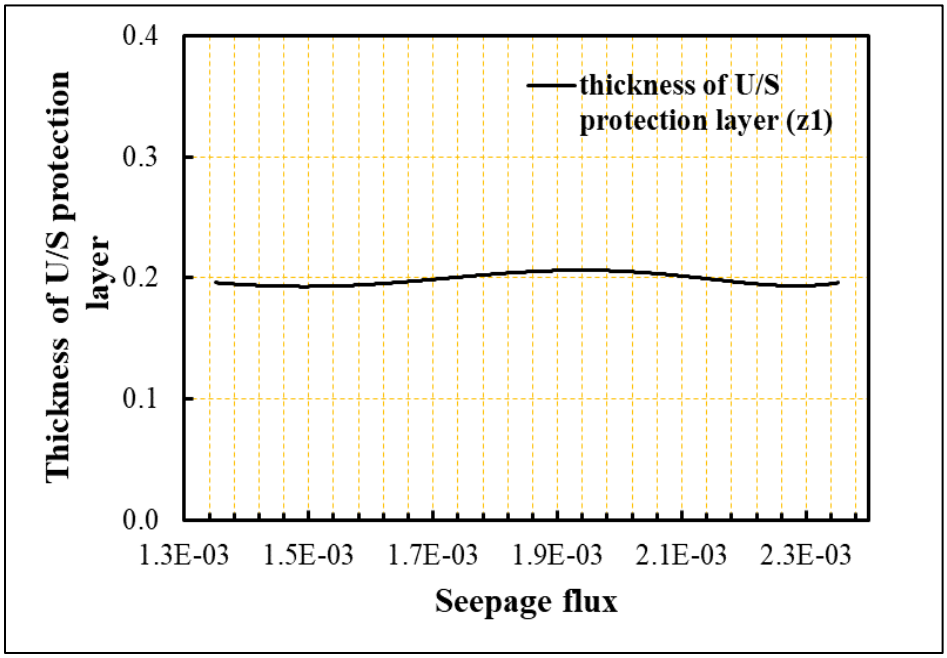


(b) Thickness of U/S protection layer versus seepage flux.

Figure (A.7): Design chart for thickness of U/S protection against different objectives for population size n=200.

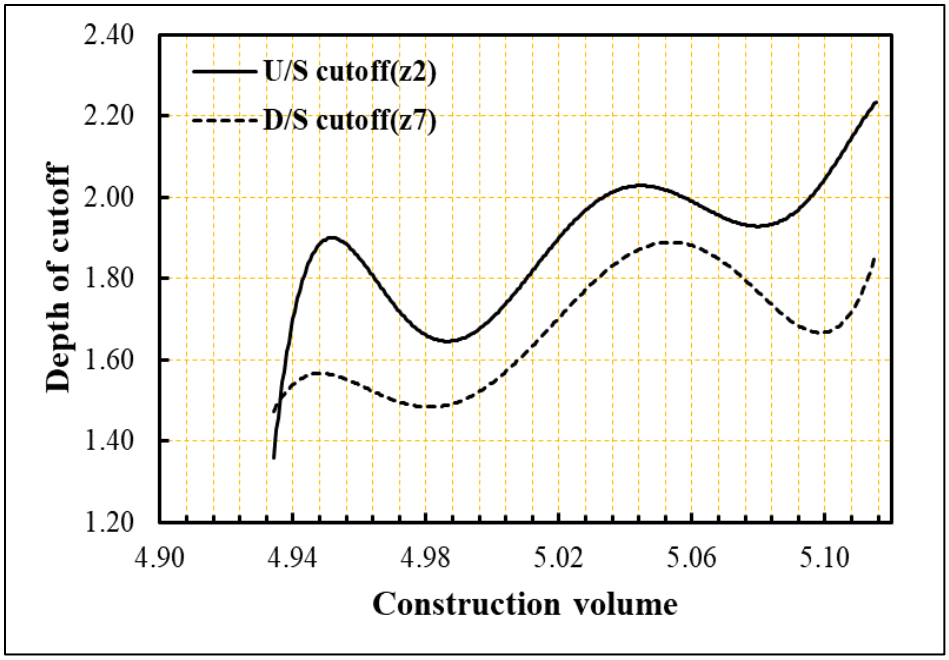


(b) Depth of cutoff versus construction volume function

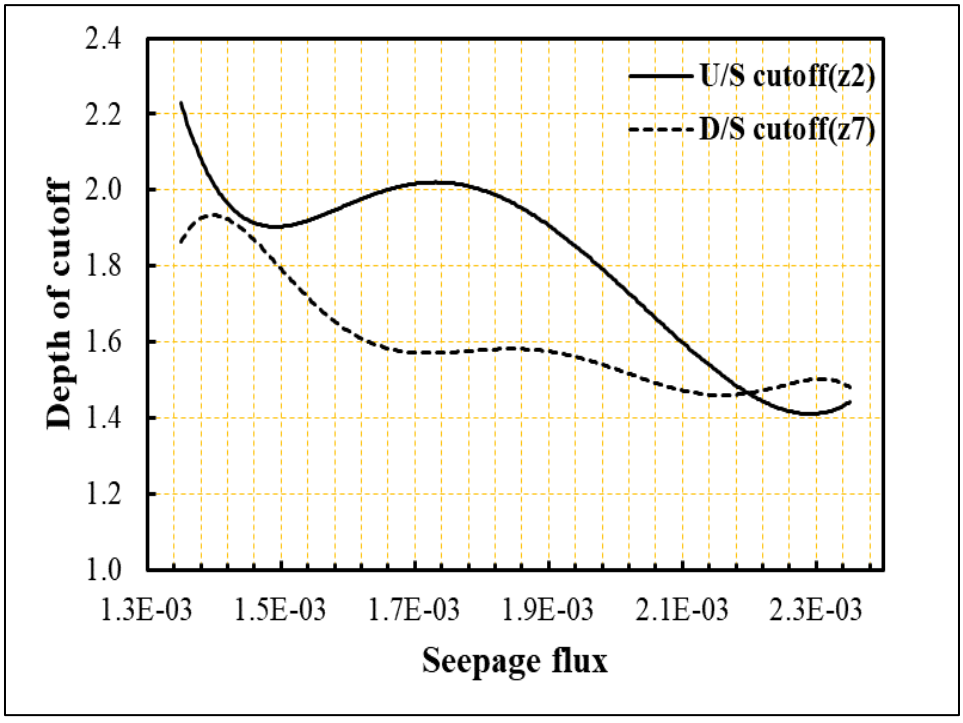


(b) Depth of cutoff versus seepage flux function.

Figure (A.8): Design chart of cutoffs depth ratio against different objectives for population size *n*=200.

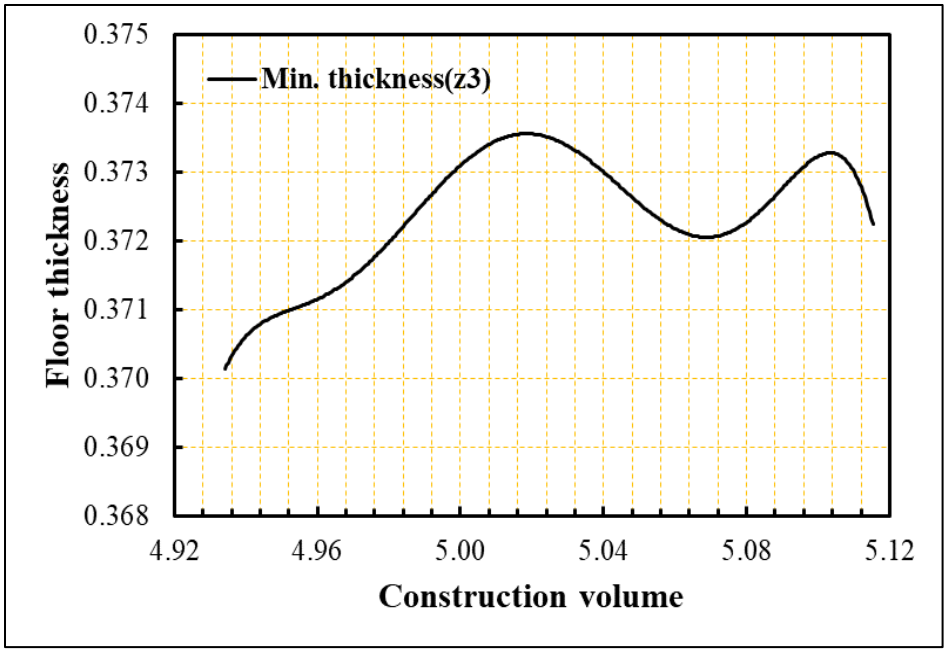


(b) Min. floor thickness versus construction volume function.

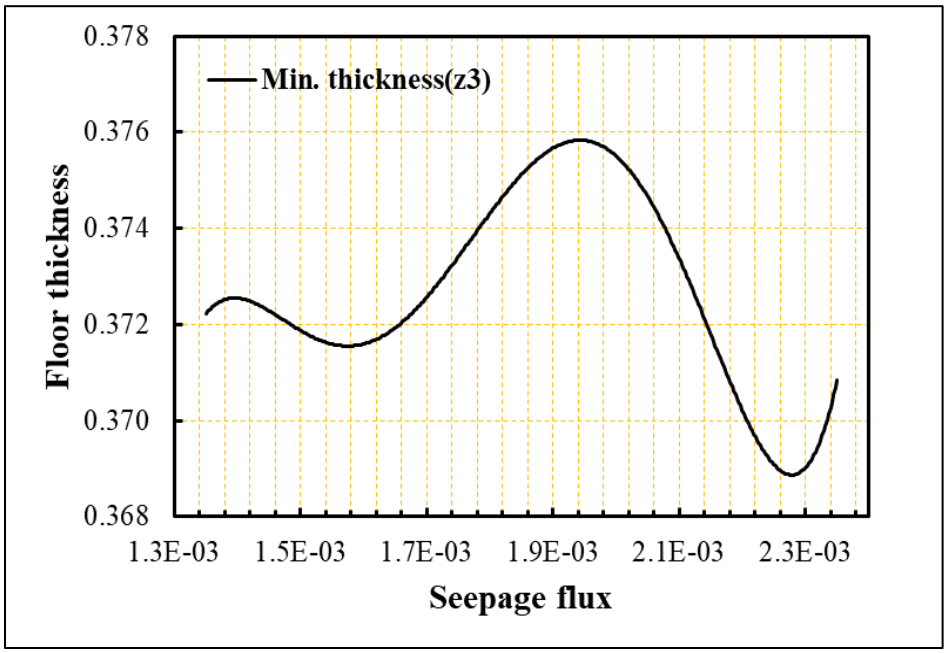


(b) Min. floor thickness versus seepage flux function.

Figure (A.9): Design chart of Min. floor thickness ratio against different objectives for population size $n$=200.

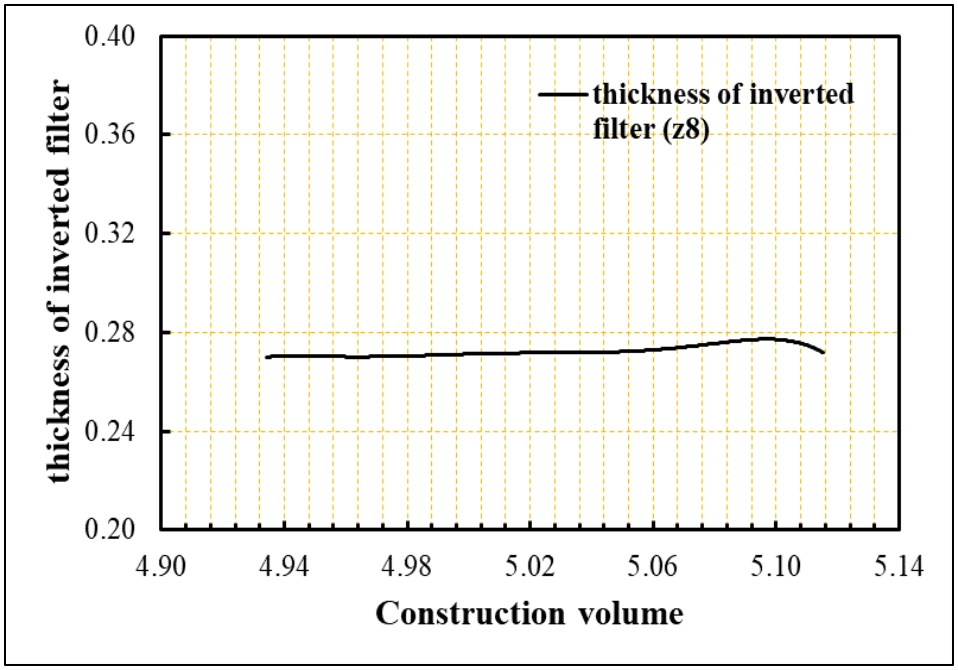


(a) Thickness of inverted filter versus construction volume.

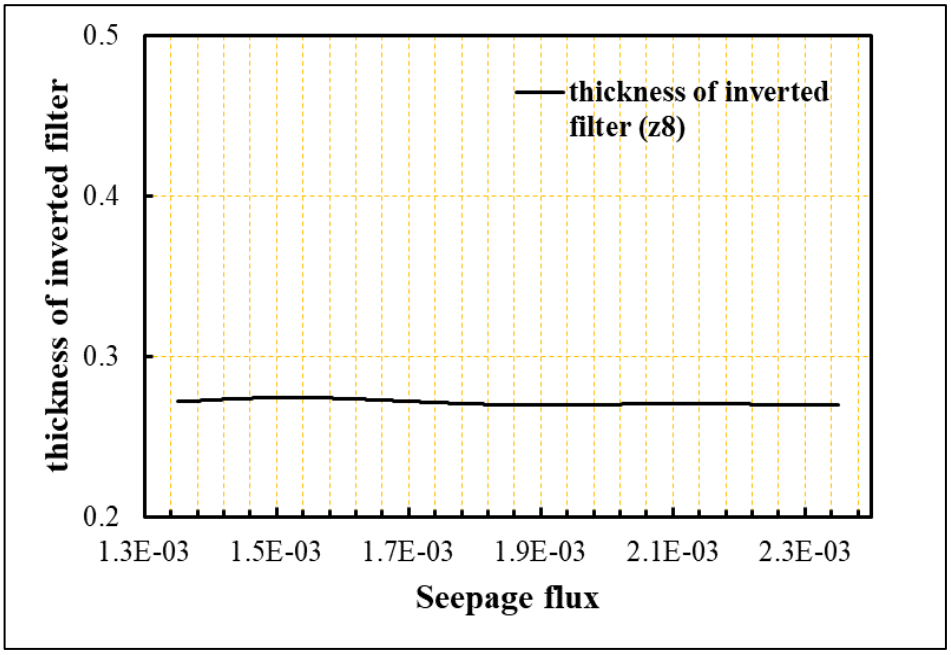


(c)Thickness of inverted filter versus seepage flux.

Figure (A.10): Design chart for thickness inverted filter against different objectives for population size n=200.

# المستخلص

غالبًا ما تتعرض الهياكل الهيدروليكية ، مثل السدود ، الهدارات ، السدات ، و النواظم لتسرب المياه تحت أساساتها بسبب ارتفاع منسوب الماء المحجوز. يمكن أن يتسبب تسرب المياه هذا في حدوث مشكلات كبيرة عندما يتم بناء مثل هذه الهياكل على تربة قابلة للأنهيار. في هذة الدراسة تم دراسة سدة مبنية على تربة جبسية و هي تربة (معروفة بأنهياريتها العالية نتيجة لذوبان الاملاح الجبسية عند تعرضها الى المياة) لأيجاد التصميم الامثل لمقطع اساس السدة في ظل ظروف وجود تربة انهيارية في اساساتها. ولتحقيق هذا الهدف تم تحضير عينات تربة جبسية باستخدام طريقة تعويض الوزن بمستويات متفاوتة من محتوى الجبس بنسبة 20٪ و 25٪ و 35٪ من وزن الجزء الناعم في عينات التربة الطبيعية. جمعت ست عينات من التربة من ضفة نهر الفرات في الكفل بمحافظة بابل، العراق. تم إجراء العديد من الفحوصات المختبرية على عينات التربة الطبيعية والجبسية المحضرة ، بما في ذلك الاختبارات الفيزيائية ، الاختبارات الكيميائية ، اختبارات النفاذية المشبعة ، اختبارات غسل الاملاح الجبسية واختبارات القص المباشر لحساب معاملات مقاومة عينات التربة الجبسية قبل اختبار الغسل وبعده.

أظهرت النتائج أن محتوى الجبس الأولي له تأثير سلبي على النفاذية المشبعة. مع تقدم عملية غسل الاملاح ، تزداد نفاذية التربة بسبب توسع وتطور المساحات الفارغة داخل كتلة التربة نتيجة ذوبان الاملاح ، مما يسمح بتسرب أكبر للمياه الناتج عن انحلال أملاح الجبس.

في هذه الدراسة تم استخدام برنامج جيو ستوديو لأجراء التحليل العددي للتسرب اسفل السدة حيث يستخدم هذا البرنامج طريقة العناصر المحددة للحصول على الحل العددي لمشكلة التسرب. تم تحليل 200 مقطع للسدة بمختلف الابعاد و قد تم تحليلها جميعا تحت افتراض بوابات مغلقة تماما. يوضح التحليل االحدودي للتسرب تحت أرضية السدة أن معدل التسرب يتناقص مع زيادة عمق جدار القطع عند المنبع ؛ و ايضآ أصبح هذا التناقص في مقدار التسرب أكثر وضوحًا عند زيادة طول أرضية السدة الكلي بسبب زيادة طول خط الزحف للمياة المتسربة تحت اساس السدة. لوحظ تناقص تدرج المخرج للمياة المتسربة مع زيادة عمق جدار القطع في اتجاه مجرى النهر ؛ أظهرت النتائج أن الحد الأدنى لقيمة التدرج الخارجي عندما يكون طول أرضية السدة الكلي وعمق القطع في اتجاة النهر يساوي (5.24 و 2.38) على التوالي ، حيث هذه القيم عند تحليل التسرب للسدة بدون ابعاد. أما تأثير ضغط الرفع الاقصى على أرضية السدة ، فقد أظهرت النتائج أن ضغط الرفع الناتج من ضغط المياة المتسربة تحت الاساس يتناقص مع زيادة عمق جدار القطع في المقدم.

من اجل ايجاد التصميم الهيدروليكي الامثل للسدة في مسألة الامثلية اللاخطية تم استخدام طريقة الخوارزمية الجينية ضمن برنامج الماتلاب. كان الهدف في هذه الدراسة هو تقليل حجم المواد الانشائية و تقليل مقدار التسرب اسفل السدة. تم تنفيذ الخوارزمية الجينية بأستخدام احجام مختلفة للمجتمع حيث كانت حجوم المجتمع (1400, 1000, 600, 200). أشارت النتائج إلى أن حجم المجتمع 600 كان كافياً للحصول على حل لمشكلة الامثلية غير الخطية المقيدة من أجل التصميم الهيدروليكي الأمثل للسدة المعنية. تم تقديم مخططات تصميمية لتطبيق مشكلة الأمثلية ، باستخدام سدة أبو صخير كمثال على التصميم لإعادة تصميم الأبعاد المثلى للسدة من مخططات التصميم الحالية في ظل ظروف وجود تربة جبسية في اساس السدة. أوضحت النتائج أن جميع أبعاد السدة قد تناقصت ماعدا عمق جدار القطع بالمقدم وسماكة طبقة الفلتر المقلوب. تم حساب معايير التصميم من حيث السلامة ضد االظاهرة الانبوبية في اساس السدة حيث يكون التدرج الفعلي للمخرج المحسوب من أبعاد السدة يساوي 0.0445 ، ومن الأبعاد المثلى 0.0433 ، وهو أقل من تدرج المخرج الحرج (0.976). تم حساب معامل الامان ضد الانزلاق من ابعاد السدة وجد انة يساوي 8.86 ومن الابعاد المحسوبة من المخططات التصميمية يساوي 7.23.

**جمهورية العراق**

**وزارة التعليم العالي والبحث العلمي**

**جامعة بابل**

**كلية الهندسة**

**قسم الهندسة المدنية**

# التصميم الأمثل لسدة مع الأخذ بالأعتبار وجود مخاطر التربة الأنهيارية

رسالة

مقدمة الى كلية الهندسة /جامعة بابل

كجزء من متطلبات نيل درجة الماجستير في الهندسة/ الهندسة المدنية /موارد مائية

من قبل

**شهلاء علي كاظم عليوي**

**بإشراف**

**أ.م.د. عماد حبيب عبيد**

**أ.م.د. زيد حميد مجيد**

2023 م

1444 هـ